On the calculation of time-domain impulse-response of systems from band-limited scattering-parameters using wavelet transform

By

Maryam Rahmani

A Dissertation
Submitted to the Faculty of
Mississippi State University
in Partial Fulfillment of the Requirements
for the Degree of Doctor of Philosophy
in Electrical Engineering
in the Department of Computer Science and Engineering

Mississippi State, Mississippi

November 2016

ProQuest LLC.
789 East Eisenhower Parkway
P.O. Box 1346
Ann Arbor, MI 48106 – 1346

On the calculation of time-domain impulse-response of systems from band-limited scattering-parameters using wavelet transform

By

Maryam Rahmani

Approved:

Michael Mazzola
(Major Professor)

J. Patrick Donohoe
(Co-Advisor)

Masoud Karimi Ghartemani
(Committee Member)

Shantia Yarahmadian
(Committee Member)

Hendrik F Arnoldus
(Committee Member)

James E Fowler
(Graduate Coordinator)

Jason M. Keith
Interim Dean
Bagley College of Engineering

Name: Maryam Rahmani

Date of Degree: November 3, 2016

Institution: Mississippi State University

Major Field: Electrical Engineering

Major Professor: Dr. Michael S. Mazzola

Title of Study: On the calculation of time-domain impulse-response of systems from band-limited scattering-parameters using wavelet transform

Pages of Study: 139

Candidate for Degree of Doctor of Philosophy

In the aspect of electric-ship grounding, the time-domain behavior of the ship hull is needed. The grounding scheme impacts the nature of voltage transients during switching events and faults, identifiability and locatability of ground faults, fault current levels, and power quality. Due to the large size of ships compared with the wavelengths of the desired signals, time-domain measurement or simulation is a time-consuming process. Therefore, it is preferred that the behavior be studied in the frequency-domain. In the frequency-domain one can break down the whole ship hull into small blocks and find the frequency behavior of each block (scattering parameters) in a short time and then connect these blocks and find the whole ship hull scattering parameters. Then these scattering pa- rameters should be transferred to the time-domain. The problem with this process is that the measured frequency-domain data (or the simulated data) is band-limited so, while calculating time-domain solutions, due to missing DC and low frequency content the time-domain response encounters causality, passivity and time-delay problems. De-

spite availability of several software and simulation packets that convert frequency-domain information to time-domain, all are known to suffer from the above mentioned problems.

This dissertation provides a solution for computing the Time-Domain Impulse-Response for a system by using its measured or simulated scattering parameters. In this regard, a novel wavelet computational approach is introduced.

Key words: Scattering-parameters, impulse response, time-domain, frequency-domain, causality, passivity, wavelet transform,

DEDICATION

To my adorable Parents: Hossein and Khadijeh

for being constant source of encouragement and making me be who I am

To my darling spouse, Saeed

for his dedicated partnership for success in my life

And

My beloved siblings

Mojgan,Mojdeh and Mehdi

For nursing me with affections and love

ACKNOWLEDGEMENTS

I would like to thank Dr. Karimi for his advisory at my first year of PhD and his passion to introduce me the methods of academic research and analyzing the practical problems and all his encouragements and supports.

I would also like to thank my committee members, Dr. J. Patrick Donohoe, Dr. Masoud Karimi, Dr. Shantia Yarahmadian and Dr. Henk F. Arnoldus, whose work demonstrated to me that introducing of mathematics, physics sciences to the fields of control, applied electromagnetic and power electronic should always transcend academia and provide a quest for posterity.

In addition, a special thank you to Dr. Shantia Yarahmadian, who introduced me to the incredible world of Mathematics, and whose enthusiasm for the "WaFou transform" had lasting effect. I thank the Mississippi State University for permission to include copyrighted pictures as a part of my dissertation. I also thank IEEE Xplore for permission to include Chapter 5 of my dissertation, which was originally published in IEEE Journal. I would also like to thank to The Office of Naval Research through for their financial support granted through N00014-15-1-2276 predoctoral grant.

TABLE OF CONTENTS

LIST OF FIGURES

CHAPTER 1

STATEMENT OF THE PROBLEM

1.1 Grounding in Electric Ships

1.1.1 Using Scattering parameters

Analysis of the power distribution system including grounding schemes and common-mode coupling to the ship hull of future all-electric ships is the first and main motivation of this dissertation. Simulation tools currently used to model terrestrial power systems do not take grounding schemes and common-mode coupling into account. Scattering parameters are suggested to help validate existing models, to support the development of specialized models designed for shipboard power systems, and ultimately facilitate the design of all-electric ships. We refer the reader to [15] for an overview of scattering parameter related activities within the Electric Ship Research and Development Consortium (ESRDC) presented at the ESTS conference-2015.

Power distribution in future Electric-ships has important considerations such as power density, load characteristics, physical dimensions, characteristic impedances, and reliability and availability requirements. Common-mode currents generated by the current carrying conductors in the close proximity of the ship hull create complex current distributions in it. These coupling modes contain implications for E-ship's power qualities such as level

of over-voltage, high frequency ringing, electromagnetic signature, level of interference in cathodic protection and degaussing systems.

Coupling transient simulation models of the shipboard power system (SPS) with finite element models applied to the ship hull is possible by using S-parameters. The method is powerful regarding the different coupling modes, including conductive, inductive, and capacitive coupling. Figure 1.1 shows a block diagram of different elements of the shipboard power system including generators, cables, rectifiers, DC-DC converters, inverters, and motors.

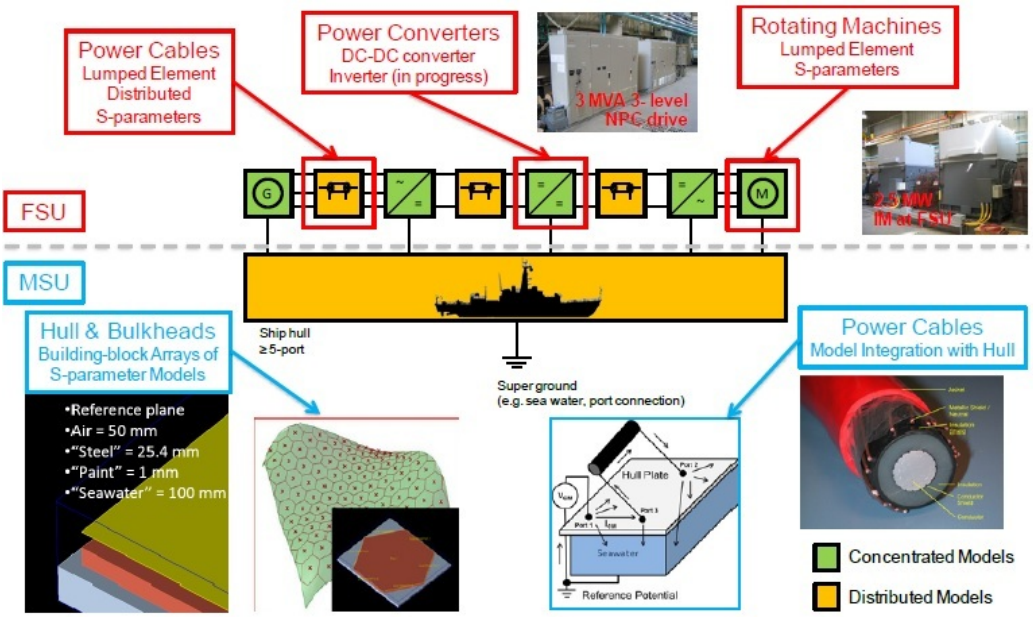

Figure 1.1

Block diagram of the different elements of the shipboard power system performed by FSU, MSU Universities

A special consideration here is the similarity of physical dimensions of the power system and the wavelength of harmonics of the power electronic switching frequencies of fast transients shown in Figure 1.2.

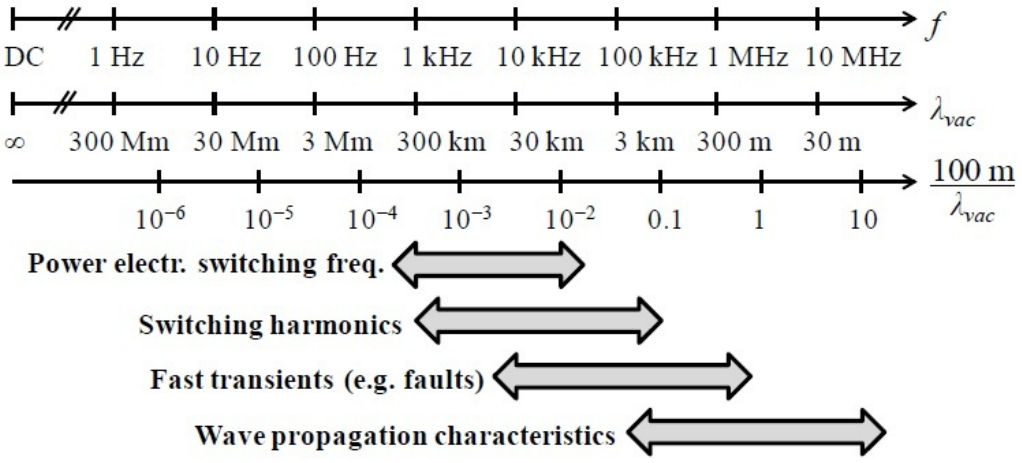

Figure 1.2

Comparison between wavelength of fast transients switching harmonic and ship-hull physical dimensions

The predominant coupling mode between the power system and the ship hull is of capacitive nature and is linear in the frequency range of our interest.

1. Introducing s-parameters to transient analysis of power systems

   Ungrounded and high impedance grounded power systems come with several intricacies. As an example, ungrounded 3-phase diode rectifiers can generate 3f harmonics from each DC rail to ground, when both AC and DC side couple capacitively to ground. Single line to ground faults in bipolar DC distribution buses can lead to transient overvoltages of up to three times the symmetrical DC voltage. The discovery of

such phenomena in simulation models shifted the research focus to the exploration of the range of validity of existing simulation models. In 2010, the ESRDC grounding team introduced scattering parameters (S-parameters) to transient power system models as a means to evaluate suitability of component models for grounding studies. Later, S-parameters were used to model common-mode coupling of components of the shipboard power system to the ship hull [15].

S-parameters can be obtained by numerical methods such as finite element analysis (FEA) or by measurement. Numerical methods usually are very complicated and time-consuming due to the large number of degrees of freedom and high aspect ratios. Therefore, straight measurement is often preferred. S-parameters can be measured by a Vector Network Analyzer (VNA) with 50Ω coaxial connectors by a specifically designed set of leads of known frequency characteristics with clamps of appropriate size at one end and high frequency coaxial connectors compatible with the VNA on the other end. There are lower and upper limits for the frequency of measurement. For instance, a current design used for S-parameter measurements at FSU-CAPS has an upper frequency limit of 10 MHz. The lower frequency is determined by the noise floor level of the VNA (mentioned in the manual) and the characteristics of the network under test.

2. Modeling Each Sub-Component

   (a) Cables and Bus Bars

   The cables and bus bars are important because of their significant influence on

amplitude and frequency of the oscillation of voltage transients. Cables can be easily modeled and physically experimented and so are a suitable choice for validation of the simulated models. The current carrying cables and bus bars were the first components which were studied by the ESRDC grounding team. During their studies, a single pole of a power cable was assumed to be a 2-port linear network considering the shield of the cable as the reference ground. Several power cables were explored and validated by FSU including a 30m long high temperature superconducting power cable. They used the measured S-parameters and also they simulated this measured S-parameter to create a lumped circuit model to validate it.

(b) Rotating Machines

Rotating machines make a major contribution to the overall coupling to the ship hull. Motors are usually fed by a variable frequency drive, which leads to switching frequency harmonics in the power system and common-mode coupling to the ship hull. The scattering parameter measurement considers the motor as a 3-port network (3 terminals as ports and the enclosure as the ground reference point), a 4-port network (3 terminals and the enclosure as ports and an external arbitrary reference point), or a 1-port network (all phases tied together as one port and the enclosure as the ground reference point).

(c) Power Electronic Converters

The common-mode coupling characteristics of shipboard power systems can be completely understood by studying Power Electronic Devices (PED) such

as rectifiers, DC-DC converters, and inverters. Behaviors of these devices are major sources of high frequency harmonics due to their fast switching character. Also, the low pass filters which are used on both the generator and load sides of these components have a dominant effect on the impedance of the common-mode current. In addition, wherever the energized part of the system comes to close proximity to a grounded conductor the parts of a PED show a significant capacitive coupling to ground.

Three parts of a PED that were considered as the major contributors to the parasitic coupling to ground in measurement were the IGBT modules, the filter inductors, and the bus bars. The heat sink of the IGBT modules and the cores of the filter inductors are grounded (the high frequency radiation is reduced), and the capacitance created between the IGBT terminals and ground can be substantial. The bus bars and power cables inside a PED are expected to have a noticeable capacitive coupling to the grounded enclosure because of their width, length, and sometimes close proximity to the enclosure. The result of the measurement is a range of capacitance which is determined in a specific frequency range.

(d) Ship Hull

S-parameter linear modeling of open-form conductors (i.e. hull and bulkheads), is computationally efficient for control of common mode currents on ships with many high-power converters and interconnecting power cables because: (1) the problem is mainly linear; (2) common-mode currents have wide bandwidth

justifying near-RF behavioral modeling methods; and (3) the possible paths of common-mode currents on ship hulls become concentrated at the bonding points of equipment chassis, safety grounding cables, armored cable sheaths, and harmonic filters. Each bonding port can be considered as an input or output port for a $n \times n$ network. The voltage and current can be computed as the port is part of a lumped-element circuit but, in fact, the electrical solution at each port is self consistently computed with respect to every other port through the internal behavioral model along with lumped elements externally bonding ports together. A process that breaks the physical description of free-form conductor shapes, such as hull plates and bulkheads, into behavioral models has been developed with industry accepted software tools such as COMSOL and ADS to extract the S-parameters for standard-shaped discrete subcomponents of hull structures. These powerful commercial tools are reliably physics-based (meaning they use finite-element methods) and are valid for the broad frequency range required for the common-mode current expected in a shipboard power system. The standard shapes are bonded together to form approximations of hull structures with unique but finite numbers of ports defining the point of bonding between the hull/bulkheads and physical components that either inject or extract common-mode currents back to the source in the power system. Once the S-parameters are extracted, time-consuming finite element methods are no longer needed to compute the voltages and currents at the bonding points to the hull. Analysis can be conducted in either the frequency or the time-domain

as needed using only behavioral modeling. It has now been demonstrated that this method can create large scale computationally efficient behavioral models based on S-parameters [34]. The specification of these S-parameter models has been extended to grounded features of cables through empirical methods based on a vector network analyzer.

3. System Analysis

   (a) Integration of S-Parameter Models in Power System Simulations

   As the major power system modeling software packages, such as MATLAB/Simulink SimPowerSystems (SPS) and PSCAD/EMTDS, do not have the capability to directly use scattering parameters, some frameworks were developed by using the components available in Simulink and SPS. In one of these methods, each S-parameter is represented by a rational function which is fitted to the corresponding S-parameter data. The order of the rational function determines the accuracy of the approximation and, as a result, the level of complexity of the final model. Then, the rational functions are used to construct transfer function blocks, which in turn are required to build the model. The complexity of the model can be determined by the number of ports, which determines the number of transfer functions, and also the rational function that is fitted to the data set. The accuracy of the model can be increased at the cost of increasing complexity and computation time.

   (b) Parametric Studies

To analyze the sensitivity of a model response to a certain input parameter, the power system model needs to be run multiple times. This can be problematic for grounding-related studies since the uncertainty of ground impedances can span several orders of magnitude. The result would be thousands of simulation cases even for just a dozen of uncertain ground impedance values. Intelligent sampling methods can substantially reduce the number of required simulation cases [18], [23]. The required computation time can often be reduced further by parallelizing the cases on multi-core CPUs, which generally works well due to the independence of each simulation case.

CHAPTER 2

REVIEW OF THE LITERATURE AND RESEARCH QUESTIONS

2.1 Introduction

The three key features of this dissertation can be summarized as impulse response, scattering parameters and wavelet transform. The following sections are specified to classify these aspects.

2.1.1 Impulse Response

Impulse response is the response of a Linear Time-Invariant (LTI) system to all frequencies. Because the impulse is such a short time pulse which includes all frequencies; therefore, it determines the behavior of the system regarded in across the entire frequency spectrum. In other words, any LTI system is completely characterized by its impulse response. By obtaining the impulse response of a system, one can have the response of the system to all types of input signals because it is simply calculated by multiplying the Laplace transform of input signal by the Laplace transform of the impulse response (called transfer function), and the output can be calculated by the inverse Laplace transform of the product.

Because the behavior of a ship hull is the desired concept, therefore evaluation of the impulse response is an important subject in the design of an electric ship.

2.1.2 Scattering Parameters

Richard W. Anderson opens his classic application note [2] on scattering parameters with the observation [39]: "Linear networks can be completely characterized by parameters measured at the network terminals (ports) without regard to the contents of the networks. Once the parameters of a network have been determined, its behavior in any external environment can be predicted."

Generally, the development of scattering-parameters is an important milestone in the history of Radio Frequency. They are powerful tools for the design and analysis of systems as n-port networks in the frequency-domain.

Historically, Jean Baptiste Joseph Fourier published his book entitled as "Analytical Theory of Heat" [4]. Even he himself didn't have an idea how drastically the trigonometric or Fourier series following with Fourier transform could revolutionize the methods of analysis and designing of systems and networks. Later on, many mathematicians dedicated to apply, improve and classify Fourier's invention. In 1828, Dirichlet formulated conditions for a function to have a Fourier Transform.

The concept of scattering parameters was first popularized around the time that Kaneyuke Kurokawa of Bell Labs wrote his IEEE article "Power Waves and the Scattering Matrix" [22] in 1965. During the 1960s, Hewlett Packard introduced the first microwave network analyzers. Several papers predated Kurokawa's from the 1950s, and one of them was written by E. M. Matthews, Jr., of Sperry Gyroscope Company entitled as "The Use of Scattering Matrices in Microwave Circuits" [26]. Also in 1960, Robert Collin discussed scattering matrix briefly in his textbook of *Field Theory of Guided Waves* [8]. Afterward,

a prolific number of publications on the application of these matrices in different networks were performed, and several companies manufactured different types of simple and vectoral Network Analysers. Therefore, utilizing scattering parameters became a more than common method to analyze systems in the frequency-domain.

Scattering parameters, which we will call S-parameters from now on, describe the behavior of an electromagnetic wave while propagating through a network. By using the S-parameter matrix, one can describe even incredibly complicated networks as a simple black-box. In a network, once an RF-signal is incident on one port, some part of the energy of the signal reflects back, some part of the energy is transmitted through the network and exits from the output port, and a small part converts to heat or electromagnetic radiation. An N-port network is described by an $N \times N$ S-parameter matrix. This matrix contains complex elements because it determines the variations of both magnitude and phase of a signal while passing through a network. S-parameters are a function of frequency, and they also depend on the network's input impedance. Each component S_{ij} of the S-parameter matrix shows the ratio of the reflected to incident wave in input port of "j" and output port of "i". Therefore, in this matrix, the diagonal elements are called reflection coefficient, and the off-diagonal elements show transmission coefficients. The following matrix represents a S-parameter matrix for an $n \times n$ network.

$$S = \begin{bmatrix} S_{11} & S_{12} & \dots & S_{1n} \\ . & & & \\ . & & & \\ S_{n1} & S_{n2} & \dots & S_{nn} \end{bmatrix}$$

S-parameters can be defined as the response of a N-port network to a voltage signal at each port. Therefore, S_{ij} represents that the incident port is "j" and the responding port is "i". For instance, the S_{21} represents that the incident voltage is applied to port 1, and the responding port is 2. If we consider the voltage on the incident port by "a" and the voltage at the responding port by "b," we can show the configuration of the S-parameter matrix by Figure 2.1:

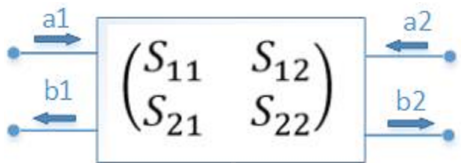

Figure 2.1

2-port network S-matrix

It is assumed that each port is terminated by an impedance of Z_0, so the S-parameters of the 2-port network is defined as follows:

$$\begin{bmatrix} b_1 \\ b_2 \end{bmatrix} = \begin{bmatrix} S_{11} & S_{12} \\ S_{21} & S_{22} \end{bmatrix} \times \begin{bmatrix} a_1 \\ a_2 \end{bmatrix}$$

$$S_{11} = \frac{b_1}{a_1} \qquad S_{12} = \frac{b_1}{a_2} \qquad S_{21} = \frac{b_2}{a_1} \qquad S_{22} = \frac{b_2}{a_2} \tag{2.1}$$

All a's and b's are complex numbers showing the ratios of the magnitude and phase of a signal from the input to the output port. The units usually are in dB and radians.

2.1.3 Wavelet Transform

In this section Fourier transform, short time Fourier transform and their limitations which lead us to use wavelet transform are discussed. Continuous and discrete wavelet transforms are studied as well.

1. **Fourier Transform**

   The general formula for Fourier and inverse Fourier transforms and the series are as follows:

$$X(f) = \int_{-\infty}^{+\infty} x(t) e^{-j2\pi f} dt \tag{2.2}$$

$$X(k+1) = \frac{1}{N} \sum_{n=0}^{N-1} x(n+1).e^{\frac{-j2\pi kn}{N}} \tag{2.3}$$

$$x(t) = \int_{-\infty}^{+\infty} X(f) e^{+j2\pi f} df \tag{2.4}$$

$$x(n+1) = \frac{1}{N} \sum_{k=0}^{N-1} X(k+1).e^{\frac{+j2\pi kn}{N}} \tag{2.5}$$

   By utilizing Fourier transform, one can store and transmit data, solve differential and difference equations, and obtain signal behavior in different domains e.g. frequency-domain. The Fourier transform or series method is applied to decompose a signal into its containing frequency components.

Fourier transform has some drawbacks. For instance, the Fourier transform cannot pick out local frequency content. For understanding the local frequency content of a signal, Short-Time Fourier Transform is utilized.

2. **Short Time Fourier Transform (STFT)**

   The general idea behind this transform consists of applying a window with a fixed width to the time-domain signal and extracting the related frequency containing of the signal inside the window and then transferring the window to the next time-slot. The general formula for STFT is as follows:

$$STFT_g(\tau, k) = \int_{-\infty}^{+\infty} f(t)g^*(t-\tau)e^{-2\pi ikt}dt \tag{2.6}$$

   As shown, STFT is function of two variables, the time and frequency, which enable us to see the time-frequency distribution of energy of a signal. The resolution of time and frequency are related by Heisenberg uncertainty principle (2.7):

$$\Delta t.\Delta k = constant \tag{2.7}$$

   It means that by increasing the width of the window, time resolution decreases and vice versa. Once a window function g is selected, both time and frequency resolutions are determined, and these resolutions are fixed for all times and frequencies. Therefore, as an alternative approach, the wavelet transform was proposed as an STFT with variable window width to overcome the resolution problem.

3. **Continuous Wavelet Transform**

   By using wavelet transform, one can analyze a signal at different frequencies with

different resolutions. At high frequencies, a good time resolution but poor frequency resolution can be achieved while at low frequencies there is good frequency resolution and poor time resolution.

Wavelet transform splits up the signal into a multitude of signals representing the same signal but all corresponding to different frequency bands and only shows which frequency bands exist at what time. The general equation of wavelet transform is represented by:

$$W\{f(t)\} = W_\psi f(a,b) = \frac{1}{\sqrt{a}} \int_{-\infty}^{+\infty} f(t)\psi^*(\frac{t-b}{a})dt \tag{2.8}$$

where a is the scale and b is the translation. It is necessary to sample the time-frequency (scale) plane. At high scales (lower frequencies) of a, the sampling rate N can be decreased. The Scale Parameter a is normally discretized on a logarithmic grid with the most common value of 2. In practical applications due to the fact that integrals will be calculated by digital computers, usually the Discrete Wavelet Transform is utilized.

A comparison between the above mentioned transforms is illustrated in Figure 2.2

4. **Discrete Wavelet Transform (DWT)**

While the DWT provides sufficient information in frequency-domain both for synthesis and analysis, it reduces the computation time compared to continuous wavelet transform (CWT) significantly and is easier to be implemented. DWT analyzes the signal at different frequency bands with different resolutions and decomposes the

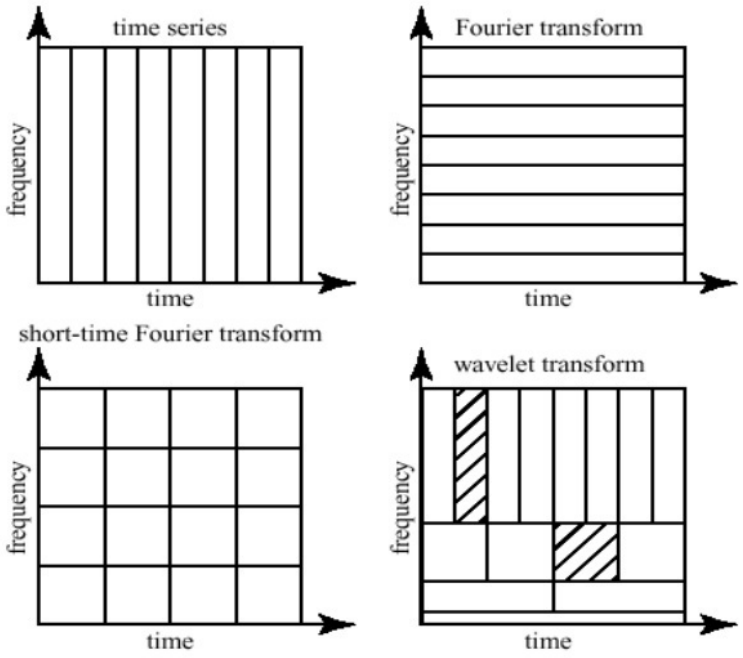

Figure 2.2

Comparison of different transformations between time and frequency-domain

signal into a coarse approximation and detailed information. This transform provides good time resolution and poor frequency resolution at high frequencies and good frequency resolution and poor time resolution at low frequencies. This property is useful because most natural signals have low frequency content spread over a long duration and high frequency content for only short durations.

Generally, the DWT is nothing but a system of filters. There are two filters involved, one is the wavelet filter, and the other is the scaling filter. The wavelet filter that calculates the details of signals is a high pass filter, while the scaling filter is a low pass filter and therefore is an averaging filter. A three level DWT is shown in Figure 2.3.

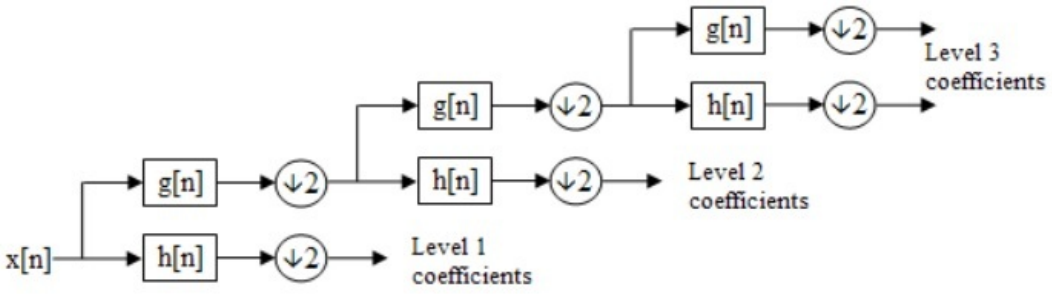

Figure 2.3

a three level filter bank performing a three level DWT

2.1.4 Frequency to Time-Domain Considerations

All the results mentioned so far are calculated, simulated, or measured in the frequency-domain, but all of them need to be shown or calculated in the time-domain. If the frequency data, here S-parameters, were complete and contained all the frequency components, then

the transformation of the signal would be straight forward and could be achieved quickly by using inverse Fourier transform:

$$f(t) = \frac{1}{2\pi} \int_{-\infty}^{+\infty} F(\omega) e^{j\omega t} d\omega \tag{2.9}$$

However, this is not the case most of the time. Due to limitations of simulation algorithms and measuring equipment, some parts of frequency data, specifically in the DC side, are missing and therefore, the frequency data is band-limited. Reconstruction of a band-limited S-parameter does not result in an accurate impulse response in the time-domain, and some problems emerge that need special consideration, which are addressed in [36] and [35].

2.1.4.1 Causality

Band-limited S-parameters can violate causality conditions even when this data is physical and accurate in-band. Causal systems satisfy Kramers-Kronig (K-K) equations 2.10:

$$u(\omega) = \frac{1}{\pi} P \int_{-\infty}^{+\infty} \frac{v(\omega')}{\omega - \omega'} \quad d\omega'$$

$$v(\omega) = -\frac{1}{\pi} P \int_{-\infty}^{+\infty} \frac{u(\omega')}{\omega - \omega'} \quad d\omega' \tag{2.10}$$

u(ω) is the real part and v(ω) is the imaginary part of S-parameter and P is the Cauchy principle value. These equations show that in a causal system, the real and imaginary part of S-parameters are dependent. The integrations are calculated from minus infinity to plus

infinity; therefore, they cover all the frequency spectrum. As mentioned before, because the typical S-parameter model is band-limited it violates the Kramers-Kronig relations and lead us to a noncausal time-domain response. For example, consider a simple exponential response function as:

$$H(\omega) = \frac{1}{1 + j\omega\tau} \tag{2.11}$$

The impulse response of this function is causal and given by:

$$h(t) = \begin{cases} 0 & t < 0 \\ e^{\frac{-t}{\tau}} & t \geq 0 \end{cases} \tag{2.12}$$

Once the assumed S-parameter function is calculated by IDFT (in Matlab or other software) the response is no longer causal and differs from 2.12 as illustrated in Figure 2.4. There are cut-off frequencies from both sides, DC and high-frequency, which is a common problem with the electromagnetic measurements and simulations. For simplicity τ is considered one. As seen in Figure 2.4, the upper plot shows the original and reconstructed signal in time-domain and the lower plot shows the frequency response of the signal with maximum frequency of 60 Hz. A window is applied to the frequency response in a way to keep a few components of the first frequency data (i.e, 17 points as shown in the figure) and eliminates the rest of frequency data. In other words, this process truncates the frequency data. The goal of applying this window is to simulate the conditions that happens in reality, i.e. a spectrum containing some missing parts of data. As can be seen in the upper plot, the red line shows the reconstructed time-domain signal which indicates non-causal behavior of the signal and also some ripples in negative time.

Although there are some correction techniques that enforce causality, such as the hypothetical causality correction method that truncates the non-causal (t<0) part of the response to zero, but the spectrum of truncated response does not match the original one and therefore, the time-domain simulation accuracy is poor.

Usually, in order to enhance a signal with the ripples, a windowing technique is applied. In this case, windowing has an adverse effect because most of the popular windows like Hanning, Hamming and Barlett are non-causal and despite smoothing the ripples, the causality condition gets worse. After applying these windowing techniques, a significant portion of the signal energy appears at t< 0.

In [6], Biemacki et al. addresses Causality Enforcement in Fast EM-based Simulation of Multilayer Transmission Lines.

2.1.4.2 Passivity

Generally in reconstruction of a signal in the time-domain from its Fourier transform, models of passive components appear non-passive due to errors in measurement or simulation. In the S-parameter matrix, if the magnitude of all the eigenvalues be less than one, it can be concluded that the matrix belongs to a passive component. A straight-forward method for enforcing passivity is to divide the matrix elements at the offending frequencies by the magnitude of the maximum matrix eigenvalue. Therefore, one of the most important considerations of reconstruction of responses in the time-domain is enforcing passivity to the impulse response of passive components.

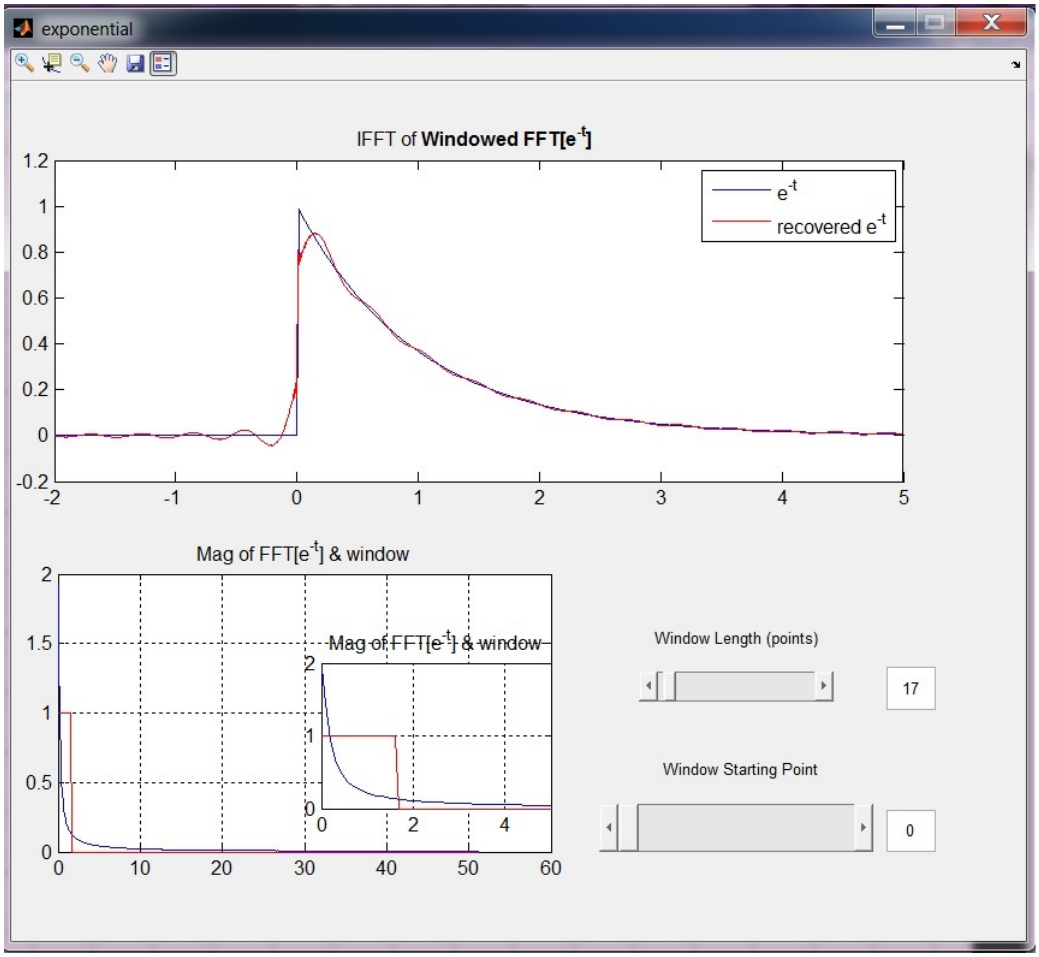

Figure 2.4

GUI figure in Matlab. The bottom plot shows the freqency response (blue) and the applied windowing (red); the top plot shows the original time-domain response (blue) and the reconstructed time-domain response from the truncated frequency response.

2.1.4.3 Time delay

While causality enforcement methods deal with system response relative to absolute time zero, there is another important consideration called time-delay, which is the response with respect to a minimum propagation delay. In every physical system there is no output before the system's base propagation delay. This constraint is frequently violated by numerical simulations and is caused by frequency-domain data truncation or band-limiting, and therefore, as a result of violating Krammer-Kronig.

2.2 Literature Review

S-parameters for every component can be produced in one of two manners: experimental and simulation. In the experimental approach, S-parameters are measured by a network analyzer with or without "device under test" (DUT) fixtures. Then it is saved in appropriate file format such as touchstone. For a simulation approach, the S-parameters are generated by one of the following methods: parametric equations, 2D and 2.5D field solvers and 3D full-wave field solvers.

One of the advantages of frequency-domain simulation is its flexibility such that it can be used directly with linear simulations. In addition, it is accurate because all of the frequency-dependent losses and higher order modes are considered during the simulation. Also it can be transferred between different simulation environments using special file formats e.g. touchstone files.

A disadvantage of S-parameter simulation occurs when using them in time-domain simulations. For this purpose one should convert the S-parameter model to pole/residue

macro-models or impulses. Conversion to impulse data requires special aforementioned considerations like causality, passivity and time-delay. There are some commercial simulation tools which are able to calculate S-parameters of structures, such as Keysight (Agilent) Advanced Design System (ADS) and Electromagnetic Professional (EMPro) and Ansoft HFSS, Microwave Office AWR , CST Microwave Studio, and COMSOL.

Reconstruction of the time-domain impulse response using a simple IDFT would be straight forward provided the S-parameters are complete and cover all of the frequency range. Due to the limitations of measuring equipment and simulation algorithms, it is not possible to have the S-parameters over the entire frequency-domain; therefore, there are lower and upper frequency bounds i.e. the S-parameters are band-limited. As discussed above, there are some considerations such as causality and passivity that should be noticed when performing any inverse transform from frequency-domain to the time-domain. The following sections address the most popular methods to compensate band-limited S-parameter defects or to convert band-limited to a complete S-parameter.

2.2.1 Reconstruction by Circuit Elements (Traditional)

Rao, Morgan et. al addresses this problem at the IBIS summit of Agilent/Tyco [9], which is one of the most important companies that provides modeling software, and the component models for the electromagnetic solution of problems in electronic and communication systems. They investigated in this work an impulse response file format for components from their S-parameters. For deriving passive component models in traditional methods a quasi-static 2D and 3D solver is used to find the equivalent inductance

(L), mutual inductance (K), and capacitance (C) to be represented as a transmission line model. These models are usually lossless except, for the series DC resistance as illustrated in Figure 2.5.

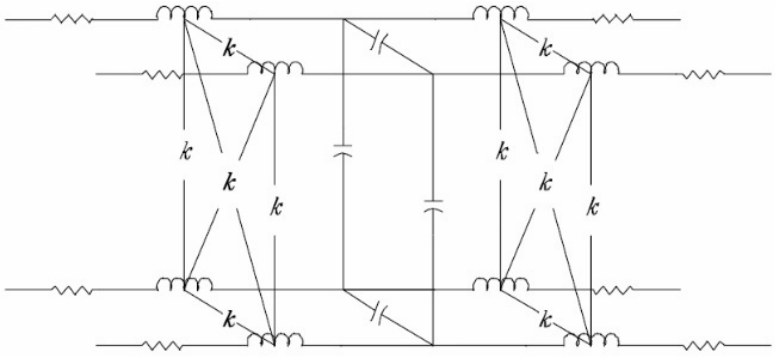

Figure 2.5

Transmission-Line model considered for a passive component in 2D and 3D solvers

One of the advantages of these types of traditional models is that the sub-circuit models can be run in transient simulation along with other active device models. The other advantage is these models are inherently passive and causal. There are some disadvantages related to these types of models. Firstly, the frequency-dependent loss and dispersion are not captured by these models completely. Secondly, the longitudinal modes and transverse currents are not adequately modeled. Thirdly, model run-time and complexity increase with shorter cross-section lengths.

One of the traditional simulation tools which solve transient simulations through time-stepping differential equations is the generic SPICE. For using this simulator one needs to

first convert the S-parameters to a lumped element circuit model. This can be performed by using the following algorithms:

1. Genetic Algorithm

   In order to utilizing this algorithm, one needs to first give a lumped element circuit structure. Genetic algorithm determines the lumped element values to fit the desired S-parameter model. Note that guessing the lumped element circuit structure ahead of time is very difficult.

2. Macro-Modeling

   A Matlab routine called *Vectfit*, which is an implementation of Fast Relaxed Vector Fitting (FRVF), computes a rational approximation from tabulated data in the frequency-domain. This routine can fit given S-parameter data to a pole/residue function. This procedure enforces passivity and finally, produces a lumped element network representing the given S-parameter data.

3. Laplace domain simulation

   This simulation uses recursive convolution to evaluate the model in one of the following forms:

   (a) Pole/residue form

$$H(s) = c + \sum_{m=1}^{M} \frac{k_m}{s - p_m} \tag{2.13}$$

(b) Pole/Zero form

$$H(s) = \frac{a(s + a_{z1} - \omega_{z1})(s + a_{z1} + \omega_{z1})...(s + a_{zn} - \omega_{zn})(s + a_{zn} + \omega_{zn})}{b(s + a_{zp} - \omega_{p1})(s + a_{p1} + \omega_{p1})...(s + a_{pn} - \omega_{pn})(s + a_{pn} + \omega_{pn})} \tag{2.14}$$

(c) Rational Polynomial form

$$H(s) = \frac{k_0 + k_1 s + ... + k_n s^n}{d_0 + d_1 s + ... + d_m s^m} \tag{2.15}$$

2.2.2 Reconstruction by Curve Fitting

Using curve fitting, one can extract the missing parts of S-parameter data and reconstruct the time-domain impulse response through simple IDFT. Some of the popular curve fitting software and toolboxes are found in Excel, Matlab, Keysight (Agilent) ADS. Among them, Matlab may be the best choice because of its exceptional features and its strength in fitting data, curves and surfaces interactively. The following tables describe the library model types for curves and surfaces.

1. Distribution

   Distribution models such as Weibull.

$$y = abx^{b-1}e^{-ax^b} \tag{2.16}$$

   a is the scale and b is the shape.

2. Exponential

   Exponential function and sum of two exponential functions.

$$y = ae^{bx}, y = ae^{bx} + ce^{dx} \tag{2.17}$$

3. Fourier

   Up to eight terms of Fourier series.

$$y = a_0 + \sum_{i=1}^{n} a_i Cos(i\omega x) + b_i Sin(i\omega x) \tag{2.18}$$

   n: number of harmonics , $1 \leq n \leq 8$

4. Gaussian

   Sum of up to eight Gaussian models.

$$y = \sum_{i=1}^{n} a_i e^{-(\frac{x-b_i}{c_i})} \tag{2.19}$$

   where a is the amplitude, b is the centroid (location), c is related to the peak width, n is the number of peaks to be fit, and $1 \leq n \leq 8$.

5. Interpolant

   Interpolating models which includes linear, nearest neighbor, cubic spline, and shape-preserving cubic spline.

   In some cases, the concern is not about extracting or interpreting fitted parameters. Instead, it is desired simply to draw a smooth curve through the data. Fitting of this

type is called nonparametric fitting. The Curve Fitting Toolbox software supports these nonparametric fitting methods:

(a) Interpolant estimates values that lie between known data points. Smoothing Spline creates a smooth curve through the data. The level of smoothness can be adjusted by varying a parameter which changes the curve from a least-squares straight-line approximation to a cubic spline interpolant.

(b) Lowess Smoothing creates a smooth surface using locally weighted linear regression in order to make smooth the data.

6. Polynomial

Polynomial models, up to degree nine.

$$y = \sum_{i=1}^{n+1} p_i x^{n+1-i} \tag{2.20}$$

where n + 1 is the order of the polynomial, n is the degree of the polynomial, and $1 \leq n \leq 9$. The order gives the number of coefficients needs to be fit, and the degree gives the highest power of the predictor variable.

7. Power

Power function and sum of two power functions.

$$y = ax^b + c \tag{2.21}$$

Power series can model a variety types of data. For example, the rate at which reactants are consumed in a chemical reaction is generally proportional to the con-

centration of the reactant raised to some power.

8. Rational

   Rational equation models, up to the 5th degree/5th degree (i.e., up to degree 5 in both the numerator and the denominator).

$$y = \frac{\sum_{i=1}^{n+1} p_i x^{n+1-i}}{x^m + \sum_{i=1}^{m} q_i x^{m-1}} \tag{2.22}$$

   where n is the degree of the numerator polynomial and $0 \leq n \leq 5$, while m is the degree of the denominator polynomial and $1 \leq m \leq 5$. Note that the coefficient associated with x^m is always one; this makes the numerator and denominator unique when the polynomial degrees are the same.

9. Sine

   Sum of up to eight sine functions.

$$y = \sum_{i=1}^{n} a_i Sin(b_i x - c_i) \tag{2.23}$$

   where a is the amplitude, b is the frequency, and c is the phase constant for each sine wave term. n is the number of terms in the series and $1 \leq n \leq 8$. This equation is closely related to the Fourier series curve fitting described in the Fourier Series section. The main difference is that the sum of sines equation includes the phase constant and does not include a constant (intercept) term.

10. Spline

    Cubic spline and smoothing spline models. This is a nonparametric fitting as described in the interpolant model section.

Utilizing one of above mentioned models one can fill up the missing parts of S-parameters and calculate time-domain impulse response simply by applying iDFT to the S-parameter matrix, but the problem is that all of them fit a circuit-based model, a curve, a polynomial, or a rational function to the S-parameter data and they are not able to find a unique curve for frequency data. Moreover, for estimating a more precise curve the number of pole-zeros, order of polynomial, number of elements in the circuit model and so on should be increased which makes the numerical computations more complex and time consuming.

2.2.3 Reconstruction Using Wavelet Transform

In this section, we discuss three research works related to the current dissertation discussed in this research. The first paper [37] (which is a mechanical problem solution), addresses the computation of the impulse response using wavelet transformation for structural system identification. The second paper [3] analyses integrated circuit systems by wavelet-based scattering matrix. The difference between these works and this dissertation is that in the first work the wavelet method is used to extract the impulse response without using S-parameter data. Although the second paper analyzes parallel transmission lines using their S-parameter data with a wavelet transform, there are two main differences between the current research and this work. The proposed method of applying the wavelet transform is different from the previous work. Also, in [3], the S-parameter data are not

band limited. The main concern of this dissertation is the band limited S-parameter problem. The third paper provides the closest analysis to the subject of the current dissertation. [21] and generates an impulse response from S-parameters for a Power Delivery Network (PDN) by using a wavelet transform. This paper addresses the three main concerns of this dissertation which are impulse response, band limited S-parameter data and wavelet transform. In this paper the frequency to time transform issues such as causality and passivity are studied as well. The main difference between [21] and the dissertation is that in this paper the wavelet transform is performed using a signal processing technique called Compressed Sensing Method while in this dissertation a compensation-iteration wavelet method is used. The other difference between this dissertation and [21] is that they use discrete wavelet transform while the wavelet used in this research is the continuous wavelet transform via Fourier transform (CWTFT).

2.2.3.1 Computing Impulse Response Using Wavelet

The importance of this paper [37] is that it presents the significance of computing impulse response in mechanical engineering problems by using wavelet transform. In this work the extraction of impulse response data via wavelet transform for Structural System Identification is addressed. In structural system identification, a determined input function is entered into a system and the output is measured, and through this, the structural model (eigen vectors) and the model parameters (eigen values) are determined. In this method using the given u and y , the A, B, C and D can be obtained [33]:

$$\dot{x}(t) = Ax(t) + Bu(t) \qquad \dot{y}(t) = Cx(t) + Du(t) \tag{2.24}$$

In this work the mechanical values of mass, damping, stiffness matrices are desired. The process is shown in flow diagram of Figure 2.7. An example is provided for a system of four spring-mass-dampers which are illustrated in Figure 2.6.

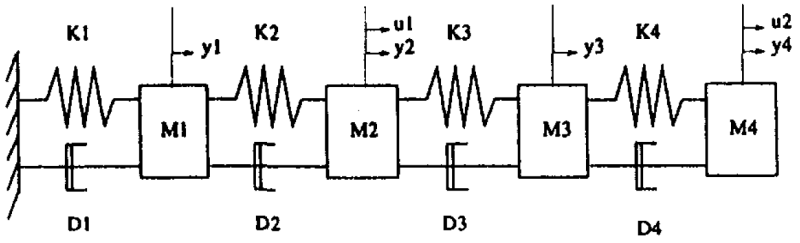

Figure 2.6

A system of four spring-mass-damper used as an example of calculating the mass, damping and stiffness.

The steps are as follows Step 1- exciting the input generation, placing the sensors and measuring the output signal using the Fast Fourier Transform. Step 2- the extraction of mathematical eigenvalues and eigenvectors. It begins with the extraction of the impulse response data (or Markov parameters) by applying an inverse FFT to the frequency response curves obtained during the first step. The extracted Markov parameters are then used to form the Hankel matrix from which one can obtain the eigenvalues and the associated eigenvectors via a singular value decomposition method. Step 3- is construction of physical modes, mode shapes and damping properties from the state space-based identified model and then constructing mass, damping and stiffness matrices.

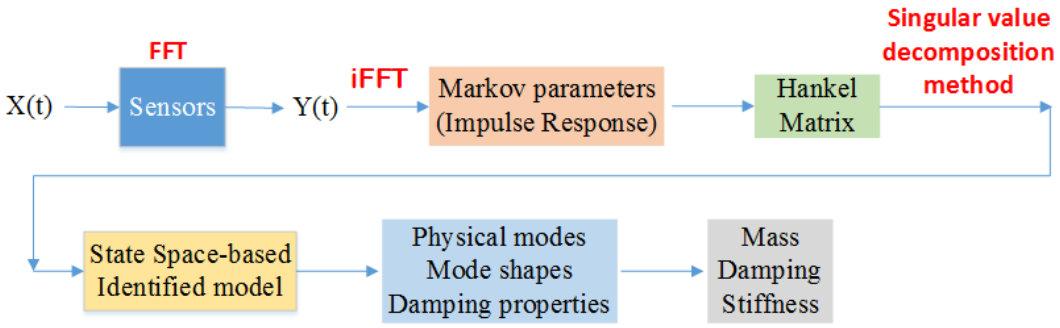

Figure 2.7

The flow diagram of computing the impulse response in the Structural System Identification.

According to [37], The FFT-based vibration signal analysis exhibits many shortcomings. The input signals must contain a frequency spectrum rich enough to be able to include the desired structural frequency components, in order that the characterization of the model come practical. For instance, when the input signal consists of a few harmonic excitations due to the inherent nature of the narrow-width frequency-domain amplitude, the resulting model is deficient. In some cases, when the input signal is pulse-shaped, this problem occurs again due to the Gibbs phenomenon. In health monitoring, several of these discontinuities happen from input signals in capturing sharp discontinuities emanating from cracks.

The main reasons for using wavelet transform instead of the Fourier transform in our research are as follows:

1. In a typical FFT-based signal processing of vibration data, the data is transformed from time to frequency-domain or in the reverse direction, while in a wavelet-based

signal processing the temporal nature of the data is preserved throughout the forward and inverse wavelet transforms.

2. The Gibbs phenomenon occurs whenever the signal shows discontinuity after applying FFT, while there is no loss of accuracy in the wavelet transform because different basis functions are orthogonal. The one that is chosen according to the nature of the signals under processing.

2.2.3.2 Wavelet-Based Scattering Matrix Analysis

The method used in [3] can be summarized in the following steps:

1. Calculating the Fourier transform of the desired $\psi(t)$ represented by $\Psi(\omega)$.
2. Multiplying the $\Psi(\omega)$ with the given S-parameter matrix, $S.\Psi(\omega)$.
3. Calculating the inverse Fourier transform of the product as $\mathbf{F}^{-1}\{S.\Psi(\omega)\}$.
4. Calculating the wavelet transform of the last step as $\Gamma = \mathbf{W}\{\mathbf{F}^{-1}\{S.\Psi(\omega)\}$
5. Computing the output by multiplying the calculated Γ matrix by input vector in the time-domain as $b(t) = \Gamma.a(t)$

The main relations used for this process are as follows. Consider the scattering matrix in the frequency-domain as a 2-port network as following:

$$\begin{bmatrix} B_1 \\ B_2 \end{bmatrix} = \begin{bmatrix} S_{11} & S_{12} \\ S_{21} & S_{22} \end{bmatrix} \times \begin{bmatrix} A_1 \\ A_2 \end{bmatrix}$$

So the equation for a N-port network in the frequency-domain is represented by:

$$B_i(j\omega) = \sum_{l=1}^{N} S_{il}(j\omega) A_l(j\omega) \tag{2.25}$$

The representation in the wavelet domain is:

$$\beta = \Gamma\alpha \tag{2.26}$$

The wavelet coefficients of the input signal (in the time-domain) with M number of scales are:

$$a_l(t) = \sum_{k=1}^{M} a_{l,k} w_k(t) \tag{2.27}$$

Taking Fourier transform of above equation yields:

$$A_l(j\omega) = \sum_{k=1}^{M} a_{l,k} W_k(j\omega) \tag{2.28}$$

By substituting (2.28) in (2.25), we find:

$$B_i(j\omega) = \sum_{l=1}^{N} \sum_{k=1}^{M} a_{l,k} S_{i,l}(j\omega) W_k(j\omega) \tag{2.29}$$

The inverse Fourier transform of 2.29 yields:

$$b_i(t) = \sum_{j=1}^{M} \sum_{l=1}^{N} \sum_{k=1}^{M} a_{l,k} \gamma_{i,l,k,j} w_j(t) \tag{2.30}$$

With some substitutions:

$$b_i(t) = \sum_{j=1}^{M} \sum_{l=1}^{N} \sum_{k=1}^{M} \gamma_{i,l,k,j} a_{l,k} w_j(t) \tag{2.31}$$

$$\beta_{i,j} = \sum_{l=1}^{N} \sum_{k=1}^{M} \gamma_{i,l,k,j} a_{l,k} \tag{2.32}$$

Where $\gamma_{i,l,k,j}$ are the elements of the matrix Γ in 2.26 i.e., $\mathbf{W}\{\mathbf{F}^{-1}\{S.\Psi(\omega)\}\}$.

Multiplying the matrix $\gamma_{i,l,k,j}$ by the wavelet transform of the input signal ($a_{l,k}$), produces the output signal $b(t)$.

One of the presented examples in this paper is shown in Figure 2.8. This example is a three-conductor line and uses the method discussed above. The results illustrate the robustness of the wavelet transform method and shows a better match with the time-domain signal as compared to the FFT method.

2.2.3.3 Impulse Response Generation from S-Parameters using Wavelet Transform

Reference [21] is the most similar work to the current dissertation. It computes the impulse response of the systems from their S-parameter data utilizing the wavelet transform. In this regard, the authors apply this method to two examples of two port transmission line and a "Power Distribution Network". The results show the superiority of the wavelet transform in predicting the impulse response of the systems compared to the Fourier transform even in the case of band limited S-parameters. The causality condition is stated by Kramers-Kronig equations 2.10 in the paper, and the passivity criteria results in $0 \leq \lambda_i \leq 1$, where λ_is are the eigenvalues of S^*S and S^* is the complex conjugate of S-parameter matrix. The passivity constraint in time-domain is also provided. The reason that the wavelet transform is used instead of the Fourier transform is as follows: The inverse Fourier transform based on band limited frequency data would be insufficient to recover precise impulse response in the time-domain. [21] takes advantage of the compressed sensing method for the reconstruction of the signal in the time-domain. This method is based

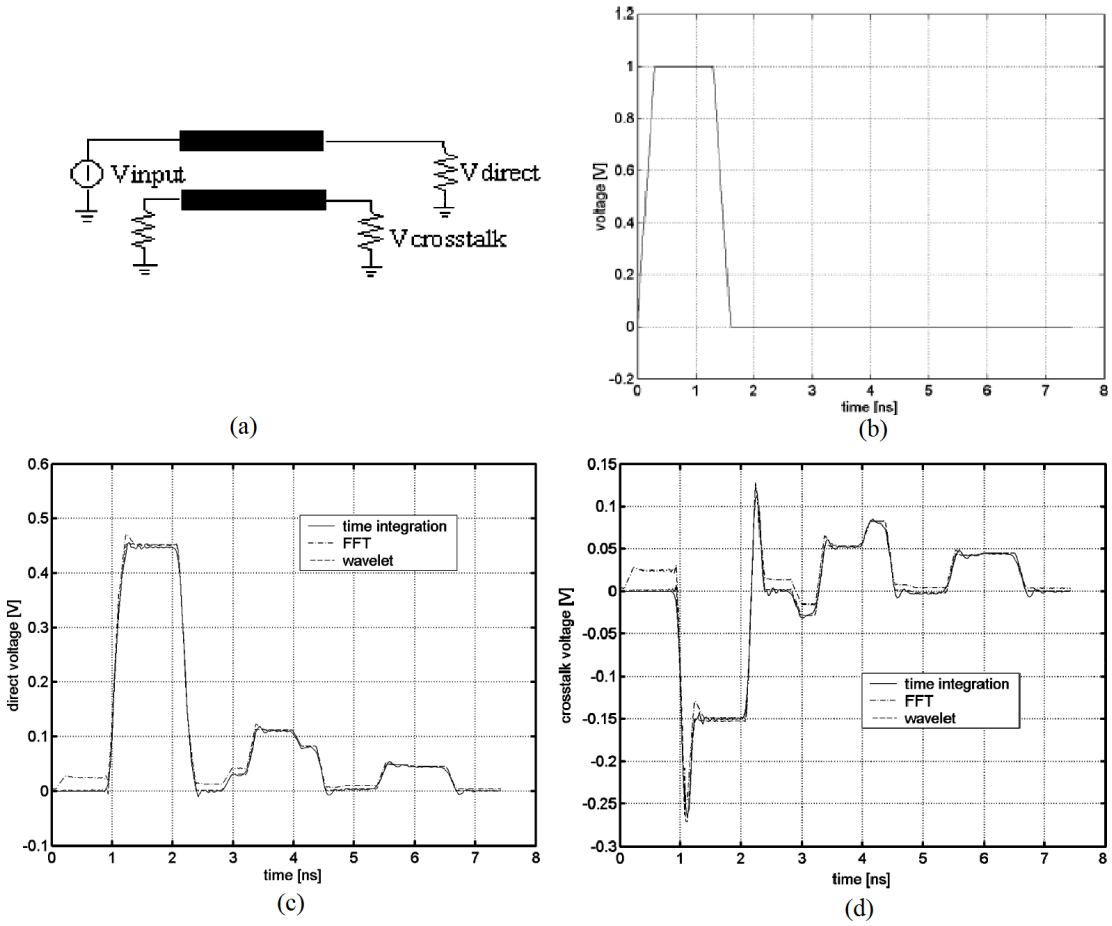

Figure 2.8

The example a) The three-conductor line b) The input voltage waveform c) Direct voltage for the low-loss line d) Crosstalk voltage for the low-loss line.

on the theory of Emmanuel Cands, Terence Tao, and David Donoho (2004) in which they proved through optimization that the sparsity of a signal can be used to recover it from far fewer samples than required by the Shannon-Nyquist sampling theorem. In other words, this method reconstructs a signal by finding solutions to underdetermined linear systems (a system of equations in which the number of unknowns are larger than the number of equations) provided that the signal is sparse and incoherent. The method can be summarized as follows. The known parameters are S-parameters and the related frequency vector, i.e.,:

$$S = \{S(\omega_1), ..., S(\omega_n)\} \qquad \omega = \{\omega_1, ..., \omega_n\}$$
$$\Psi(\omega) = \frac{1}{2a} e^{-\frac{(\sigma+\omega)^2}{2a^2}} (1 + e^{\frac{2\sigma\omega}{a^2}} - 2e^{\frac{\sigma(\sigma+2\omega)}{2a^2}} K) \tag{2.33}$$

$$\begin{pmatrix} \Psi_1(\omega_1)_R & ... & \Psi_m(\omega_1)_R \\ . & & \\ . & & \\ \Psi_1(\omega_n)_R & ... & \Psi_m(\omega_n)_R \\ ..... & & \\ \Psi_1(\omega_1)_I & ... & \Psi_m(\omega_1)_I \\ . & & \\ . & & \\ \Psi_1(\omega_n)_I & ... & \Psi_m(\omega_n)_I \end{pmatrix} \begin{pmatrix} c_1 \\ C_2 \\ . \\ . \\ . \\ C_m \end{pmatrix} = \begin{pmatrix} S(\omega_1)_R \\ . \\ S(\omega_n)_R \\ ------ \\ S(\omega_1)_I \\ . \\ S(\omega_n)_I \end{pmatrix}$$

Here $\Psi(\omega)$ is the Fourier transform of the Morlet wavelet function. σ, a and $K = \sigma^2/2$ are adjustable parameters. $\Psi(\omega)_R$ and $\Psi(\omega)_I$ are the real and imaginary part of the wavelet. The objective function is :

$$||\mathbf{Ac} - \mathbf{S}||_{L2}^2 : min \qquad subject \quad to \qquad ||\mathbf{c}||_{L1} \leq N$$

Where N is a threshold to control the sparsity of the solution **c**. They also have used the "Inverse Quadratic Polynomial" wavelet :

$$\psi(t) = \begin{cases} \frac{1}{B^2+t^2} & t \geq 0 \\ 0 & otherwise \end{cases} \tag{2.34}$$

Where B is a time derived from transmission line telegraphers equation. They use a computational algorithm called "LARS" (Least Angle Regression) to find **c** matrix, and then calculate the input function as:

$$h(t) = \sum_{i=1}^{m} c_i \psi(t)$$
$$\psi(t) = e^{-\frac{(at)^2}{2}}(cos(\sigma t) - K)$$

Then, they show that their results meet the causality, stability and passivity constraints. Some of the results are shown in Figs. Figure 2.9 Figure 2.10 [21].

It can be concluded from the shown results that the wavelet transform demonstrates better performance when compared to the Fourier transform.

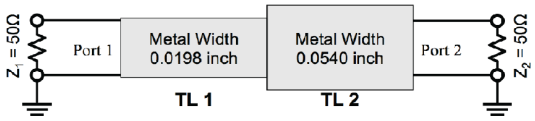

Two-port transmission line test case; two microstrip lines cascaded (TL = Transmission Line).

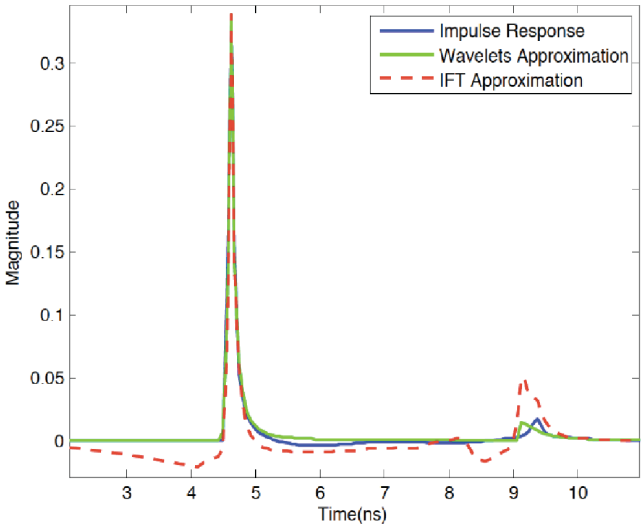

Result of the mismatched test case. We can observe the multi-reflection on the impulse response. Our recovery based on wavelets shows significantly better performance than the inverse Fourier transform method in respect of preserving the delay and passivity.

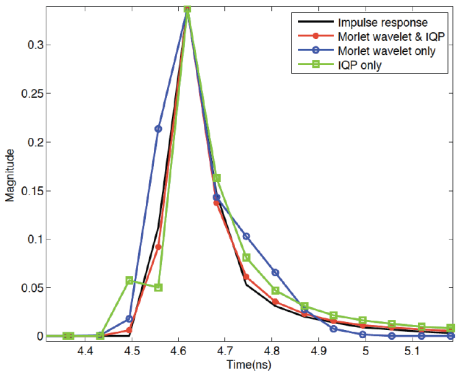

(a) Zoom-in of the first wave.

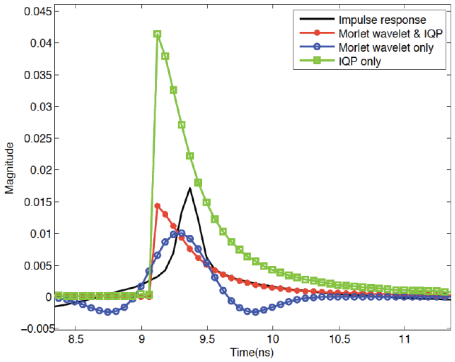

(b) Zoom-in of the second wave.

Figure 2.9

The test case of transmission line mismatch with the related results

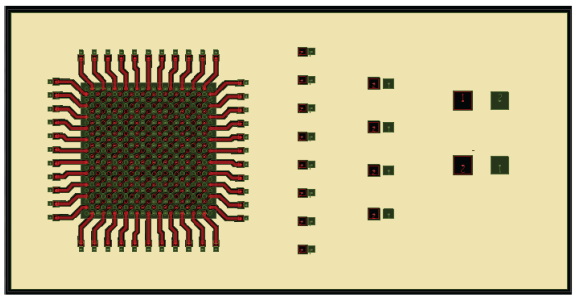

A simple power distribution network

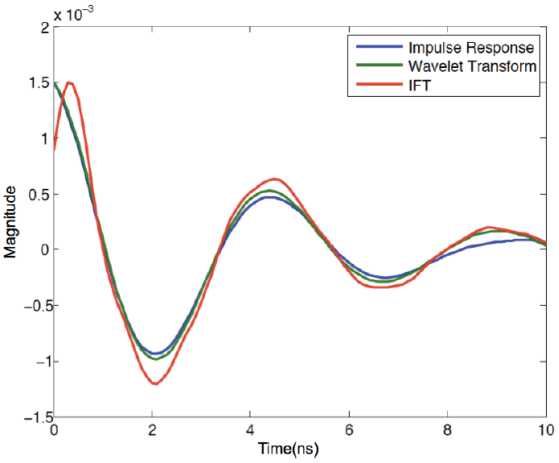

Impulse response of the PDN

Figure 2.10

The test case of the Power Distributer Network and the related results

2.2.4 Summary

Cizek in 1970 provided a robust method for calculating the Discrete Hilbert Transform (DHT) on the base of the Discrete Fourier Transform (DFT), and he defined the related expressions [7].

Narayana et al. in [30] and [29] used Hilbert transform for the interpolation and the extrapolation of frequency-domain responses. The causality of a system requires that the real and imaginary parts of its frequency-domain data be related with the Hilbert transform. They illustrated how the Hilbert transform relationship can be utilized to interpolate/extrapolate measured frequency-domain response of devices. Using the properties of sequences and their Fourier and Hilbert transform, any periodic, real, time-domain sequence of $h[n]$ can be expressed as a sum of an even and an odd sequence.

They used an iterative technique consisting of a sequence of transformations between the time and frequency-domains. They illustrated that the time-domain even sequence is produced by inverse Fourier transform of the real sequence of the frequency-domain data. Similarly, the odd sequence of the time-domain data is the result of the inverse Fourier transform of the imaginary sequence of the frequency-domain data. By using the iterative method via transferring between time and frequency-domain they completed the missed parts of the frequency-domain data. The limitation of this method is that it requires a minimum number of effective bits of data to successfully perform such data interpolation/extrapolation. Also, the regions of validity of this approach is not defined. The biggest drawback of this method is that it can be utilized just for recovering the measured frequency data degenerated or totally corrupted by noise. Therefore, all the recovered parts of data are in the middle band of the spectrum, and they have not provided a method for extrapolating the missing data from the DC side or from the higher side of the cut-off frequency.

In 1996, Narayana et al. introduced another method for interpolation/extrapolation of the frequency-domain responses and compared it with their previous method of the Hilbert transform [31]. Their new method was a direct method based on the principle of a model-based parameter estimation (analytic continuation). They consider the frequency data as a ratio of two polynomials $H(s)$. Based on the available nth derivative of $H(s)$, they try to calculate the coefficients of those polynomials. The limitation is the solution can be unique if the total number of samples are grater than or equal to the total number of unknown coefficients. This method calculates and completes the data corrupted by noise just in the middle of measured spectrum. Despite the strength of this method, it does not

provide a solution for extrapolating the lower and higher sides of the measured or simulated frequency data.

Collin and Rao in [39] study the considerations of the inverse Fourier transform in three aspects of causality, passivity and time-delay. They use the Hilbert transform to force the causality condition. The patent [35] that Rao received for this research , "Optimization of spectrum extrapolation for causal impulse response calculation using the Hilbert transform," proves that for passivity all the elements of S-parameter matrix should be divided by the largest eigenvalue in the frequencies, which the component value is larger than one. In this approach, the recovered samples are placed in the measured or simulated frequency range, not beyond it or on the DC side.

In the following section, the contribution of this dissertation is discussed.

2.3 Dissertation Question

The method that has been discussed so far, usually uses an initial guess and after a period of trial and error, estimates the approximate curve, which shows a good match with the real curve. The important point is that all of the aforementioned methods can calculate the missing data, which is usually corrupted by noise, in the whole spectrum of the measured or simulated data (interpolation). The concern of this dissertation is to provide an approach to calculate the missing DC component of a measured or simulated band-limited frequency data (extrapolation). In this research, Keysight simulation software, Advanced Design System (ADS), and Matlab is used. Finding the exact value of the DC point (and associated low-frequency data) is a challenging problem. In this regard, several different

methods are proposed. For instance, a section of ADS 2014 help, which pointed to this problem is shown in Figure 2.11

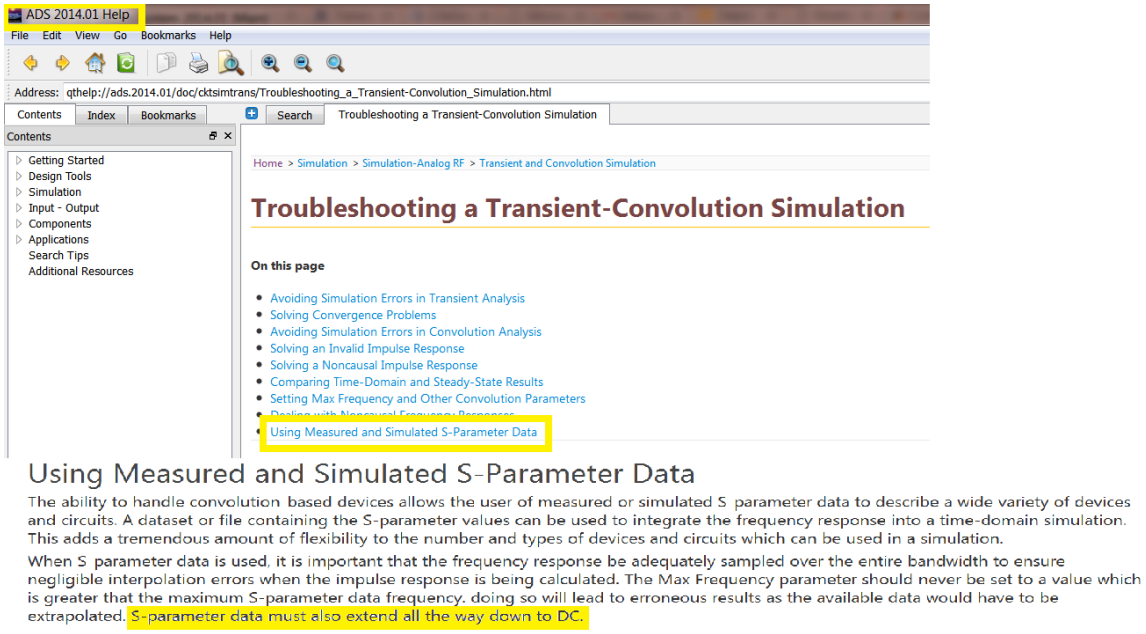

Figure 2.11

ADS help points to the importance of having DC point in the spectrum.

Other example on the required conditions for converting the S-parameters to the time-domain and the defects of using a band limited S-parameter data set is illustrated in the context of Figure 2.12. This document is a current document on the Tektronix website on the Serial Data Link Analysis (SDLA) application note (page 6) [1].

In the following, a report related to band limited S-parameter is shown from Gigatest Labs [32].

Converting S-parameters to the Time Domain

The time domain is another useful view for analyzing the S-parameter data for correctness or to troubleshoot problems that can occur. The IFFT can be used to make this conversion, however, several mathematical steps must be performed before the IFFT function can be applied.

The procedure for converting the S-parameter to the time domain is as follows:

1. Extrapolate the S-parameter from the start frequency point back to DC. Since S-parameters are commonly obtained from a VNA measurement, the data set will not contain DC unless it was measured independently and added to the file.
2. Extrapolate or truncate to set the stop frequency to the Nyquist point at ½ the sample rate.
3. Create the data set for frequencies from Nyquist to the sample rate by copying the complex conjugate of the data from the first point after DC to Nyquist in reverse order. The details are not given here, however, this step requires intricate knowledge of the FFT. The copy is slightly different for an even number of points compared to an odd number for the IFFT length. For example if the IFFT has an even length then Nyquist will fall exactly on one of the samples in the frequency domain. If the IFFT length is odd then Nyquist will be half way between two sample points in the frequency domain. Any time an FFT is computed the frequency domain has both the data of interest from DC to Nyquist and a complex conjugate image of the same data from Nyquist to the sample rate. The last point in the FFT is one sample short of the sample rate value because the FFT is a circular function and the sample rate and DC are at the same point.
4. **Compute the IFFT of the resulting S-parameter data.** If this step is performed correctly then the IFFT of the S-parameter data will result in time domain data that is real only, with the imaginary part equal to zero.

Figure 2.12

Tektronix Serial Data Link Analysis (SDLA) application note (page 6), which describes the necessity of extrapolating to DC frequency for a reliable time-domain response.

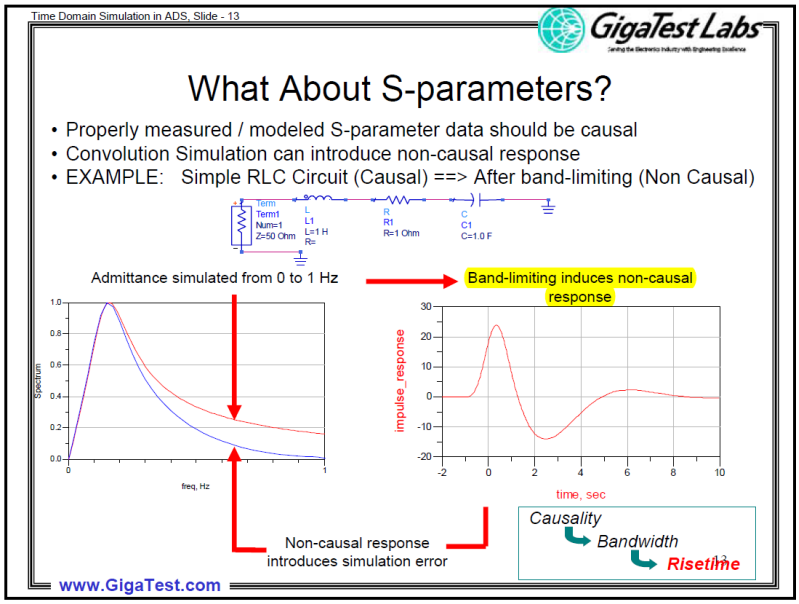

Figure 2.13

Gigatest Labs slide on bandlimited S-parameter 2008

In Figure 2.14, a few slides of "UBM Electronics" presented in the DesignCon 2012 (the premier conference for chip, board, and systems design engineers) are shown in which the DC point is noted as an important feature in transient simulations [27].

In the following, a report related to the band limited S-parameter is shown.

The main contribution of this dissertation is to provide a precise method of using wavelet transform for calculating the impulse response of systems using **band-limited** S-parameter data. In the following, a short summary is provided to list the reasons why the wavelet method is selected.

2.3.1 Why Continuous Wavelet Transform?

Continuous wavelet transform of a signal is calculated by the following relation:

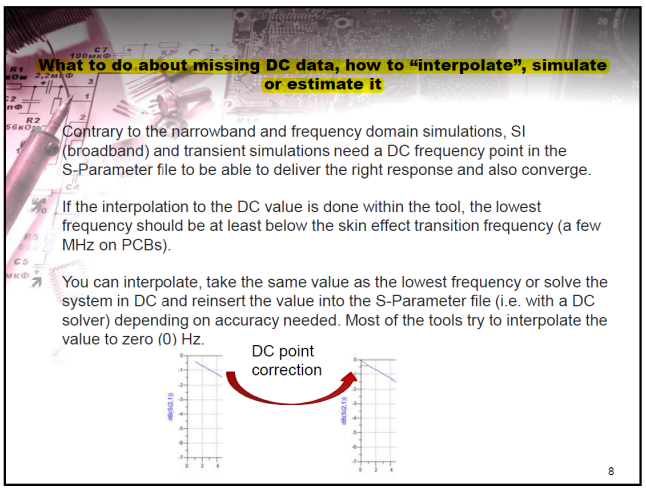

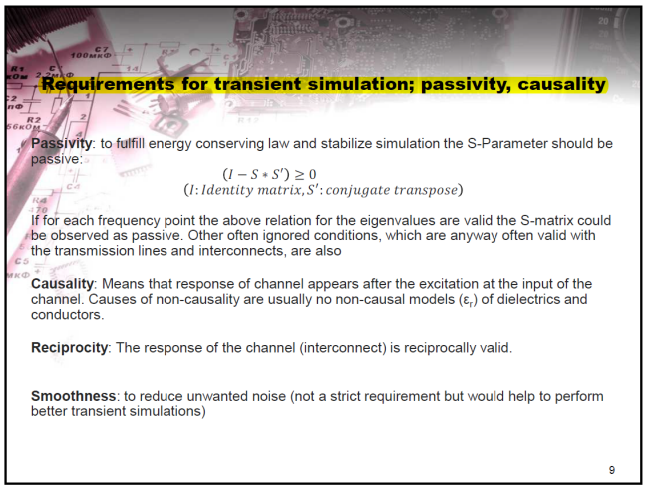

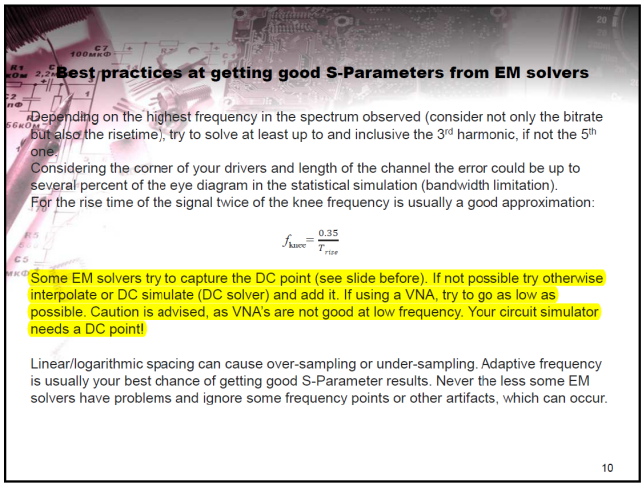

Figure 2.14

A few slides of "UBM Electronics" company presented in the DesignCon 2012.

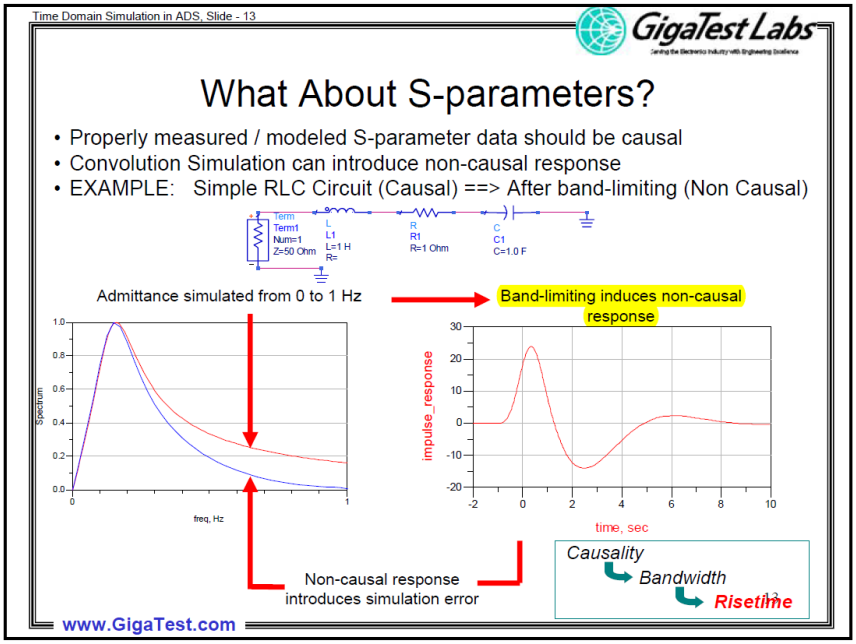

Figure 2.15

Non-causal impulse response resulted from a band-limited S-parameter

$$Wf(t) = \frac{1}{\sqrt{|a|}} \int_{-\infty}^{+\infty} f(t)\overline{\psi(\frac{t-b}{a})}dt \tag{2.35}$$

The methods of calculating the wavelet transform and its special considerations are not discussed in this section because it is covered completely in the next chapter. This section examines the significant properties of wavelet transform, which motivated us to apply this kind of transformation to the problem.

Wavelet Properties :

Wavelet transform involves several interesting properties that recommended them as the best choice of transformation for this problem.:

1. Linearity

$$W_\psi(\alpha f + \beta g) = \alpha W_\psi(f) + \beta W_\psi(g) \tag{2.36}$$

2. Translation

$$W_\psi(T_c f)(a,b) = W_\psi(f)(a, b-c) \tag{2.37}$$

$$T_c f(t) = f(t-c)$$

3. Dialation

$$W_\psi(D_\psi f)(a,b) = \frac{1}{\sqrt{c}} W_c(f)(\frac{a}{c}, \frac{a}{c}) \tag{2.38}$$

$$D_c f(t) = \frac{1}{c} f(\frac{t}{c})$$

Using the above properties and the important multi-resolution property of wavelet transform one can process and transform a signal to the time-domain more precisely. Most S-parameter curves look like the Figure 2.16:

As shown in the picture, at lower frequencies, the S-parameter (here S_{21}) is almost smooth. The oscillations start at higher frequencies due to noise effects in measurements or the simulation algorithm instabilities. Therefore, for analyzing the S-parameter data we need a non-uniform kind of sampling. One of the best choices would be the wavelet transform, which can transform the signal into multi-resolution format, making it possible to study the most important frequencies of the desired application with finer resolution and

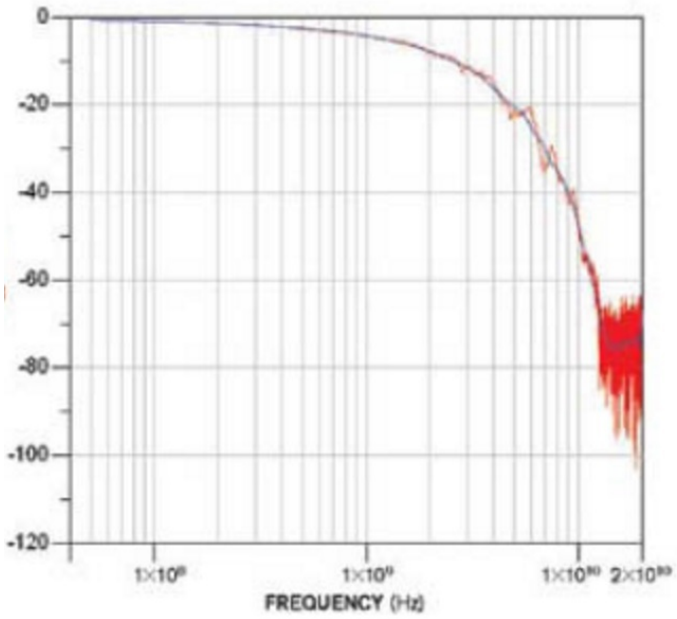

Figure 2.16

2-port network S-parameter

the other frequencies which are not of great interest with a coarser resolution. Figure 2.17 illustrates the schematic diagram for the proposed method.

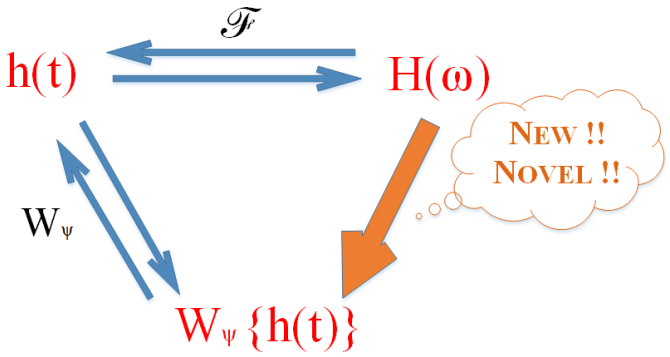

Figure 2.17

Diagram of the wavelet approach

CHAPTER 3

THEORETICAL ANALYSIS

In this chapter, the theoretical base of this work is discussed based on the wavelet transform. Wavelet-based signal processing has been known and utilized for decades. The difference is that the wavelet transform is generally applied to images in x-y plane and signals in the time-domain, but in this research it is applied to frequency-domain signals, which demands some particular considerations.

3.1 Applying Wavelet Transform to Frequency-domain

The main reason for applying wavelet transform to data in the frequency-domain is that it is assumed that only the frequency spectrum of the system model is available and reconstruction of a signal in the time-domain is required based on the frequency-domain data. As discussed before, if the signal were unlimited in bandwidth, then the inverse Fourier transform (iFFT) would be the best choice to reconstruct the signal in the time-domain. Due to limitations of frequency measurement equipment like network analyzers and frequency-domain simulation software, the signals are band-limited and applying iFFT does not lead to error free results. Therefore, it is required to develop a robust reliable method to perform this transform.

Generally, the wavelet transform is applied to the signals of real type or in the time-domain. These kinds of signals are real, and applying the wavelet transform is straightforward, but this is not the case when it is applied to a data in the frequency-domain. Frequency-domain signals are complex, and both real and imaginary values of the signal need to be extracted. Fortunately, causality condition requires the real and imaginary parts of the signal be related via Krammer-Kronig's relation (2.10). Therefore by applying the wavelet transform only on the real part of the band limited spectrum, the imaginary part can be calculated which provides the magnitude and phase of the missing parts of the bandlimited signal (here S-parameters).

There are some theoretical analysis steps for applying the wavelet transform to the frequency-domain. The schematic diagram for the proposed method is illustrated in Figure 3.1.

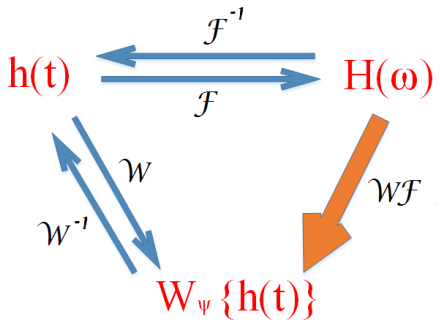

Figure 3.1

The schematic diagram of the method applied in this dissertation

3.2 Mathematical Analysis

In this section, the mathematical basis of the method is provided via the following steps:

1. **Continuous Wavelet Transform in Time-Domain**

   The wavelet transform of any function in time-domain is determined by (3.2) provided that (3.2) be satisfied, i.e., the energy of the signal in the time-domain is finite:

$$Wf(t) = W_\psi f = \int_{-\infty}^{+\infty} f(t)\overline{\psi_{a,b}}dt \tag{3.1}$$

$$\psi_{a,b} = \frac{1}{\sqrt{|a|}}\psi(\frac{t-b}{a})$$

$$\int_{-\infty}^{+\infty} f^2(t)dt < \infty \tag{3.2}$$

   The inverse wavelet transform is defined as:

$$f(t) = W^{-1}\{Wf(t)\} = \frac{1}{C_\psi}\int_{-\infty}^{+\infty}\int_{-\infty}^{+\infty} W_\psi(a,b)\frac{1}{\sqrt{a}}\psi(\frac{t-b}{a})\frac{dadb}{a^2} \tag{3.3}$$

$$C_\psi = \int_{-\infty}^{+\infty}\frac{|\Psi(\omega)|^2}{|\omega|}d\omega < \infty \tag{3.4}$$

   C_ψ is admissible constant and should satisfy $0 < C_\psi < \infty$, in other words it should be a function with compact support.

2. **Calculating the Fourier Transform of the Mother wavelet**

With wavelets, three operators affect the mother wavelet ψ : complex conjugate, time-shift and scaling. The Fourier properties are reviewed first. These properties are defined through the following equations:

(a) Complex Conjugate:

$$F\{f(t)\} = \int_{-\infty}^{+\infty} \overline{f(t)} e^{-i\omega t} dt = \overline{\int_{-\infty}^{+\infty} f(t) e^{i\omega t} dt} = F(-\omega) \tag{3.5}$$

(b) Time Shifting:

$$\mathcal{F}\{f(t-b)\} = e^{-ib\omega} F(\omega) \tag{3.6}$$

(c) Scaling:

$$\mathcal{F}\{f(at)\} = \frac{1}{|a|} F(\frac{\omega}{a}) \tag{3.7}$$

Now the Fourier transform of the mother wavelet can be calculated:

$$\mathcal{F}\{\psi(\frac{t}{a})\} = |a|\Psi(a\omega)$$

$$\mathcal{F}\{\frac{1}{\sqrt{|a|}}\psi(\frac{t-b}{a})\} = \frac{1}{\sqrt{|a|}}|a|\Psi(a\omega)e^{-ib\omega}$$

$$\mathcal{F}\{\frac{1}{\sqrt{|a|}}\psi(\frac{t-b}{a})\} = \sqrt{|a|}\Psi(a\omega)e^{-ib\omega} \tag{3.8}$$

3. **From Fourier Transform to Wavelet Transform**

Parsvale's identity states that the total energy of the signal in the time-domain is equal to the energy in the frequency-domain up to $\frac{1}{2\pi}$.

$$\int_{-\infty}^{+\infty} f_1(t)\overline{f_2(t)}dt = \frac{1}{2\pi}\int_{-\infty}^{+\infty} F_1(\omega)\overline{F_2(\omega)}d\omega \tag{3.9}$$

Using Parsval's identity it can be concluded 3.10:

$$W\{f(t)\} = (W_\psi f)(a,b) = \frac{1}{\sqrt{|a|}}\int_{-\infty}^{+\infty} f(t)\overline{\psi(\frac{t-b}{a})}dt =$$

$$\frac{1}{2\pi}\int_{-\infty}^{+\infty} F(\omega)\sqrt{|a|}\ \ \overline{e^{-ib\omega}}\ \ \overline{\Psi(a\omega)d\omega}$$

$$(W_\psi f)(a,b) = \frac{1}{2\pi}\int_{-\infty}^{+\infty} F(\omega)\sqrt{|a|}e^{+ib\omega}\overline{\Psi(a\omega)}d\omega \tag{3.10}$$

Now Figure 3.1 can be complete as illustrated in Figure 3.2 :

4. **Applying Inverse Wavelet Transform to Fourier Transform**

The expectation is that applying the inverse wavelet transform to the wavelet transform of the Fourier transform should result in the original signal in the time-domain. Some considerations are required to be performed for this purpose. It needs a few mathematical operations that is illustrated below. Calculation of the inverse wavelet transform is performed with the Matlab wavelet toolbox. Matlab applies this transform to the time-domain signal, and the wavelet transform is required to be applied to

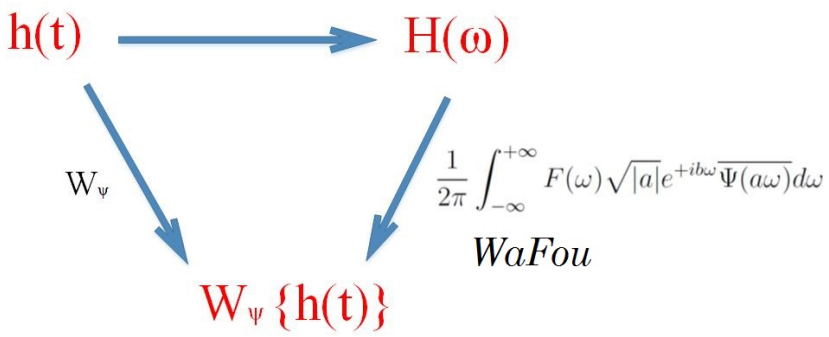

Figure 3.2

Diagram showing the transform from Fourier to Wavelet

the frequency-domain data; therefore, a relation between the normal inverse wavelet transform in the time-domain and the frequency-domain should be found. This new wavelet transform of frequency-domain data is named *WaFou*. By considering 3.10, the inverse wavelet transform can be written as below [20]:

$$f(t) = W^{-1}\{(W_\psi f)(a,b)\}(t) =$$
$$\frac{1}{2\pi C_\psi}\int_{-\infty}^{+\infty}\int_{-\infty}^{+\infty}(\int_{-\infty}^{+\infty} F(\omega)\sqrt{|a|}e^{+ib\omega}\overline{\Psi(a\omega)}d\omega)\sqrt{|a|}\{\frac{1}{\sqrt{|a|}\psi(\frac{t-b}{a})}\frac{dadb}{a^2}$$

Therefore:

$$W^{-1}\{(W_\psi f)(a,b)\}(t) =$$
$$\frac{1}{2\pi C_\psi}\int_{-\infty}^{+\infty}\frac{da}{a^2}\sqrt{|a|}\int_{-\infty}^{+\infty} F(\omega)\overline{\psi(a\omega)}(\int_{-\infty}^{+\infty} e^{+ib\omega}\frac{1}{\sqrt{|a|}}\psi(\frac{t-b}{a})db)d\omega$$

and

$$W^{-1}\{(W_\psi f)(a,b)\}(t) =$$
$$\frac{1}{2\pi C_\psi}\int_{-\infty}^{+\infty}\int_{-\infty}^{+\infty}\frac{1}{\sqrt{|a|}}\psi(\frac{t-b}{a})(\int_{-\infty}^{+\infty}F(\omega)e^{+ib\omega}\overline{\psi(a\omega)}d\omega)\frac{dadb}{a^2}$$

The last integral is equal to $(W_\psi f)(a,b)$, therefore :

$$(W_\psi f)(a,b) = \int_{-\infty}^{+\infty}F(\omega)e^{+ib\omega}\overline{\psi(a\omega)d\omega}$$

$$W^{-1}\{(W_\psi f)(a,b)\}(t) =$$
$$\frac{1}{2\pi C_\psi}\int_{-\infty}^{+\infty}\frac{da}{a^2}\sqrt{|a|}\int_{-\infty}^{+\infty}F(\omega)\overline{\psi(a\omega)}(\int_{-\infty}^{+\infty}e^{+ib\omega}\frac{1}{\sqrt{|a|}}\psi(\frac{t-b}{a})db)d\omega$$

After some simplification we get:

$$\int_{-\infty}^{+\infty}e^{+ib\omega}\frac{1}{\sqrt{|a|}}\psi(\frac{t-b}{a})db = \frac{1}{\sqrt{|a|}}\int_{-\infty}^{+\infty}e^{-ib(-\omega)}\psi(\frac{b-t}{-a})db$$

$$\sqrt{|a|}e^{it\omega}\Psi(a\omega) \quad , \qquad \mathcal{F}\{f(t)\} \ = \int_{-\infty}^{+\infty}f(t)e^{-i\omega t}dt = \int_{-\infty}^{+\infty}f(b)e^{-i\omega b}dt \tag{3.7}$$

$$W^{-1}\{(W_\psi f)(a,b)\}(t) =$$
$$\frac{1}{2\pi C_\psi}\int_{-\infty}^{+\infty}\frac{da}{a^2}\sqrt{|a|}(\int_{-\infty}^{+\infty}\overline{\psi(a\omega)}F(\omega)\sqrt{|a|}e^{+i\omega t}\psi(a\omega)d\omega)$$

Finally the relation for the inverse wavelet transform of the Fourier transform of the signal is achieved:

$$W^{-1}\{(W_\psi f)(a,b)\}(t) = \frac{1}{2\pi C_\psi}\int_{-\infty}^{+\infty} e^{+i\omega t}F(\omega)d\omega(\int_{-\infty}^{+\infty}\frac{da}{|a|}|\Psi(a\omega)|^2) \quad (3.6)$$

CHAPTER 4

METHODOLOGY

The main goal of this dissertation is to compute the time-domain impulse response of the ship hull and its related equipment and cables from its band limited scattering parameter model. To pursue this goal, a valid example is needed to make sure the code works properly. For this reason, first, the CWTFT and iCWTFT are applied to an exponential function which represents the general shape of S-parameters. Second, a linear combination of exponentials is considered, the algorithm is applied again, and the results are investigated. In the results chapter (chapter 6), it is shown that this algorithm satisfies the necessary requirements of the reconstruction process. In the next step, the algorithm is applied to the practical problem of the ship hull, and the impulse response is shown in the results (chapter 6) as well. In the following sections the CWTFT and iCWTFT algorithms along with the aforementioned steps are discussed comprehensively.

4.1 Continuous Wavelet Transform Using Fourier (CWTFT)

In the previous section the CWT and CWTFT formula were derived as:

$$W\{f(t)\} = (W_\psi f)(a,b) = \frac{1}{\sqrt{|a|}} \int_{-\infty}^{+\infty} f(t)\overline{\psi(\frac{t-b}{a})}dt =$$

$$(W_\psi f)(a,b) = \frac{1}{2\pi} \int_{-\infty}^{+\infty} F(\omega)\sqrt{|a|}e^{+ib\omega}\overline{\Psi(a\omega)}d\omega \tag{4.1}$$

A Matlab code written to run this algorithm is illustrated in Figure 4.2. According to this algorithm a time-domain input signal is given. This signal $e^{-|t|}$ is continuous, but in Matlab only sampled data from the signal are available. $e^{-|t|}$ is a time-domain continuous signal. As shown in Figure 4.1, the number of scales is determined such that the length of the scale vector be equal or larger than the time-domain signal length and totally cover it. It is assumed that the length of the signal is equal to N and the number of the scales is M. Now, a linear or logarithmic vector of scales can be defined as follows:

1. Linear:

   $s_0 = 2 * T_s \qquad ds = 0.1 \qquad scales = s_0 + (0 : NbSc - 1) * ds$

2. Logarithmic:

   $s_0 = 0.02 * T_s \qquad ds = 0.4875 \qquad scales = s_0 * 2^{(0:NbSc-1)*ds}$

T_s is the sampling time, ds is the wavelet width coefficient, and $NbSc$ is the number of scales. Then a frequency vector ω is defined with length N as shown in Figure 4.2.

In the next step, the Fast Fourier transform (FFT) of the signal is calculated with the same number of points. Then, the FFT of the mother wavelet, Ψ, is evaluated. Depending

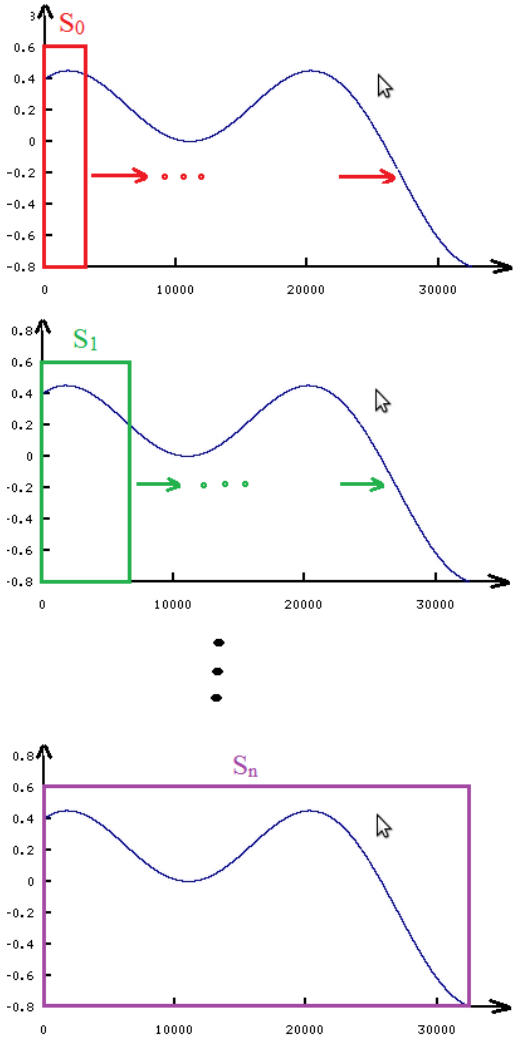

Figure 4.1

How to select the correct number of scales with regard to the linear of logarithmic scaling

on which wavelet function is selected, the FFT result would be different. Some types of mother wavelet functions that have exact analytical Fourier transform formula that are used in this dissertation, are listed below:

1. Derivative of Gaussian (DOG) $\hat{\Psi}(s\omega) = -\frac{1}{\sqrt{\Gamma(m+1/2)}}(js\omega)^m e^{-(s\omega)^2/2}$
2. Mexican Hat $\hat{\Psi}(s\omega) = -\frac{1}{\sqrt{\Gamma(5/2)}}(js\omega)^2 e^{-(s\omega)^2/2}$
3. Analytic Morlet $\hat{\Psi}(s\omega) = \pi^{-1/4} e^{-(s\omega-\omega_0)^2/2} U(s\omega)$
4. Non-Analytic Morlet $\hat{\Psi}(s\omega) = \pi^{-1/4} e^{-(s\omega-\omega_0)^2/2}$
5. Non-Analytic zero mean Morlet $\hat{\Psi}(s\omega) = \pi^{-1/4}\{e^{-(s\omega-\omega_0)^2/2} - e^{-\omega_0^2/2}\}$
6. Paul $\hat{\Psi}(s\omega) = 2^m\sqrt{m(2m-1)!}(s\omega)^m e^{-s\omega} U(s\omega)$

In Figure 4.2, the FFT of the DOG wavelet is considered. Then, regarding the formula provided in Eq. 3.10, the Fourier transform of the signal is multiplied by the Fourier transform of the wavelet. Afterwards, the inverse Fourier transform (iFFT) is applied to the calculated wavelet coefficients to create the wavelet transform of the signal.

4.2 Inverse Continuous Wavelet Transform Using Fourier (iCWTFT)

In the previous section, the wavelet transform of the signal is calculated through Fourier transform $W\{F(\omega)\} = W\{f(n)\}$. In this section, the inverse Wavelet transform is applied to the calculated wavelet coefficients using Eq. 3.3 and 3.4:

$$f(t) = W^{-1}\{Wf(t)\} = \frac{1}{C_\psi}\int_{-\infty}^{+\infty}\int_{-\infty}^{+\infty} W_\psi(a,b)\frac{1}{\sqrt{a}}\psi(\frac{t-b}{a})\frac{dadb}{a^2} \qquad (4.2)$$

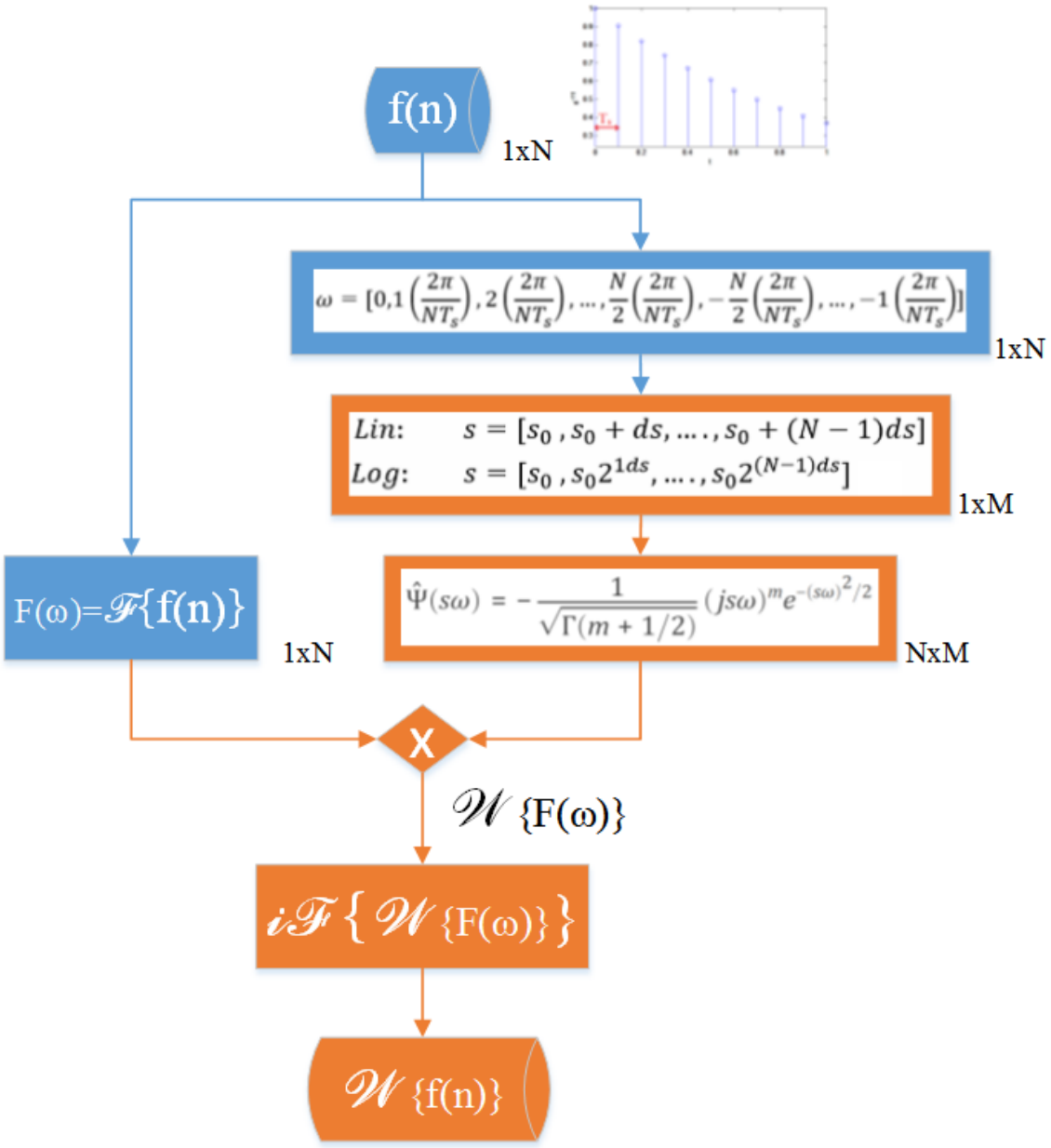

Figure 4.2

Algorithm of calculating CWTFT of signal $f(n)$ in Matlab

$$C_\psi = \int_{-\infty}^{+\infty} \frac{|\Psi(\omega)|^2}{|\omega|} d\omega < \infty \tag{4.3}$$

4.3 CWTFT on exponential function

In this part, an exponential function of $e^{-|t|}$ is considered. A Matlab GUI code is written for this computation, and different types of wavelet transform are applied to the signal. This GUI can change the frequency resolution of the spectrum or even the maximum frequency. Also, this GUI has the ability to force any number of elements on the DC side of the spectrum to zero. The reconstructed time-domain signal is observed in this situation. The applied enhancement to the signal is discussed in the next section.

Figure 4.3 and Figure 4.4 compare different parameters that affect the amount of similarity between the reconstructed signal and the original signal. In Figure 4.3, two signals are reconstructed using Paul and DOG wavelets. Although the reconstructed signal using Paul wavelet demonstrates more similarity to the original signal but still both of the reconstructed signals using, FFT and CWTFT, have a downward shift (decreased mean of the signal) due to the missing DC point . In Figure 4.4, the effect of the bandwidth limitation on the reconstructed signal is shown. As seen, when the bandwidth of the signal is more limited (left), the deviation from the original signal is more severe.

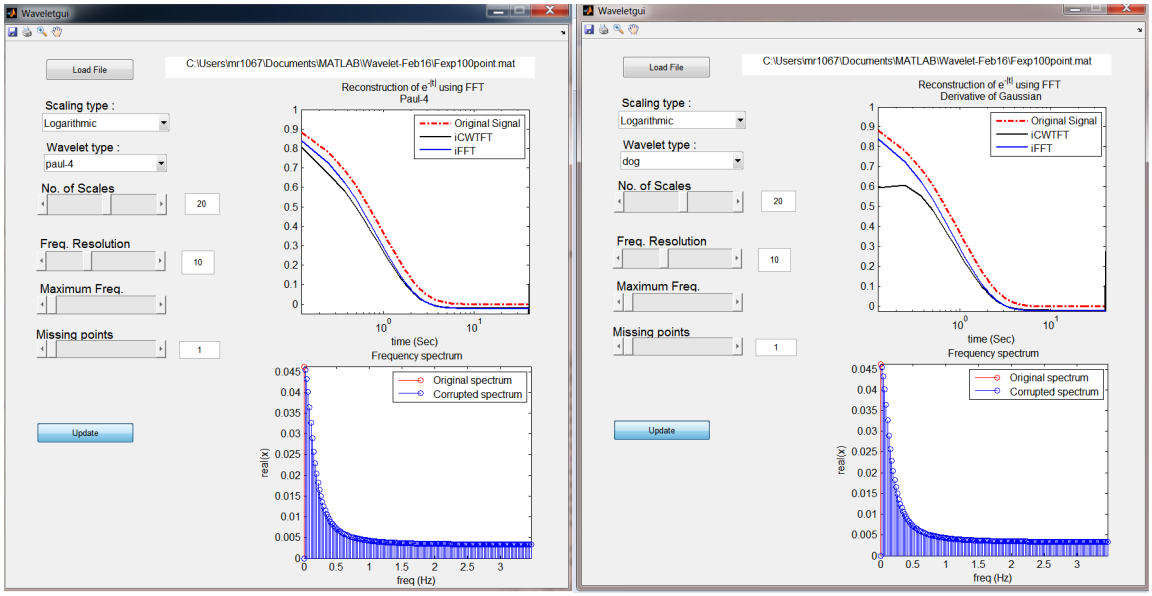

Figure 4.3

Illustration of different wavelet types with DC missing point **Left**: Paul **Right**: DOG wavelet

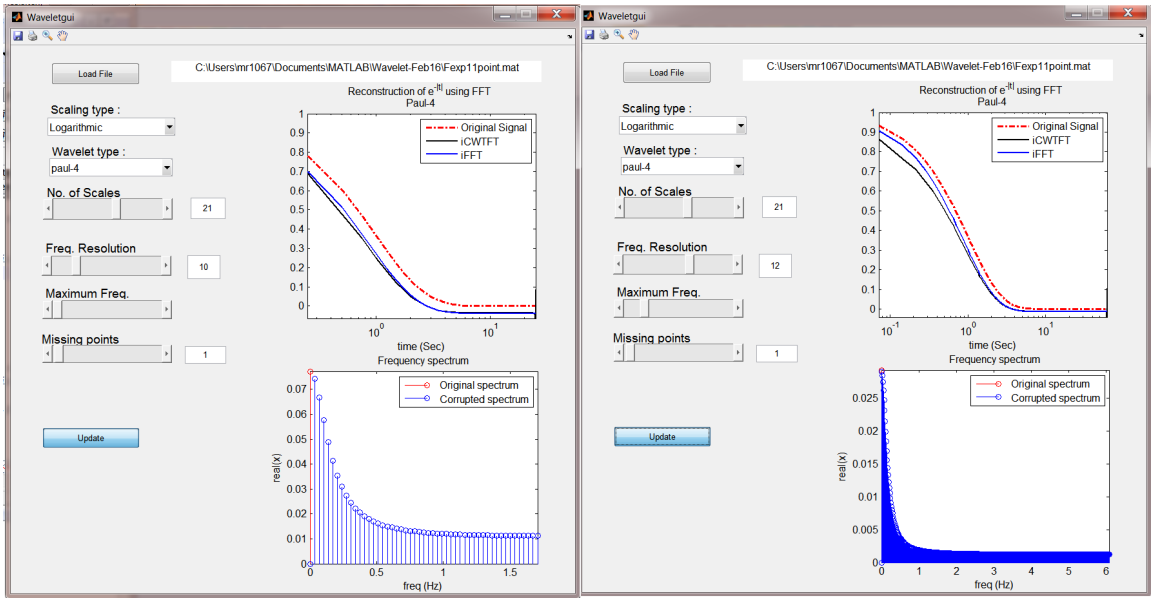

Figure 4.4

Illustration of the bandwidth limitation effect of the spectrum with DC missing point on the time-domain reconstructed signal

4.4 CWTFT on Linear Combination of Exponentials along with Spectrum Enhancement

After the experiments performed for a simple exponential function, one can execute the same process for a linear combination of exponentials e.g. binomial because several S-parameter functions can be expressed as $ae^{-|ut|} + be^{-|vt|} + ce^{-|wt|} + ...$

As illustrated in Figure 4.5, a two-term exponential $7e^{-|5t|} + 8e^{-|2t|}$ is reconstructed, but in this experiment the spectrum of the signal is improved every time that CWTFT is applied. The enhancement steps are as follows:

1. The f(n) signal is inserted to the system as an input.

2. FFT is applied to this input signal.

3. The DC element (zero frequency) is forced to zero.

4. The wavelet transform and then the iCWTFT of the signal are calculated. Therefore, the signal is reconstructed in the time-domain, and because of the missing DC frequency component, it is different from the original signal.

5. Again, the FFT is applied to the reconstructed signal.

6. This time the spectrum is different from the original spectrum in the previous stage. The spectrum is modified as follows:

   (a) In general algorithm, the number of the missing points of the DC-side of the spectrum to the first available point in the given spectrum is called k (In the illustrated example $k = 1$ because it is assumed that the only missing point is the

DC frequency). The difference between the value of the frequency element of $k+1$ with the same element in the previous spectrum is multiplied by a scaling factor, and this value is used as the first iteration value of the DC component. The scaling factor is obtained with trial and error and works for the exponential binomial with coefficients from 0.001 to 1000 and even beyond it as shown in Figure 4.5. In Figure 4.6, the range of variations of power in an exponential binomial is shown.

(b) The other components of the spectrum, $k+1$ to the end, are forced to their previous values in the previous spectrum.

The process is iterated by the length of the scales vector and reconstructs the signal in the time-domain.

7. This process is repeated until the last scale is applied. The length of the scales vector is chosen such that the scales cover the entire time-domain signal length. Therefore, as shown in the Figure 4.7, the value of the DC component converges. The convergence occurs because the multiplied scaling factor, has an inverse relation with the scales magnitude, so increasing the scale size adds smaller amounts to the DC component. In addition, the length of the scale vector, i.e. the number of the iterations is proportional to the length of the signal in the time-domain.

4.5 CWTFT of Bandlimited S-parameters along with Spectrum Enhancement

In both of the previous sections, the processes were started from the time-domain signals, but in this section, the practical problem of this dissertation is considered. In this

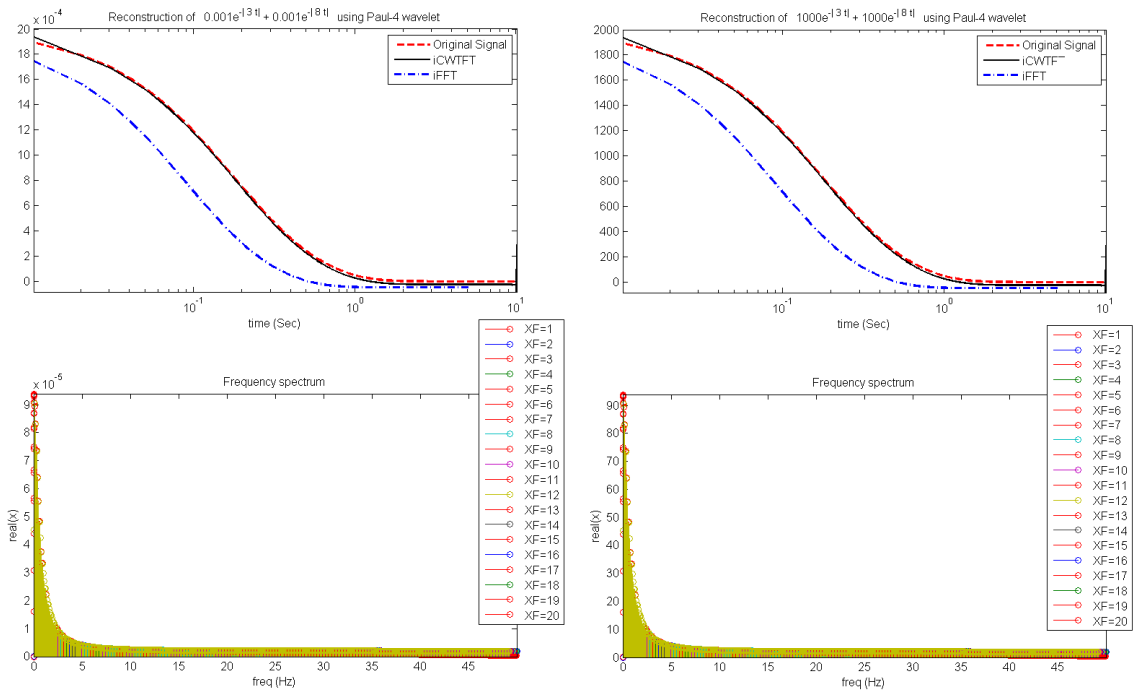

Figure 4.5

Reconstruction of the exponential binomial with different coefficients from 0.001 to 1000.

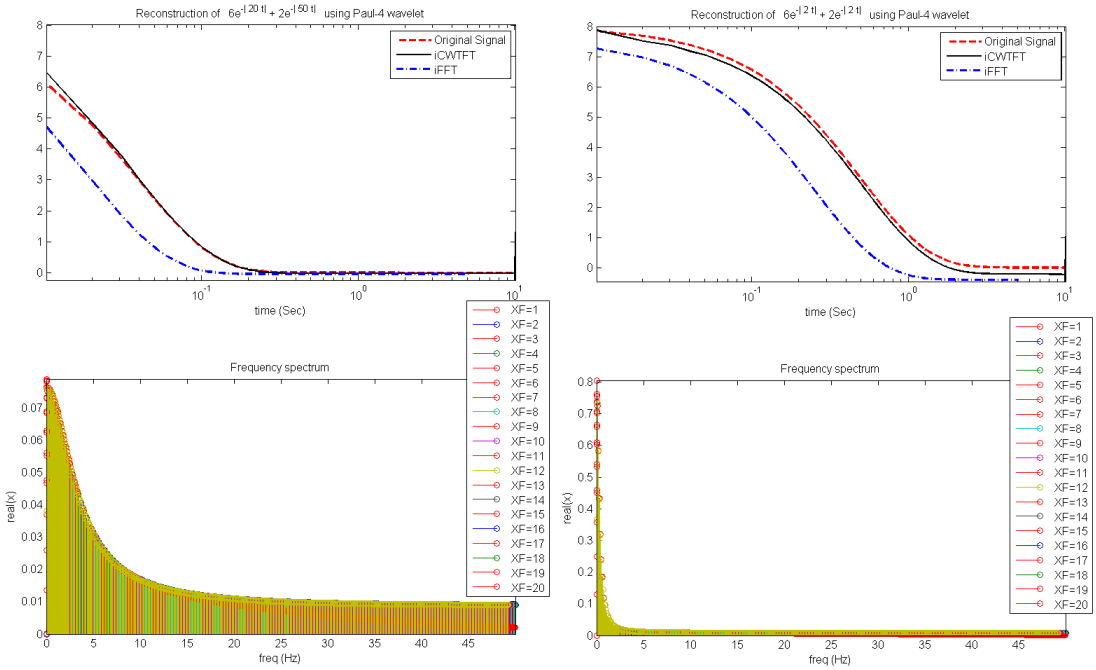

Figure 4.6

Reconstruction of the exponential binomial with different powers from 2 to 50.

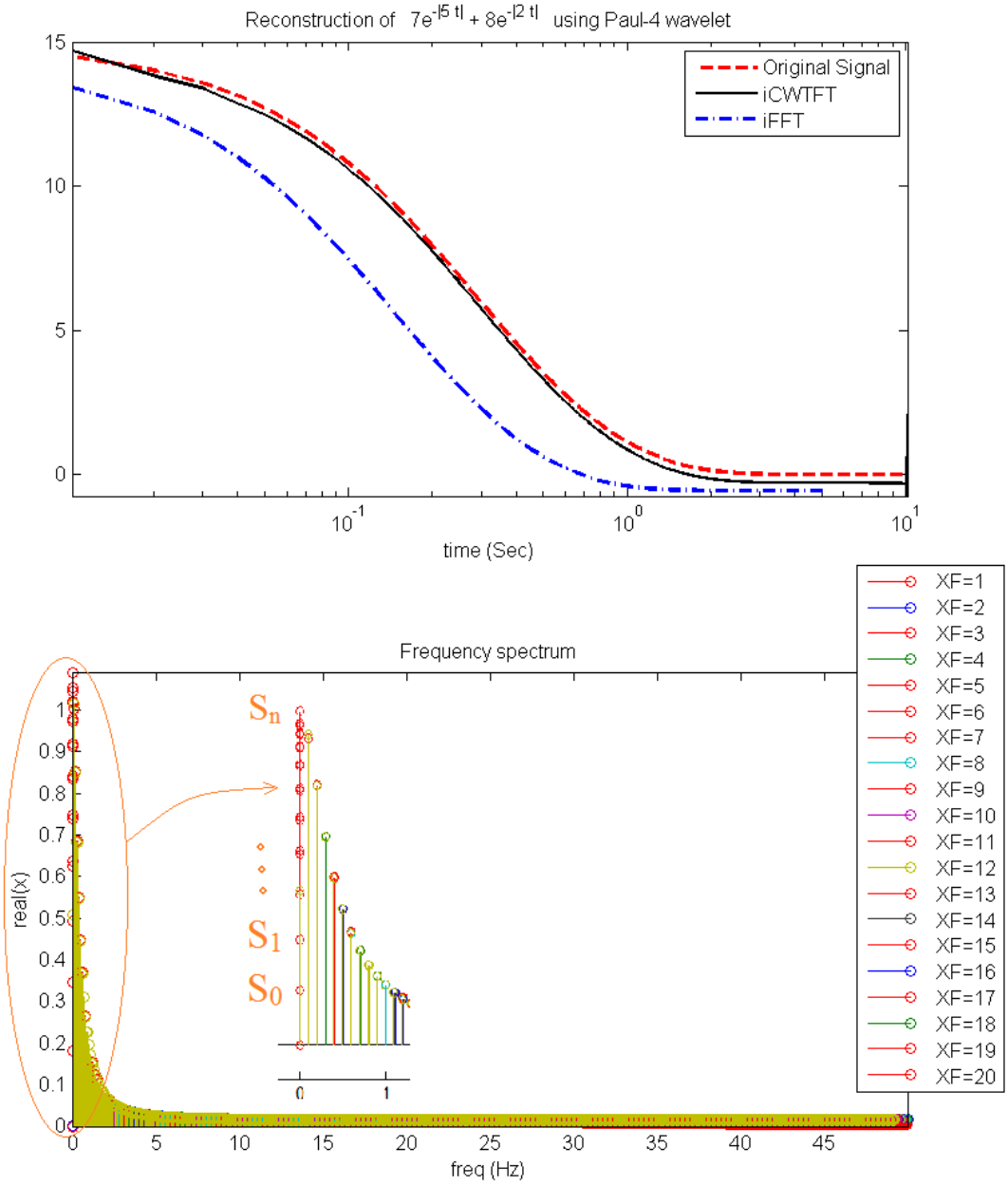

Figure 4.7

Up: the time-domain original and iCWTFT, iFFT reconstructed signals. **Down**: the frequency spectrum and the recovered DC element of it.

problem, no information on the time-domain signal is available, and the only accessible data is the frequency data or the spectrum of the signal. Therefore, the starting point of the process should be shifted from the time-domain to the frequency-domain. As it is illustrated in Figure 4.2, the flow diagram shows the general process of the signal reconstruction in the time-domain. In this problem, the process is started from the frequency-domain, and only the orange blocks are included in the process. The blue blocks are excluded because the FFT of the signal and the ω vector already exist in the given spectrum. In addition, this frequency data (S-parameters) is band limited and is always missing the DC component. The method used in this dissertation to complete the missing DC frequency element and computing the system impulse response is sketched in the Flow diagram of Figure 4.8 and Figure 4.2.

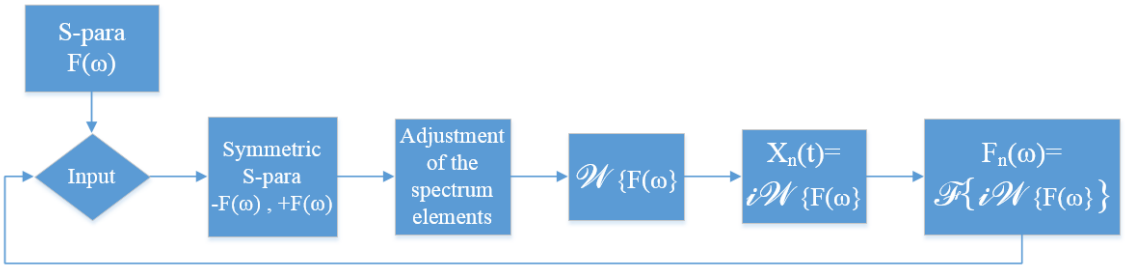

Figure 4.8

Flow diagram of the signal processing

The process is almost similar to the steps mentioned in 4.4. It can be summarized as follows:

1. The real part of the given S-parameter data is extended with even symmetry, and the imaginary part is extended with an odd symmetry to obtain the reconstructed signal in the time-domain as a real signal.

2. The continuous wavelet transform is applied to the spectrum.

3. The inverse continuous transform is applied to the wavelet coefficients calculated in the previous section, and the time-domain signal is computed which is the 1^{st} because the DC element is missing in the spectrum.

4. In the next iteration, the spectrum of the reconstructed signal is calculated one more time. The difference between the $k+1$ element in the current and the previous spectrum is multiplied by a scaling factor. k is the number of the missing points that is equal to one for this example.

5. The CWTFT and iCWTFT are applied to the signal, to reconstruct the signal in the time-domain.

6. The above process is iterated M times. M is the length of the scales vector.

The result of reconstruction of the signal (or the Impulse response) is demonstrated in Figure 6.22. As noted in the theoretical analysis, the S-parameter matrix elements are the impulse response of the related ports in the frequency-domain. Therefore, the reconstruction of the signal in the time-domain provides the time-domain impulse response.

CHAPTER 5

COMPLETED PROJECTS

5.1 Modeling of Common Mode Currents on the Ship Hull Using Scattering Parameters

Physics-based modeling is used to form a multiport S-parameter behavioral model of the ship's structure [34]. It models distributed currents and potentials throughout the open-form conductor of the ship hull. As the ship uses ungrounded power systems, it encounters common-mode current flow. Parasitic paths from the energized portion of the power system can conduct common-mode current throughout the ship hull and bulkheads, and any conductive structures bonded to the ship such as equipment chassis and protective armoring around power cables. The analysis starts with partitioning the structure into finite elements. A two-part work-flow converts physics-based models of elementary pieces of the ship into a complete multi-port S-parameter behavioral model of an arbitrarily large portion of the ship's structure. This multi-port model can be connected to other models of components, such as power cables and fixed loads and sources, that allow a standard circuit-based solver to find solutions for voltages and currents as functions of time or frequency at any of the ports. The modeling method provides rapid system-level design including the placement of sources, loads, filters and interconnecting power cables in order to predict and therefore

mitigate the effects of common-mode current in ship systems without using an overly optimistic treatment of the hull as a perfectly conducting ground plane.

5.1.1 Behaviorial Modeling of Common-Mode Current

1. Multi-Port Linear Modeling

   Common-mode currents in the electric ship arise primarily from converters in both the distribution system and in the loads. As a general rule, the bandwidth is rather broad as a result of fast switching in converters. The projected use of wide bandgap (WBG) devices in advanced power converters makes it likely that designers will need modeling and simulation tools appropriate for the near RF bandwidth of such fast switches. Common-mode current can couple to the ships structure through unavoidable parasitic paths, such as between semiconductor switches and heat sinks.

2. S-parameter Modeling

   Two advantages of using S-parameters in this case are that they are suitable for computing broadband voltages and currents at arbitrary numbers of ports on the ships structure where equipment and cables are bonded to the structure. Also, the S-parameter model is linear and so is, for the most part, the system being modeled. Furthermore, S-parameter models can be used in either the frequency or the time-domain for the assessment of the potential for electromagnetic interference and other dynamic properties and for rerouting connections or for compensation with passive components.

5.1.2 Modeling Approach

The example, as shown in Figure 5.1 , consists of a hull plate in contact with seawater supporting an isolated DC power system consisting of two power cables connecting a medium voltage source to a load. The source is connected between the energized conductors of the two cables, as is the load on the other side of the compartment. The hull plate is 3 m $\times$ 3 m square. The cable has an armored sheath that is grounded for safety by risers that bond the sheath to the hull plate at eight locations on the plate. There is no galvanic connection between the center energized conductors and the armored sheath. Common-mode currents are induced by a step change in the source voltage of 5 kV. The modeling approach involves a three part work flow. The process begins by defining a library of elementary structural pieces. The finite element analysis is used to extract S-parameters for each elementary piece and the larger structure is reconstructed with the elementary pieces and a second S-parameter model is extracted with ports corresponding to the bonding points of equipment to the hull and/or bulkheads of the ship. This final S-parameter model allows evaluation of common-mode currents flowing into or out of ports.

1. Physics-Based Models of the Sub-elements

   Physics-based modeling, shown in Figure 5.2, was used to extract four unique S-parameter models of sub-elements. The only difference between these sub-elements is the number of edges with ports defined about the perimeter. EMPro by Agilent is the software tool in which CAD models of the sub-elements are drawn. An example of a corner sub-element is shown in Fig. 3(a). EMPro automatically meshes these

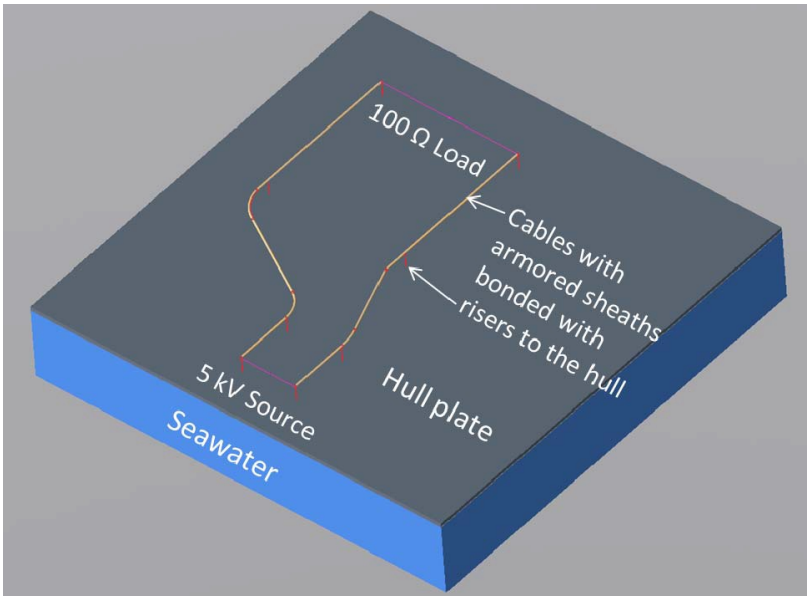

Figure 5.1

Hull and power system layout for the common-mode current modeling

physical models and solves the S-parameter extraction problem using the method of finite elements. This model is computed over a bandwidth of 100 MHz.

2. Constructing the Behavioral Model

   Figure 5.2-b illustrates the arrangement using the four unique sub-element S-parameter models. (wire bonds not shown in Figure 5.2-b). Three ports are used in this example, but this number can be scaled up or down to manage the error between the behavioral model and the physical reality. Once the sub-elements are wired together to approximate the complete hull section, then a second S-parameter extraction calculation is done. However, this time the extraction is not by finite-element analysis, but by linear multiport network analysis using only the ports that will remain in the

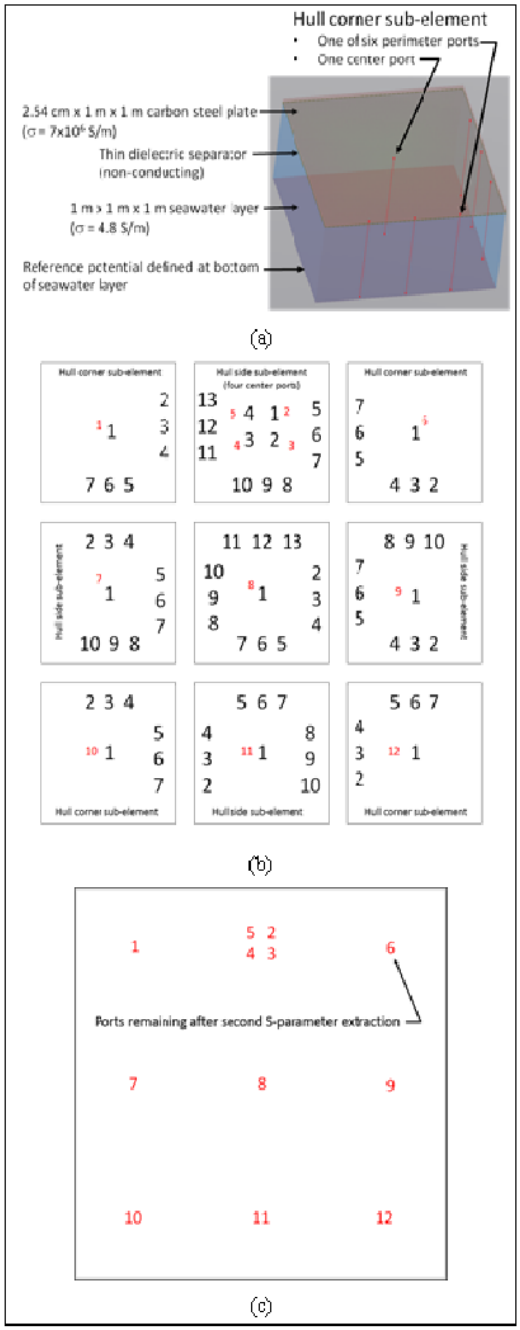

Figure 5.2

Work Flow of Behavioral Modeling

complete behavioral model. These ports are smaller in number than the number of perimeter ports and are numbered in red font in Figure 5.2-b. This step is performed in the ADS software tool by Agilent. The result is a single 12-port linear model of the entire hull plate as shown in Figure 5.2-c. The extraction process is very fast because it is behavioral instead of physical. After that, the 12-port behavioral model can be connected to cable and equipment S-parameter models, and the resulting speed of calculation for the voltages and currents at each port depends only upon the much smaller number of remaining ports.

5.1.3 Modeling Results

In this section, a comparison is made between a time-domain simulation of the example problem computed with the behavioral model in ADS and one done with a finite-element simulation of the same system in EMPro.

1. Constructing the Complete Behavioral Simulation

   The complete behavioral model for the example calculation is shown in Figure 5.3. At the center of the diagram is the 12-port S-parameter model of the hull-seawater section (12p block). An S-parameter model available in ADS was used to introduce cables to the behavioral simulation. The ports of the model that access the outer shield on either end off the cable (representing the armored sheath of a real marine cable) are connected to the hull ports in the same locations as shown in Figure 5.1. Therefore, the configuration is electrically the same as drawn in this figure. The displacement currents in the water were computed in EMPro and found to be typically

10000 times smaller than the currents in the hull plate. Therefore, at the depth of the simulated water column the surface is essentially an equipotential. The important consequence of this is that the voltages computed at each port during the time-domain simulation are relative to the same reference potential in both the behavioral and the physical models, and thus the computed potential difference between ports approximates those that would be observed on the ship.

2. Comparison of Computed Results

   Figure 5.4 shows the computed port transient currents at ports 2, 3, 9, and 12 using the behavioral model. Figure 5.5 shows the surface currents computed by finite element analysis for the complete system shown in Figure 5.2 using EMPro at one instant in time $= 100\mu s$.

5.2 Behavioral Modeling for Stability in Multi-Chip Power Modules Using Scattering Parameters

5.2.1 Introduction

Packaging plays a major role in determining performance for the wide band-gap (WBG) systems. WBG devices are sufficiently fast to excite resonances in small parasitic elements. This challenge becomes even harder once it comes to the designing of multi-chip modules (MCM) for wide band-gap (WBG) semiconductors and managing the parasitic impedances associated with intra-module interconnections and construction details. In other words, for designing WBG modules, one may encounter the same challenge but more complex in

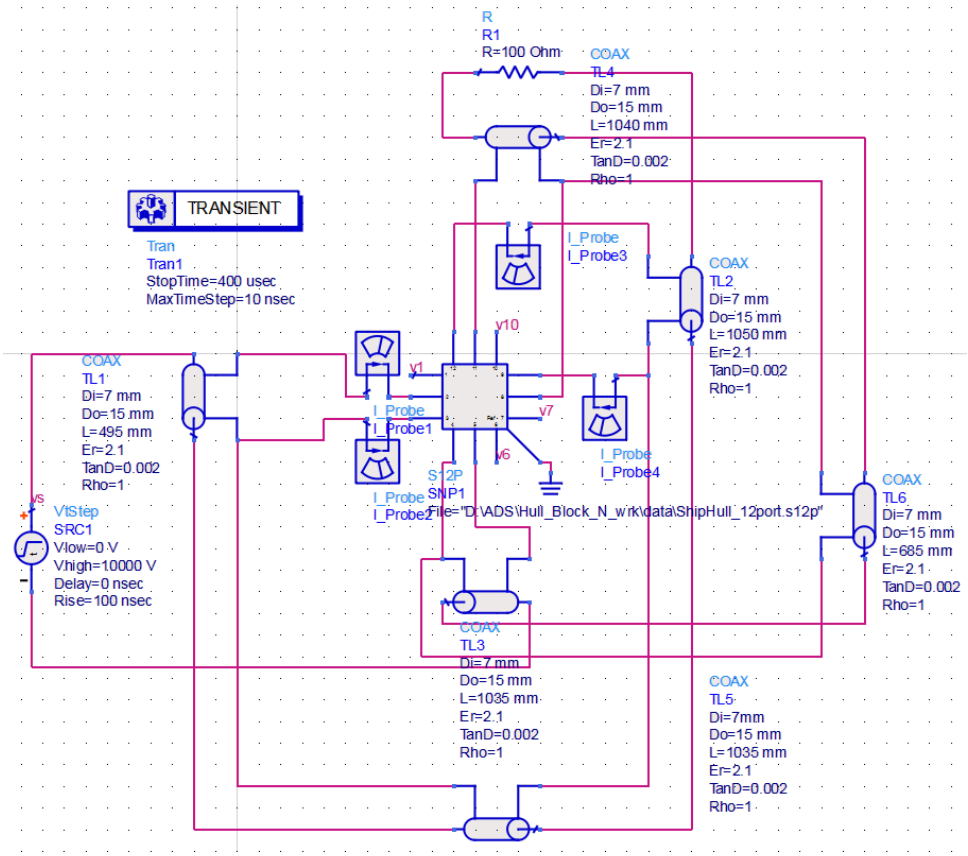

Figure 5.3

Transient simulation using the behavioral model in ADS

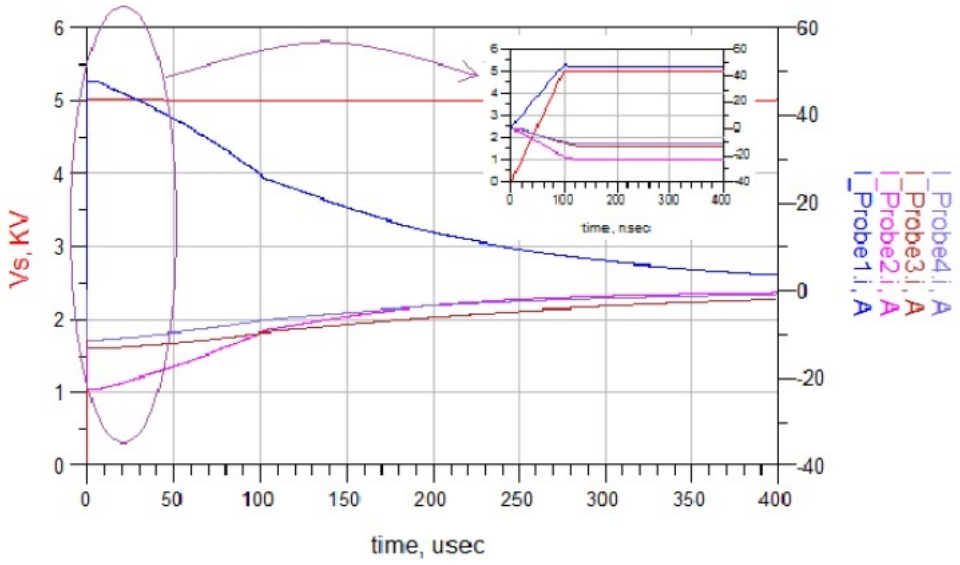

Figure 5.4

Source voltage and port currents computed using the behavioral model in ADS

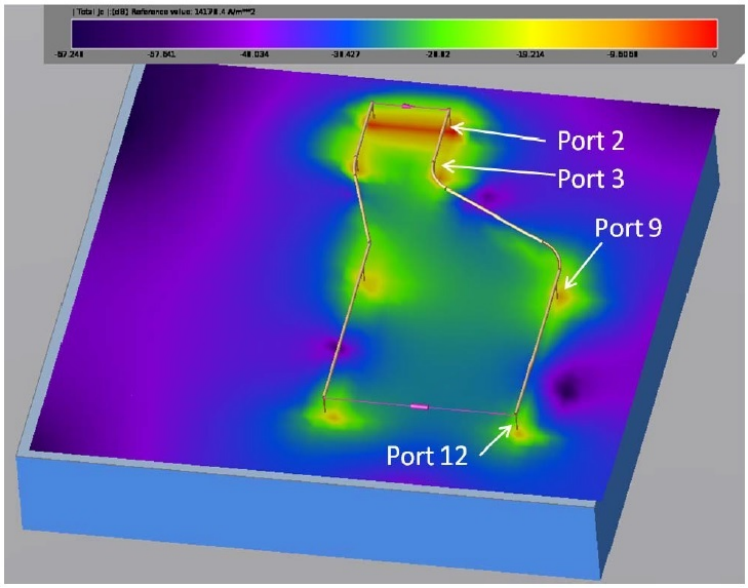

Figure 5.5

Magnitude of the surface currents at $t = 100\mu$ s computed by EMPRO

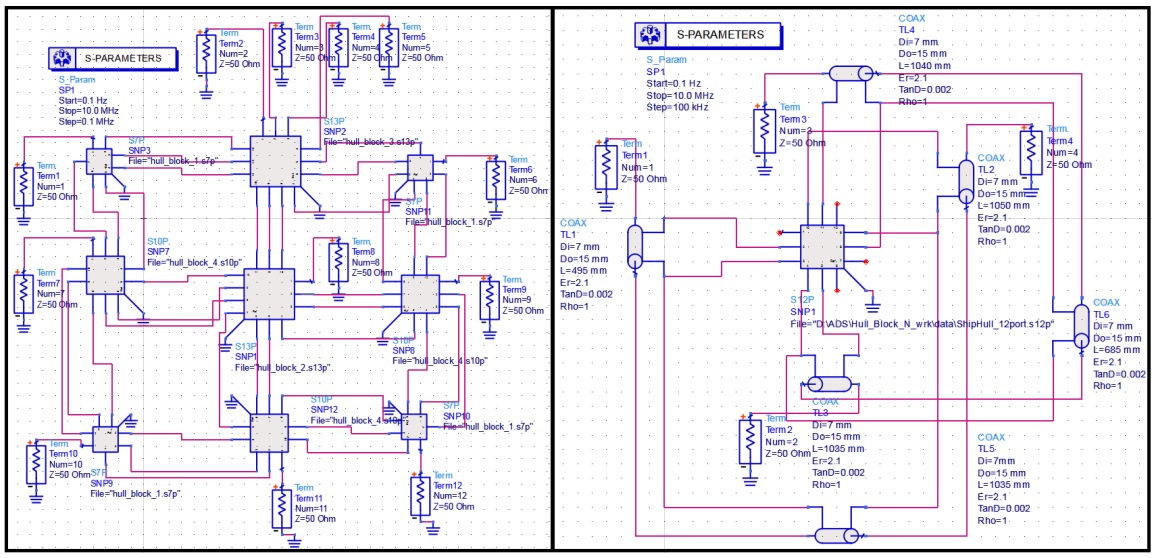

Figure 5.6

Left: Combination of 9-Block S-parameters and calculation of 12-port S-parameter block. **Right**: Calculation of 4-port S-parameter by adding two cables.

regarded to discrete packaging. In WBG modules, the die to die interconnects as well as mutual coupling between bond-wires should be considered.

For instance, the individual die are connected in parallel with wire-bonds, DBC traces, and bus bars introduce parasitic inductance and capacitance into the system. Parasitic inductance in the gate loop of a circuit switched by WBG devices has been studied [25] which shows that interconnect inductance can result in circuit instability and even device failure. On the other hand, capacitors in key locations on the DBC can provide beneficial compensation. For MCMs, complete frequency-domain behavioral models are needed due to the complexity of interconnects, the high power levels, and the integration of multiple die.

In [11], a 1200V, 600A silicon carbide JFET half-bridge module for drop-in replacement of a 600-V, 600-A IGBT intelligent power module has been developed. A body diode in the SiC vertical-channel JFET is used in this switch topology to allow SiC Schottky barrier diodes to be utilized as the anti-parallel rectifier without any undesirable conduction through a MOSFET body diode. Casady et al. in [19] introduced a 1200V Enhancement-mode SiC VJFET Power Module. This power module is a normally-off SiC VJFET. The initial switching results show that there are some undesirable oscillations at turn-on which drives the device into conduction for a short period before remaining off. Also, gate voltage measured internal to the module shows oscillation at the die level. Stability considerations for SiC field effect transistor is addressed in [24]. The presence of parasitic inductance in gate makes this circuit susceptible to self-sustained oscillation that occurs at turn-off of the active switch after the Miller period.

Bayerer et al. discussed the parasitic inductance in gate drive circuits in [5]. Muller et al. analyzed the effects of parasitic stray inductances in the gate and drain circuit on the switching performance of fast-switching devices in [28]. Their experiments show switching losses are larger by approximately a factor of five in comparison to small coupling inductance values which is valuable in the design of power modules and for the integration of discrete products using fast-switching devices. In [25], the issue of instability in half-bridge circuits switched with wide-band-gap transistors is addressed. The near-ideal features of these switching devices, considering the presence of parasitic elements, can introduce self-sustained oscillation. The available power density of the device associated with the parasitic elements in the circuit is related to susceptibility to self-sustained os-

cillation. Considering this susceptibility, wide band-gap devices such as SiC and GaN transistors can be categorized as a class approaching to the radio frequency-domain.

A solution for active gate drive in [38] is provided in order to improve SiC JFET switching dynamics. It suggests an active gate design to reduce the occurrence of natural and forced oscillations at turn-off of the SiC JFET. The susceptibility of the circuit to sustained oscillations is reduced as well as the stress on the gate-source junction. In [10], stable high dV/dt switching of SiC JFETs using simple drive methods is addressed. It discussed that the excitation of resonant modes during switching in SiC JFET resulted from its capability of very high dv/dt is related to its low on-resistance and low intrinsic capacitance. To achieve stable operation, a precise consideration of the parasitic inductances in circuit layout can yield very high dV/dt switching requiring the modest series gate resistance.

As can be inferred from all these referenced studies, the main purpose of using WBG devices in power electronics is their fast switching while these rapid changes in voltage and current at the commutation nodes in typical power electronic topologies cause above mentioned challenges. The management of electromagnetic emissions (both conducted and radiated) is required at the source of the driving dV/dt to use WBG devices in compliance with limits on electromagnetic interference [14], [13] and [12].

This work utilizes frequency-domain data (S-parameters) to analyze and calculate a behavioral model of a complicated power circuit board including multiple power WBG devices that demonstrate near RF behavior in emission or conduction. Designing power circuits with fast switching devices like WBGs requires special considerations because they excite resonances in small parasitic elements and create some undesired oscillations in the

circuits. Time-domain simulation and analysis of these devices is straightforward but time consuming, and the time required for solution increases dramatically as the complexity and the size of these circuits increases. In the frequency-domain it is feasible to extract the characteristics of the circuit board as a $N \times N$ black box (matrix) with N ports which are the internal connections of power transistors and other components with the power module. This process is computationally efficient.

In this work, a direct-bonded copper substrate (DBC) is introduced as an example circuit that all simulations and experiments are performed with. In section 5.2.3, the physical modeling of the structure both in the time-domain and the frequency-domain is discussed. In section 5.2.4, behavioral modeling using different multiport linear modeling is studied and the reason for choosing Scattering parameters (S-parameters) a suitable approach is discussed. At the end and in the section 5.2.5, different available modeling environments that have been used in this paper for simulation or validation purposes are introduced.

5.2.2 Device Under Test

A direct-bonded copper substrate (DBC) is the exemplar problem chosen for performing all simulations and experiments in this work. The DBC is $3.8\times$ 7 cm and is made of 1.58-mm thick FR4 printed circuit board with copper traces formed on the top and a solid copper layer on the bottom. The DBC has been modeled using four ports for the drain, gate, Kelvin source and Kelvin pad as illustrated in Figure 5.7. This board layout was used in an actual custom application using an AlN DBC in which SiC junction field effect transistors were bonded on the drain bus as labeled and wire bonds were used to connect

the die to the gate and Kelvin source buses respectively. For modeling and experimental purposes, the hypothetical drain, gate, Kelvin source, and Kelvin source pad form the four ports of the behavioral model. As shown in Figure 5.7, $RG-174$ coaxial cables were used to define the ports for the experimental work.

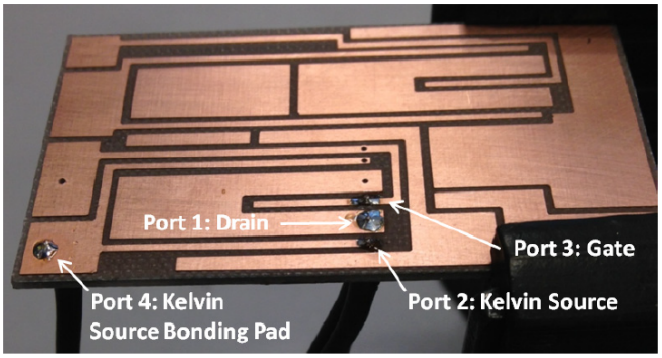

Figure 5.7

DBC made from a FR4i milled printed circuit board. Ports are defined with RG-174 coaxial cable probes with the shields soldered to the copper plane on the bottom of the board.

5.2.3 Physical Modeling

Physical models could be created using electromagnetic 3D software utilizing analysis engines such as finite-elements (FE) or finite-difference time-domain ($FDTD$). The model provided by this method is robust and reliable. Complicated structures and circuits can be modeled with this approach including very complex geometries. The weakness of this method is that it is computationally expensive and incompatible with other behavioral modeling.

5.2.3.1 Time-Domain Analysis

Finite-difference time-domain (FDTD) is a numerical analysis technique used for calculating approximate solutions to the associated systems of differential equations and is a computational electrodynamics modeling approach. FDTD solves Maxwell's equations in the time domain. This means that the calculation of the electromagnetic field values progresses at discrete steps in time. FDTD solutions can cover a wide frequency range with a single simulation run because it is a time-domain simulation method and it can deal with nonlinear material properties in a natural way. The main reason for using the FDTD approach is the excellent scaling performance of the method as the problem size grows. As the number of unknowns increases, the FDTD approach quickly outpaces other methods in efficiency. FDTD is provided by many electromagnetic-related software. In this work, Keysight EMPro is used to calculate the surface current of the structure in different time steps after exciting a port with a step function (to be discussed in more detail in 5.2.5.2). Figure 5.9 shows the surface current after $60ns$ when the source is excited with a Gaussain pulse with a width of $30ns$.

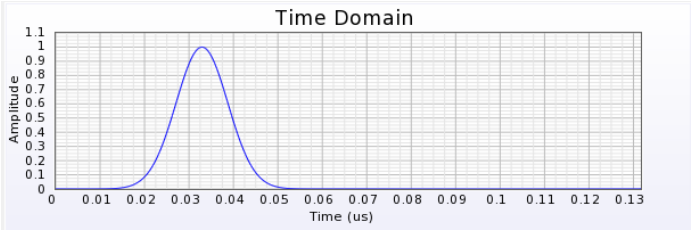

Figure 5.8

Excitation of a Gaussian input pulse on port 2 with a width of $30ns$.

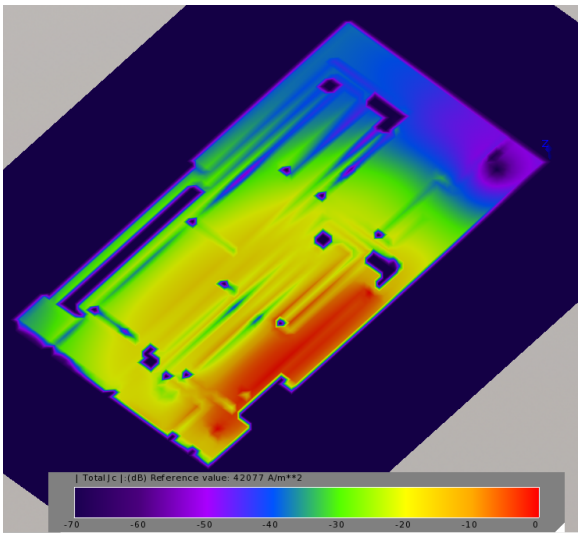

Figure 5.9

Illustration of DBC surface current by applying a Gaussian pulse function of 1V and width of $30ns$ at the time of $60ns$.

The required time for this simulation depends on the density of the mesh that the software calculates and as the frequency of interest or the complexity of the structure increases the mesh becomes finer and accordingly the time required to compute the simulation increases.

5.2.3.2 Frequency-Domain Analysis

Finite element method (FEM) is a numerical technique used to calculate approximate solutions to boundary value problems in partial differential equations. It divides the whole structure into simpler parts called finite elements and solves the Maxwell equations for each element and illustrates the frequency behavior of a structure when excited with a wave voltage or current. For the DBC of Figure 5.7, the finite-element calculation is per-

formed via EMPro software and S-parameters of the structure at the mentioned four ports is calculated. This method is discussed further in section 5.2.5.2. Figure 5.10 shows the DBC geometery and the mesh for performing finite-element analysis.

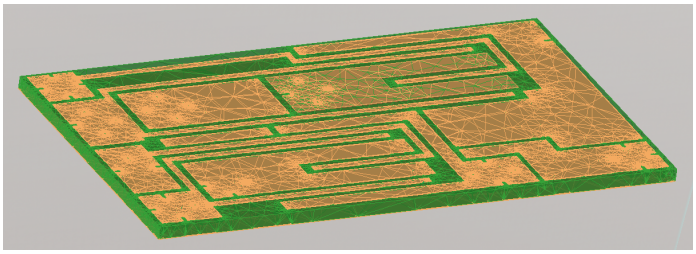

Figure 5.10

The CAD rendering of the DBC structure and the mesh for performing finite-element analysis.

5.2.4 Behavioral Modeling

Behavioral modeling involves calculating the structures behavior at the boundaries of a black box and describing the relationship between boundary variables with a matrix of frequency-dependent coefficients. This allows the boundary variables to be connected to other components in a circuit and the resulting self-consistent solution of the whole structures behavior in the time or frequency-domain to be computed.

5.2.4.1 Multiport Linear Modeling

Packaging of power modules with fast switching semiconductors like WBGs requires special consideration of the components near-RF behavior [25]. The device under test (DUT) is a DBC board, which, due to its passive character, yields linear behavior that can be modeled completely using multiport linear modeling. One of the advantages of behav-

ioral modeling is that it is computationally efficient and is usable in multi-chip module (MCM) and die integration where the semiconductor devices contribute virtually all non-linearity in the system. The non-linear behavioral modeling of semiconductor devices is well known. Such models can be integrated with the linear behavioral model of the DBC at the boundaries of both models to form a complete system.

In the designing of MCM for wide band-gap (WBG) semiconductors, the management of parasitic impedances associated with intra-module interconnections and construction details is a challenge. For instance, the individual die which are connected in parallel with wire-bonds, DBC traces, and bus bars introduce parasitic inductance and capacitance into the system. Interconnect inductance can result in circuit instability and even device failure according to a study done on Parasitic inductance in the gate loop of a circuit switched by WBG devices. On the other hand, capacitors in key locations on the DBC can provide beneficial compensation. For MCMs, complete frequency-domain behavioral models are needed due to the complexity of interconnects, the high power levels, and the integration of multiple die.

Figure 5.11 shows a DBC which has been digitized and modeled with Keysights EMPro physics-based modeling suite. The DBC is $3.8cm \times 7cm$ and is made of 0.8-mm thick AlN with copper traces formed on the top and a solid copper layer on the bottom. EMPro extracts the four S-parameters representing the complete behavioral model between ports 1 and 2 shown in the figure.

An optional wire bond is also shown in the figure. When the wire bond is absent, ports 1 and 2 are isolated, but when the wire bond is present, there is a galvanic connection.

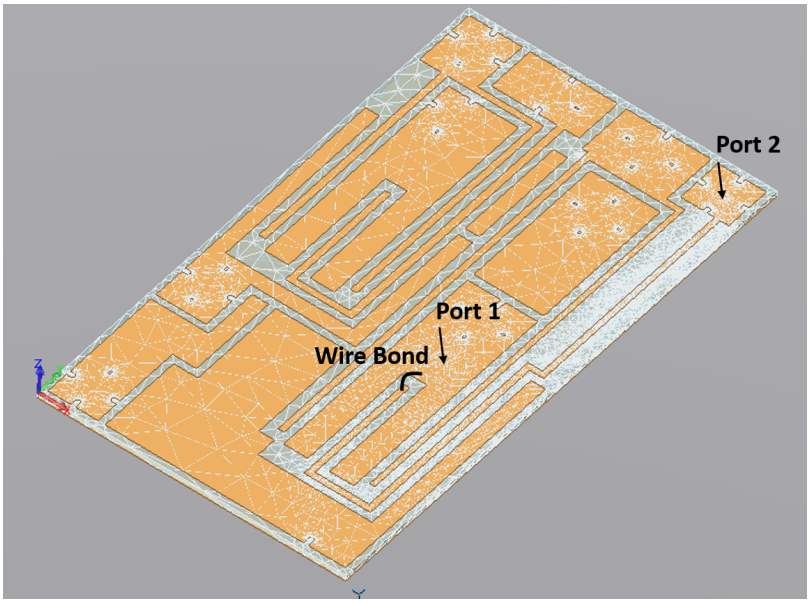

Figure 5.11

Meshed model of a DBC used in a half-bridge MCM for an application with SiC transistors and diodes.

Measurements were made (see Figure 5.11) with an Agilent Vector Network Analyzer E8062A and calibrated 50ω probes as shown in Figure 5.13.

The results cover the range $0.3MHzto100MHz$ typical of the parasitic oscillations found in MCM. Figure 5.12 (a) and (b) show the computed and measured S_{11} and S_{21} magnitudes when the wire bond is absent while Figure 5.12 (c) and (d) show the same parameters when the wire bond is present. For the first case, the results are clearly capacitive, while for the second case, they are resistive at low frequency and inductive at high frequency. In real applications, the simultaneous modeling of both extrema is needed in a geometrically accurate form to achieve acceptable time-domain model performance with

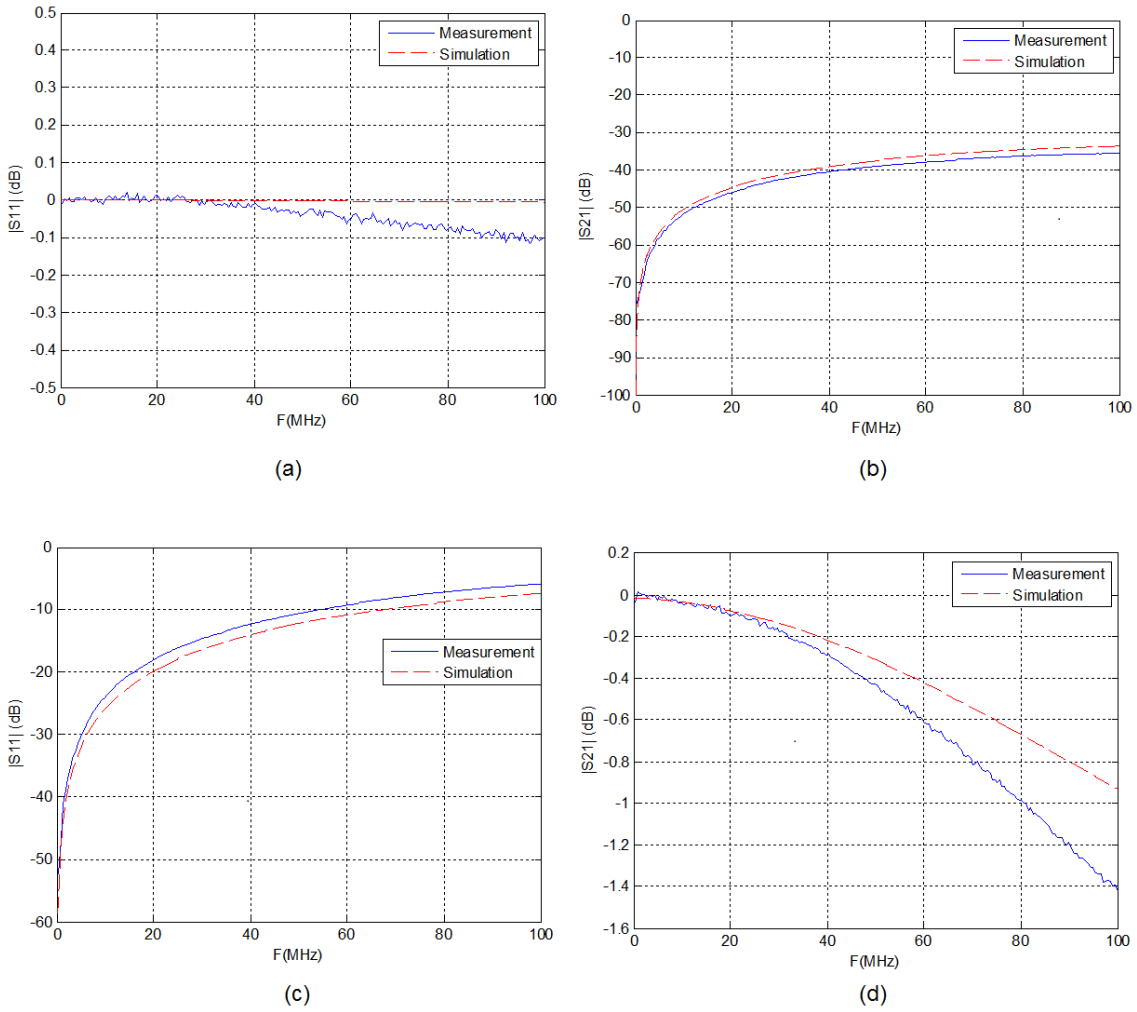

Figure 5.12

Computed and measured a) $|S_{11}|$ and b) $|S_{21}|$ for the case that the wire bond is absent. Computed and measured c) $|S_{11}|$ and d) $|S_{21}|$ for the case that the wire bond is present. The small deviation at higher frequency between simulation and experiment is an artifact of the residual uncompensated probe inductance and uncertainty in the exact AlN thickness.

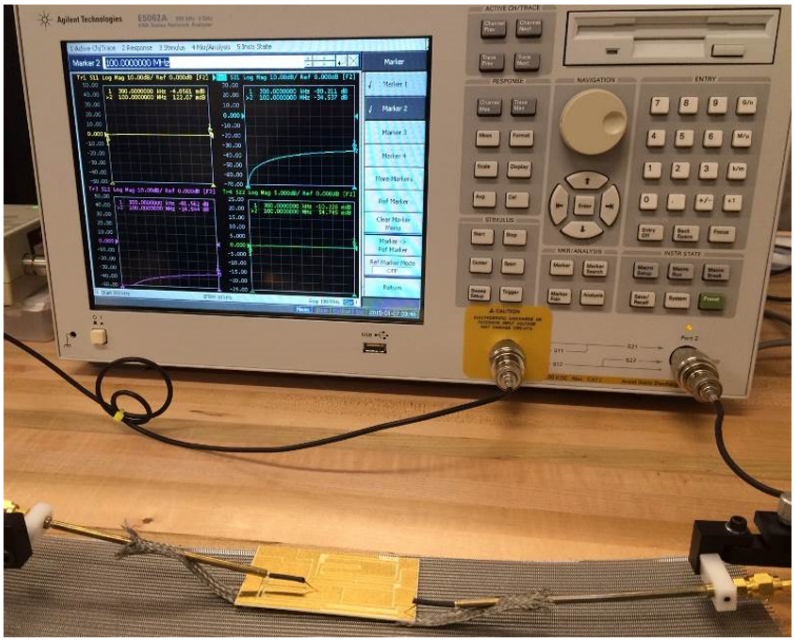

Figure 5.13

Setup of the measurement of DBC related to the results illustrated in Figure 5.12

assemblies of semiconductor dice and wire bonds. The multi-port S-parameter behavioral model excels at this task.

5.2.4.2 S-parameter Modeling

In measuring the system characteristics, different parameters are available, such as h, y and z parameters. Measuring these parameters requires that the output and the input both be shorted or opened completely. At high frequency this requirement turns into an important problem because it requires tuning stubs which in turn can cause oscillation in semiconductor devices. In contrast, when measuring S-parameters, the device under test is placed between two 50ω impedances at input and output, and this rarely causes instability and oscillation. The other advantage of using S-parameters stems from the fact

that the S-parameters can be measured simply by coaxial cables because the magnitude of traveling waves is almost constant on a transmission line. S-parameters relate to the traveling waves that are scattered or reflected when an n-port network is excited. As shown in Figure 5.14, S-parameter modeling convention treats port variables as traveling waves rather than voltage or currents and thus overcomes measuring difficulties in extracting model parameters at RF frequencies.

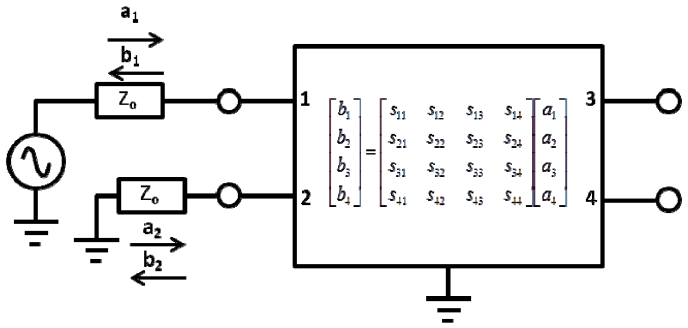

Figure 5.14

Definition of a four-port S-parameter behavioral model where each port is referenced to a common ground terminal. In this example, port one is connected to an active source, while port two is connected to a passive load.

The main hypothesis behind using S-parameters in this work is associated with the fast switching property of WBG devices. Fast switching generates broad spectral power in the tens to hundreds of MHz resulting in parasitic coupling of this energy to other parts of the DBC which leads to problems with half-bridge switching instability. Also parasitic coupling of this energy to the grounded surfaces leads to common- mode current and resulting conducted EMI. Second, there are established engineering methods for RF

transistor packaging in which S-parameters are ensconced in the commercially available modeling software and measurement instruments. The inference being that new power packaging designed for WBG semiconductor devices needs to borrow from the RF experience. The S-parameter model can be used in either the frequency or the time domain for the assessment of stability and other dynamic properties and for rerouting connections or for compensating with passive components.

5.2.5 Commercial Modeling Environments

5.2.5.1 Advanced Design System (ADS)

Keysight (Agilent) Advanced design system (ADS) is an electromagnetic design software that can be used for RF, microwave and high speed digital applications.

In this work, after extracting the S-parameters in Keysight EMPro, it is possible to place the calculated S-matrices in a data box in the schematic environment of ADS and calculate the time domain-behavior of the whole system as illustrated in Figure 5.15. As shown in Figure 5.16, a step-input signal of $20ns$ is applied to port 4 (Kelvin pad) shown in Figure 5.18, and the resulting induced voltages on drain and gate are measured using an osciloscope as shown in Figure 5.16.

A comparison between the simulated and measured signals are illustrated in Figure 5.17.

5.2.5.2 Electromagnetic Professional (EMPro)

Keysight Electromagnetic Professional (EMPro) is another electromagnetic design software for analyzing the 3D electromagnetic effects of components such as high-speed IC packages, bondwires, PCB interconnects. This software is utilized in this work to create a

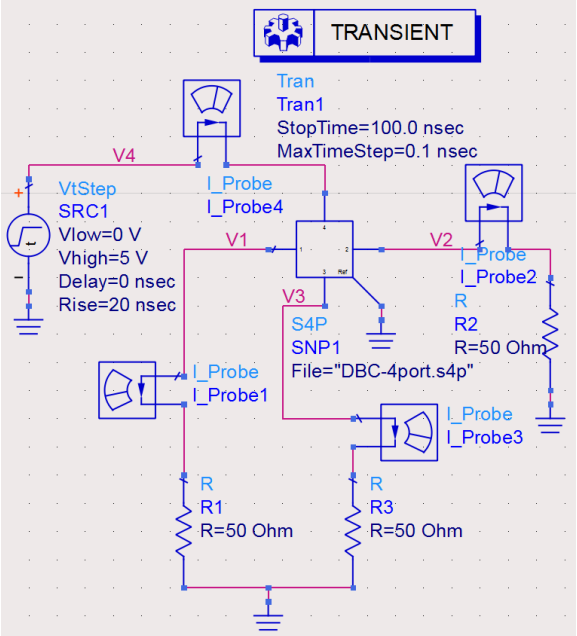

Figure 5.15

The ADS schematic environment showing the S-parameter data box and the four probes for measuring current and the voltages on the ports and the $20ns, 5V.$ step-function source.

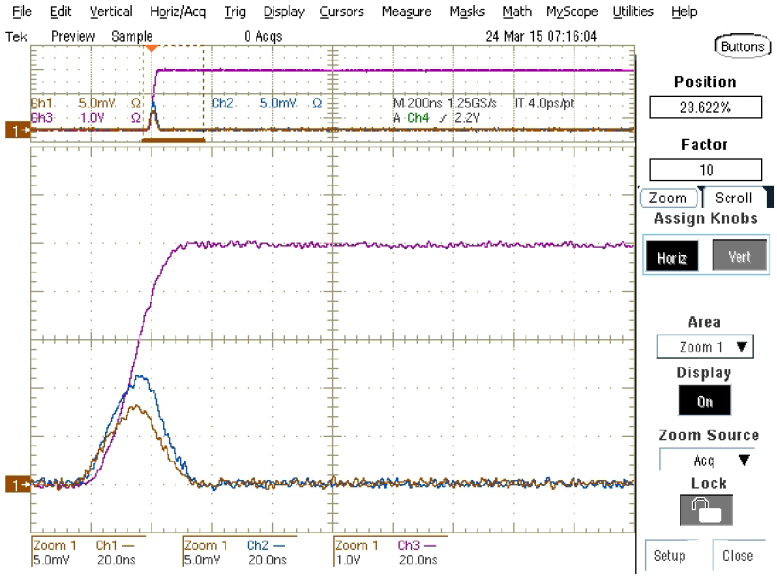

Figure 5.16

Time-domain measured voltages for a step-input with a $20ns$ rising time using a oscilloscope.The gate and the drain are shown in mV.

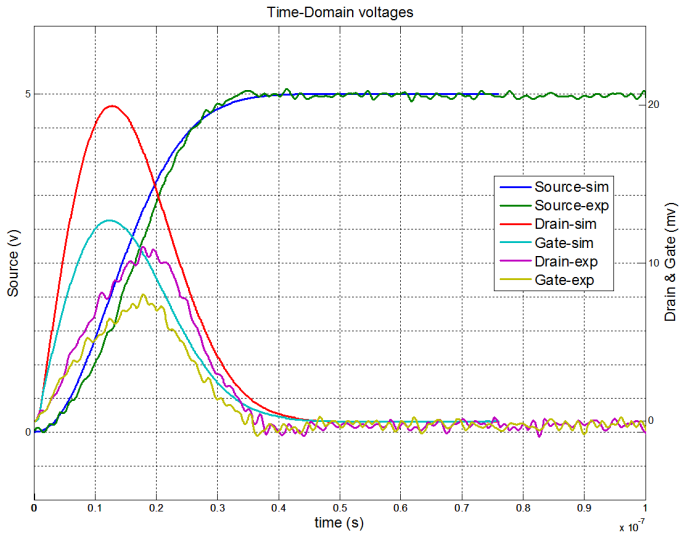

Figure 5.17

Comparison of the time-domain gate, source and drain voltages resulted from simulation and measurement by applying a step-signal with $20ns$ rise time and $5V$ to a DBC-board. The graphs show acceptable agreement between measurement and simulation.

3D component that can be simulated together with 2D circuit layouts and schematics within ADS, using electromagnetic-circuit cosimulation (as shown in section 5.2.5.1). Empro is capable of running 3D electromagnetic simulations in frequency-domain and time-domain e.g. Finite Element Method (FEM) and Finite Difference Time Domain (FDTD). The example DBC-board created in EMPro is shown in Figure 5.18.

The simulation of DBC-board in the time-domain using EMPro FDTD technology was shown in Figure 5.9. The FEM meshed representation of DBC-board which provides a solution in the frequency-domain is shown in Figure 5.10 and compared with experimental data in Figure 5.12.

5.2.5.3 Matlab SimRF/RFtoolbox

The S-parameter resulted form the behavioral simulation in EMPro and the S-parameter obtained from measurement by a network analyzer both are stored in touchstone format files. In order to use this behavioral model in other environments, some interface actions are needed. In Mathworks Matlab, the RFtoolbox provides the commands of read and write to save or load this file format and to extract the related network parameters such as S-matrices.

Also Mathworks Simulink SimRF provides an S-parameter block which use measured or simulated S-matrix data to calculate the frequency-domain behavior of the matrix in combination with other S-matrices or circuit components. Figure 5.19 shows the schematic that is used to calculate the time-domain drain and gate voltages after the source is excited with a $20ns$ and $5V$ step function.

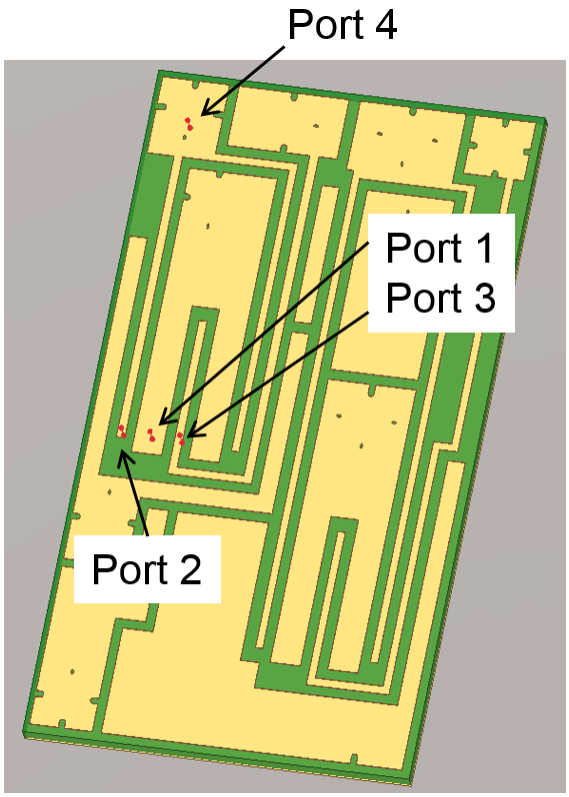

Figure 5.18

DBC board created and simulated in Keysight EMPro on a FR4 substrate. Ports are showing Drain, Kelvin source, gate and Kelvin pad respectively.

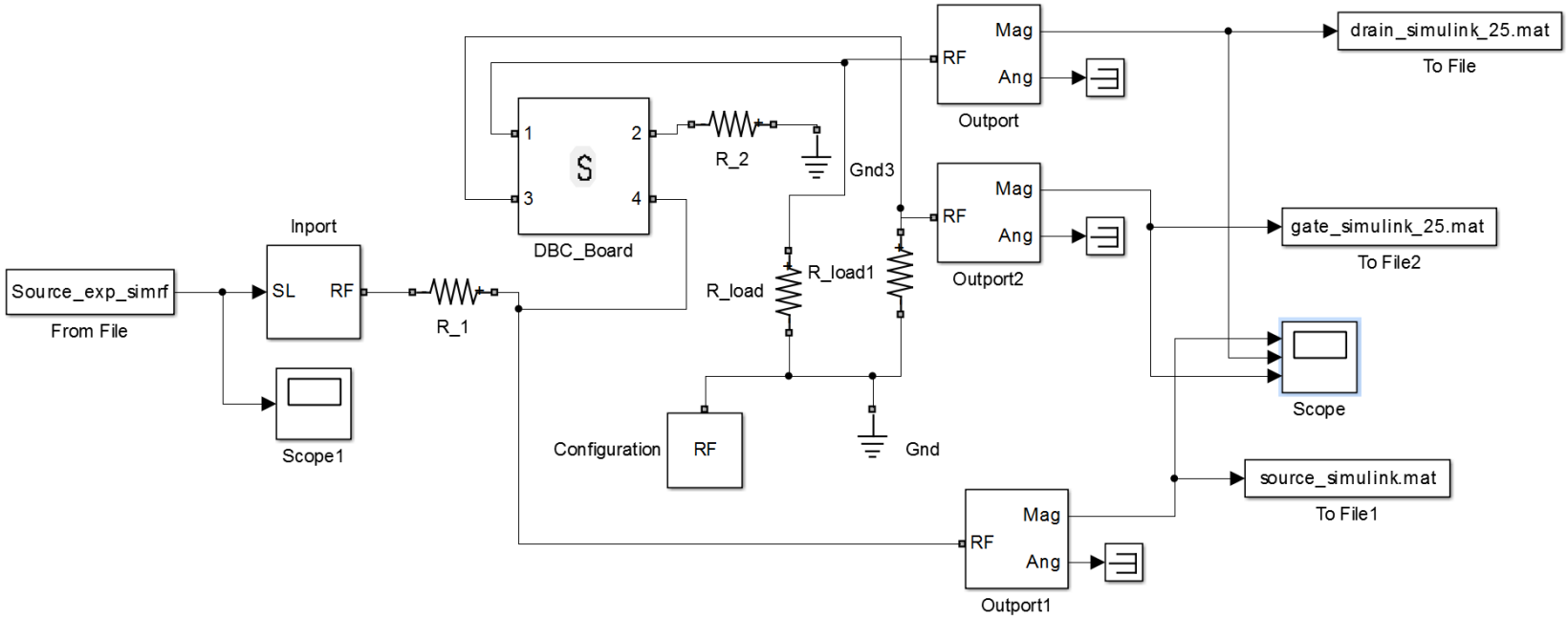

Figure 5.19

The SimRF schematic used to simulate the time-domain behavioral of the DBC board. As illustrated this time-domain is extracted from S-parameter characteristics of the system.

The output of the oscilloscope in the schematic is illustrated in Figure 5.20. The curves from top to bottom show the source, drain and gate voltages respectively. The calculated voltages are similar to the calculated voltages in Figure 5.17.

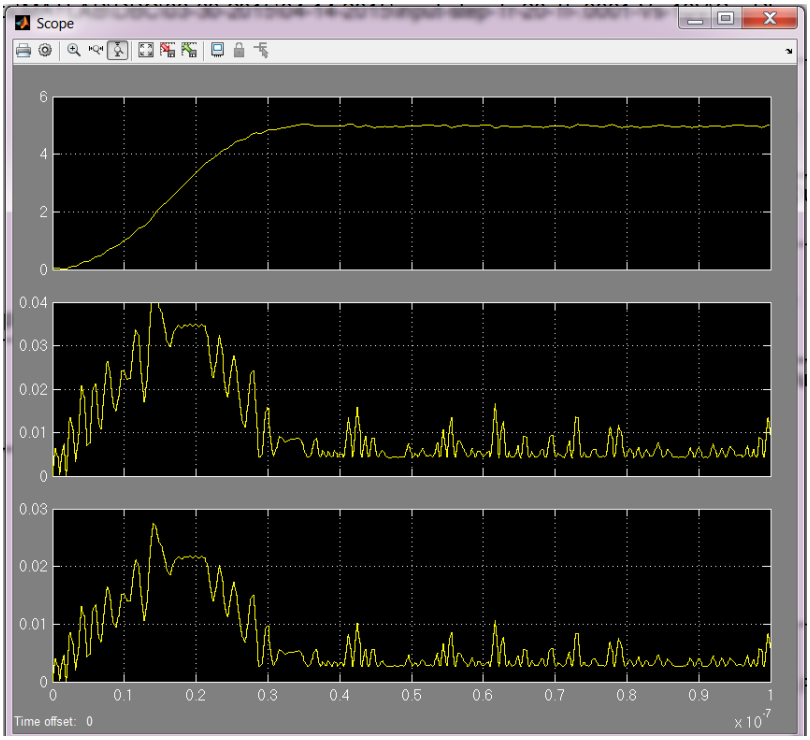

Figure 5.20

The outputs of the oscilloscope in SimRF schematic. From top to bottom, images show the source, drain and gate voltages, respectively.

CHAPTER 6

RESULTS

In this chapter the so far accomplished results are reviewed. In order to implement the methods discussed in this dissertation, different software packages are available that implement Fourier and wavelet transforms with reasonable calculation speeds. Several mathematical workouts are required here to be able to study the systems. Therefore, a new algorithm with special features in a robust software implementation is required to perform the transfer back and forth of the signal between the time and frequency-domains. For evaluation of this result some other software is used that will be reviewed later on.

6.1 Transferring Band-limited S-parameter to Time-Domain in Matlab

In this section a very simple decaying exponential signal is considered.

$$h(t) = \begin{cases} e^{\frac{-t}{\tau}} & \text{if } t \geq 0 \\ 0 & \text{if } t < 0 \end{cases} \tag{6.1}$$

The Fourier transform of this function is as follows:

$$H(\omega) = \frac{1}{1 + j\omega\tau} \tag{6.2}$$

For simplicity $\tau = 1$. Therefore:

$$h(t) = \begin{cases} e^{-t} & \text{if } t \geq 0 \\ 0 & \text{if } t < 0 \end{cases} \qquad H(\omega) = \frac{1}{1 + j\omega} \tag{6.3}$$

A code is developed in Matlab to transfer this signal from the time-domain to frequency-domain. The reason is that both the time-domain and frequency-domain transformations of a signal should be available to execute the iterative algorithm. In this project, the time-domain data are not accessible and is the main unknown of this problem that should be determined.

In the frequency-domain, we truncate, i.e., some parts of the signal is forced to zero in order to keep similarity to the original signal. This is done by multiplying the signal with a window with a length equal to a fraction of the length of the original signal. For this purpose a GUI code is written in Matlab to illustrate the real-time effects of the window width and position on the reconstructed signal in time-domain.

Figure 6.1 through Figure 6.5 illustrate this process:

The length of the original signal is 514 points, and as illustrated. Different windows with different widths varying from 513 to 4 points are applied to the signal. The bottom plot shows the frequency-domain spectrum. The blue curve shows the frequency transformation of the exponential function and the red curve is the applied window. The upper plot shows the time-domain representation of the signal. The blue curve is the time-domain curve of the original signal and the red curve is the reconstructed time-domain signal made from the truncated frequency-domain signal.

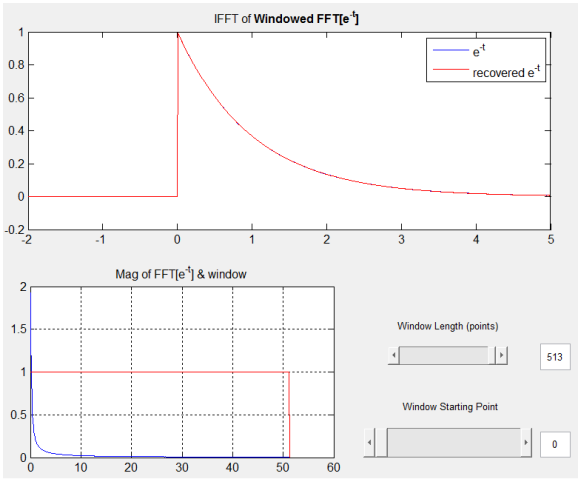

Figure 6.1

Effect of no window on Inverse Fourier transform

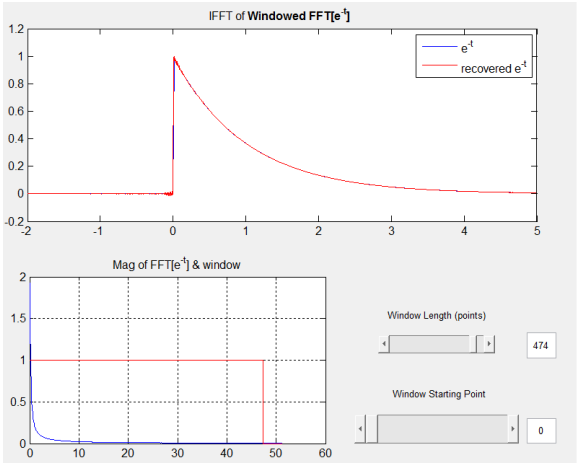

Figure 6.2

Effect of 474-point window on the Inverse Fourier transform

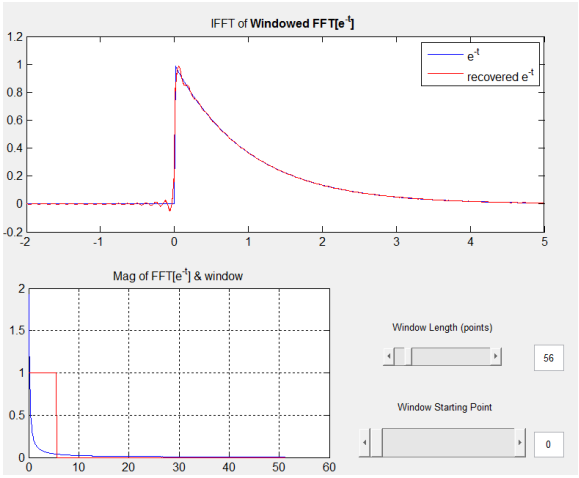

Figure 6.3

Effect of 56-point window on the Inverse Fourier transform

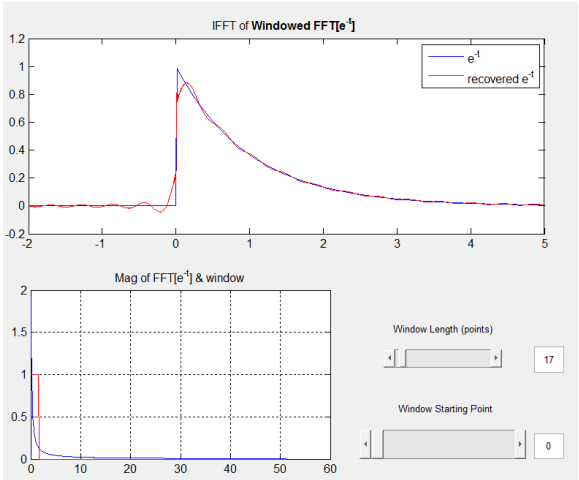

Figure 6.4

Effect of 17-point window on the Inverse Fourier transform

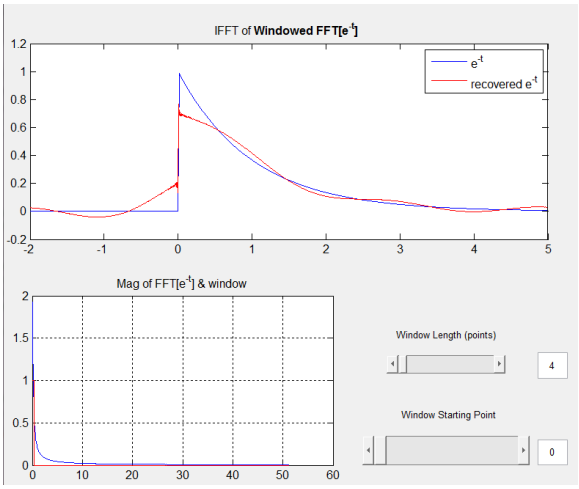

Figure 6.5

Effect of 4-point window on the Inverse Fourier transform

As shown, there is not that much information in the higher frequencies and for exponential signal most of the energy is concentrated in the DC and close to DC frequencies. Therefore, when the length of window changes from 514 to 56 it does not affect the reconstructed signal significantly, while when the width of the window changes from 17 to 4, the signal in the time-domain is completely degenerated. It can be concluded that a complete frequency-domain spectrum results in an exact time-domain reconstructed signal, but when the signal spectrum is truncated the reconstructed signal is not causal anymore.

The starting point of the window examined above is zero frequency or the DC frequency. If the window is shifted a little bit to the right and is started from frequencies higher than the DC, the reconstructed signal gets degenerated moderately and turns to a non-causal signal. Therefore, it can be concluded that lower frequency data in the spectrum play a key role in the reconstruction of the signal in the time-domain. Figure 6.6

through Figure 6.8 show the critical effects of starting point of windowing on the quality of the reconstructed signal in the time-domain.

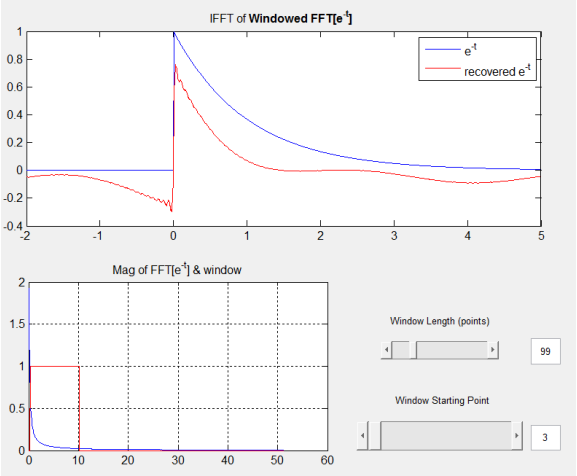

Figure 6.6

The effect of starting point of 3 on the Inverse Fourier transform of the signal

These results show that calculating the missing frequency data has a critical role in the reconstruction of the signal in the time-domain.

6.2 Results

The main three features for the reconstruction of a signal in the time-domain from frequency data are the casuality, passivity and time-delay. Time delay is not discussed here because it requires the same considerations as causality. In the following, the algorithm for eliminating the reconstruction errors is discussed.

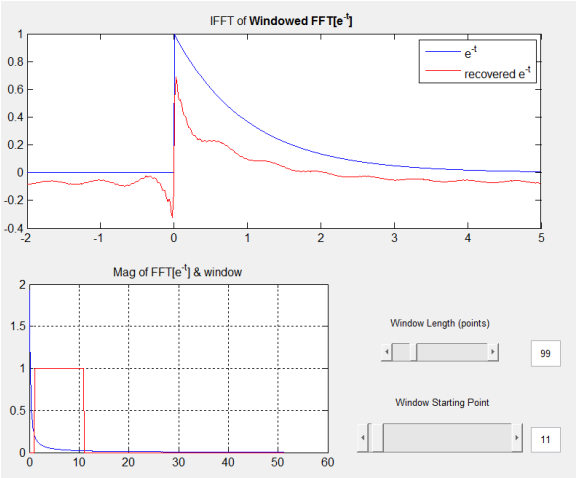

Figure 6.7

The effect of missing the first 11 points on the Inverse Fourier transform of the signal

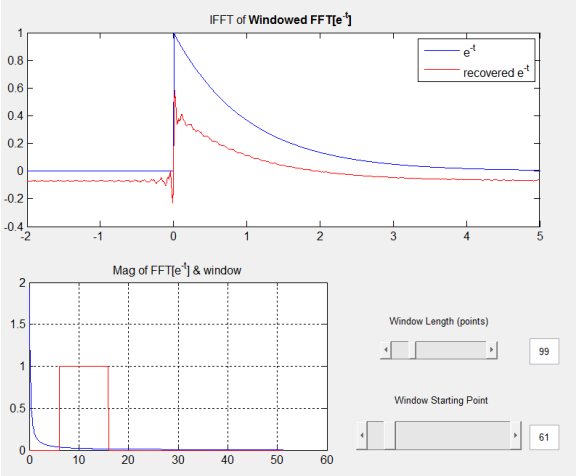

Figure 6.8

The effect of missing the first starting 61 points on the Inverse Fourier transform

6.2.1 Passivity

Forcing passivity to signals in the time-domain requires three simple steps:

1. The eigenvalues of the S-parameter matrix with a value more than one in all frequencies should be explored. These eigenvalues make the S-parameter of the component non-passive.

2. Evaluating the passivity constraint is performed as follows:

$$|S_{11}|^2 + |S_{21}|^2 \leq 1$$

3. Dividing all the elements of S-parameter matrix by the largest found eigenvalue.

Through these simple steps one can convert the non-passive S-parameter matrix to a passive one. This modification is run in matrix level, and there is no curve of schematic to shown the result.

6.2.2 Causality

As discussed before, the lowest frequency limitation of the simulations or measurement instruments determines the lower band limit of the available S-parameter spectrum. It seems like that the signal is filtered with a completely sharp filter. This sharp filter in the frequency-domain gives a broad response in the time-domain. We might try applying a smooth amplitude roll off (windowing) in the frequency-domain. It can be performed for magnitude curve, but there is no method to roll off smoothly the phase angle data. Anyhow, amplitude windowing can eliminate some of the sharp time-domain oscillations

ringing or *Gibbs* phenomena, but it makes the time-domain pulse even broader, and so the non-causality problem grows [39].

To reconstruct the pulse accurately, a different approach should be considered to be able to calculate and add the missing data to the available band-limited S-parameter data. In practice, as the measured component is physical, its response beyond the measurement cut-off frequency will roll off smoothly. Therefore, windowing is not required any more, and the amplitude and phase should be extrapolated. Extrapolating the amplitude is as simple as fitting a low order polynomial curve to the measured amplitudes, but extrapolating the phase still seems a challenging problem which demands new effort.

On the other hand and according to the Kramers-Kronig relation, discussed in chapter 3, the necessary and sufficient condition for a system to be causal is that the real and imaginary components of the frequency response are related through Hilbert transform.

Consider the Fourier transform:

$$f(\omega) = \int_{-\infty}^{+\infty} f(t)e^{-ib(-\omega)}dt = \int_{-\infty}^{+\infty} [cos(\omega t)f(t) + jsin(\omega t)f(t)dt] \qquad (6.4)$$

In the time-domain, cosines and sines are even and odd functions, respectively. For waveforms in general, there is not a specific relationship between the sum of the cosines (the even component) and the sum of the sines (the odd component), while in the causal waveforms the Kramers-Kronig rule is established. If an even waveform is multiplied by the step function:

$$h(t) = \begin{cases} +1 & \text{if } t \geq 1 \\ -1 & \text{if } t < 1 \end{cases} \tag{6.5}$$

the odd waveform is achieved. With elementary algebra. This is the necessary and sufficient condition to make the even and odd components exactly cancel each other to zero for all points with negative time. So we can write a causal waveform as:

$$h_{causal}(t) = h_e(t) + h(t)h_e(t) \tag{6.6}$$

The $h_e(t)$ and $h(t)h_e(t)$ terms generate the real and imaginary parts of the Fourier integral, respectively.

On the other hand, in the frequency-domain, it can be shown that:

1. Multiplication in the time-domain is equivalent to convolution in the frequency-domain.

2. The Hilbert kernel of $\frac{2}{j\omega}$ is the Fourier transform of $h(t)$.

The Hilbert kernel is used as the convolution function in the Hilbert transform. It can be concluded that the imaginary part of the spectrum in the frequency-domain results from the Hilbert transform of the real part of the signal in the time-domain. By knowing the real part, the imaginary part can be calculated and having the imaginary part results in the real part using the Hilbert transform. If the real part is called r and the imaginary part i, the Hilbert transform of r would be $H(r)$; Therefore, the imaginary part is calculated as $i = H(r)$. In this state, the real part of the spectrum is extrapolated using binomial curve

fitting techniques. Utilizing Eq. 6.7, the imaginary part and the phase of the spectrum can be determined as follows:

$$A^2 = r^2 + H^2(r)$$
$$\phi = tan^{-1}(\frac{H(r)}{r}) \tag{6.7}$$

Using the above mentioned relations provided in [39], the time-domain response of a S-parameter matrix can be calculated but the problem is that the missing parts are extrapolated via curve fitting methods. The current dissertation uses another approach to be capable of estimating the missing parts of the frequency-domain spectrum with the same or better precision. Therefore, the method of wavelet is addressed in this dissertation that demonstrates a robust and reliable alternative for the above mentioned methods.

6.2.3 Wavelet Transform

For wavelet transform step, the Matlab wavelet toolbox was used but due to band-limiting character of S-parameters, one needs to complete the spectrum first and then use the toolbox. Although the other toolboxes in Matlab, such as Matlab Simulink Simrf and Matlab RFtoolbox, perform the conversion, they use the traditional methods of curve fitting to extrapolate the frequency-domain spectrum and then continue with their transformation. For this reason, an exponential signal with an added noise is considered. Figure 6.9 and Figure 6.10 illustrate the real and imaginary values of the Fourier transform of an exponential signal. The blue curve shows the exponential spectrum and the red curve shows the same exponential with added noise.

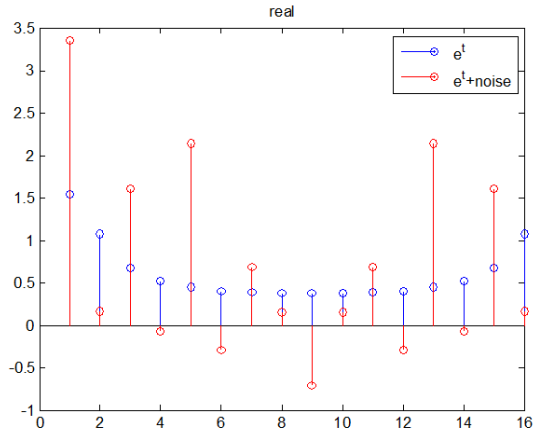

Figure 6.9

Blue cuvre, real value of the spectrum of exponential function. Red curve, real value of the spectrum of the exponential function with noise

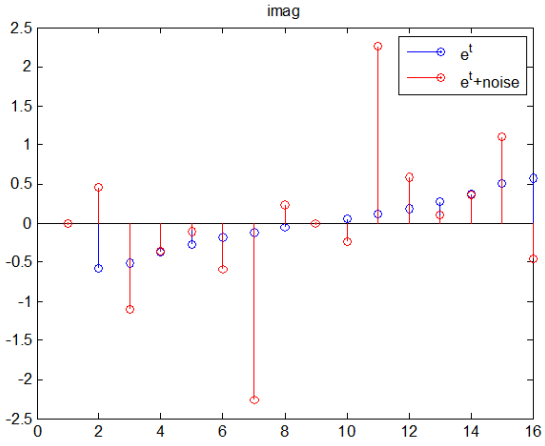

Figure 6.10

Blue cure, imaginary curve of the spectrum of the exponential function. Red curve, imaginary curve of the spectrum of the exponential function with the added noise

In this step, the Fourier transform of the spectrum of aforementioned signal (which is the Fourier transform of the original time-domain signal) is calculated and shown because the spectrum is not truncated and thus is complete, this operation reconstructs the original exponential signal precisely, as shown in Figure 6.11 .

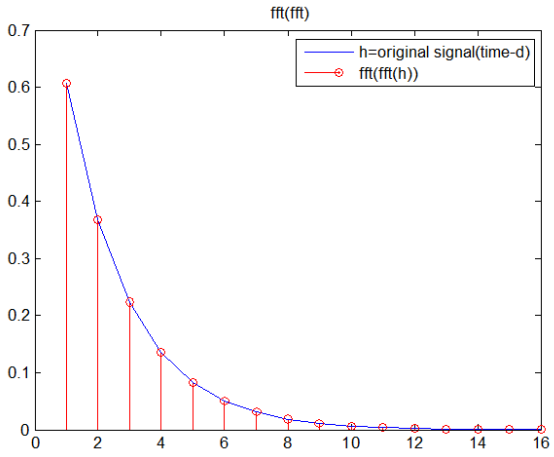

Figure 6.11

Inverse Fourier transform of the spectrum (Fourier transform) of exponential signal

As the next step, Haar wavelet transform, which is one of the simplest mother wavelets is applied to the original signal of exponential function and the Fourier transform of the signal. Figure 6.12 and Figure 6.13 show the approximate and detail coefficients of this transform, respectively. As illustrated, the result looks different for the signal and its Fourier transform. It is not far from our expectation. The red stems show the wavelet transform of the spectrum and the blue stems show the wavelet transform of the time-domain signal.

Figure 6.14 illustrates the coefficients of discrete and continuous coefficients of wavelet transform using symlet2 mother wavelet and one-dimensional wavelet decomposition.

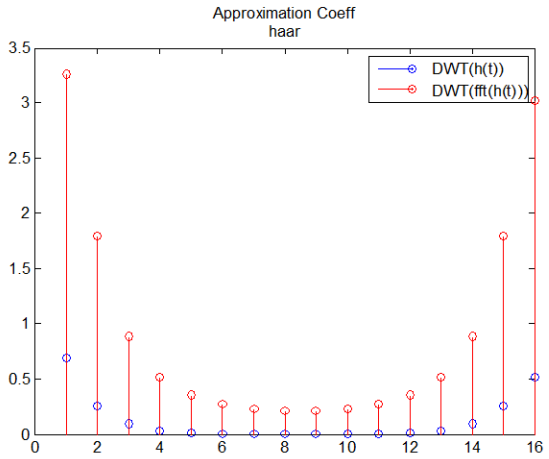

Figure 6.12

Approximate coefficients of Haar transform on the exponential and spectrum of exponential function

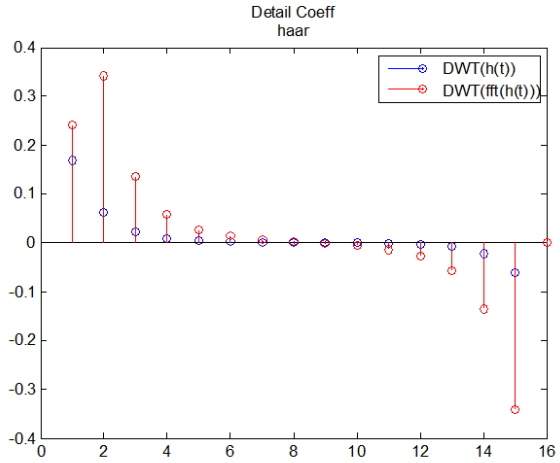

Figure 6.13

Detail coefficients of Haar transform on the exponential and spectrum of exponential function

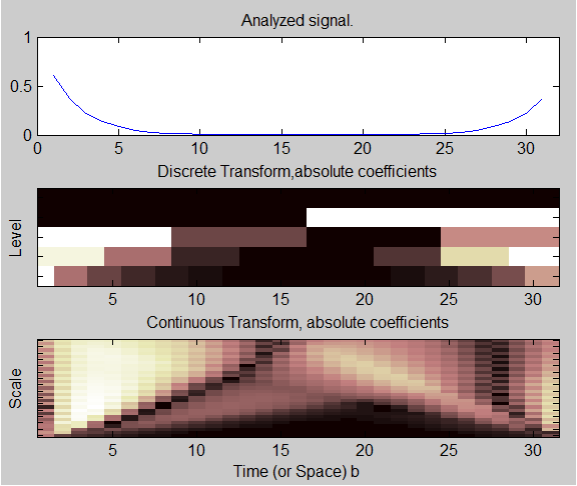

Figure 6.14

Effect of starting point of 3 on Inverse Fourier transform

Therefore, it is required to prove a method that uses the frequency-domain data and is capable of generating the exact time-domain impulse response of the system.

6.3 Validation

Several softwares are provided to calculate the inverse Fourier transform. These softwares use some kind of algorithms for converting band-limited S-parameters to complete the spectrum by using curve fitting, rational functions and other well-known methods. Among them, the most straight-forward software packages introduced so far are as following:

1. **Keysight (Agilent) Advanced Design System (ADS)**

   Through it's S-parameter simulation tool.

2. **RFtoolbox**

   A RF Matlab toolbox, through two main commands of ”timeresp” and ”impulse” which calculates impulse response of S-parameters.i

3. **Simrf**

   a RF toolbox in Matlab Simulink.

All these methods require a value for DC component in the given S-parameter data otherwise they do not guarantee the causality and validity of the results. Therefore, in this dissertation an alternative method for calculating the DC point is provided.

6.4 S-parameter Curve Types

The types of the S-parameters curves differs regarding to the system frequency range of operation. For instance, some of RF, microwave and antenna devices curves are illustrated in Figure 6.15.

The frequency-domain spectrums faced in this research include simple curves with the resonance points or oscillations because the range of operation of the systems are at the lower limit of the frequency range. Therefore, the S-parameter curves can be approximated with simple functions such as exponential functions. Samples of corresponding S-parameter curves are illustrated in Figure 6.15.

6.5 Reconstruction of Exponential Function Using Wavelet Transform

In this section, a very simple exponential function is used:

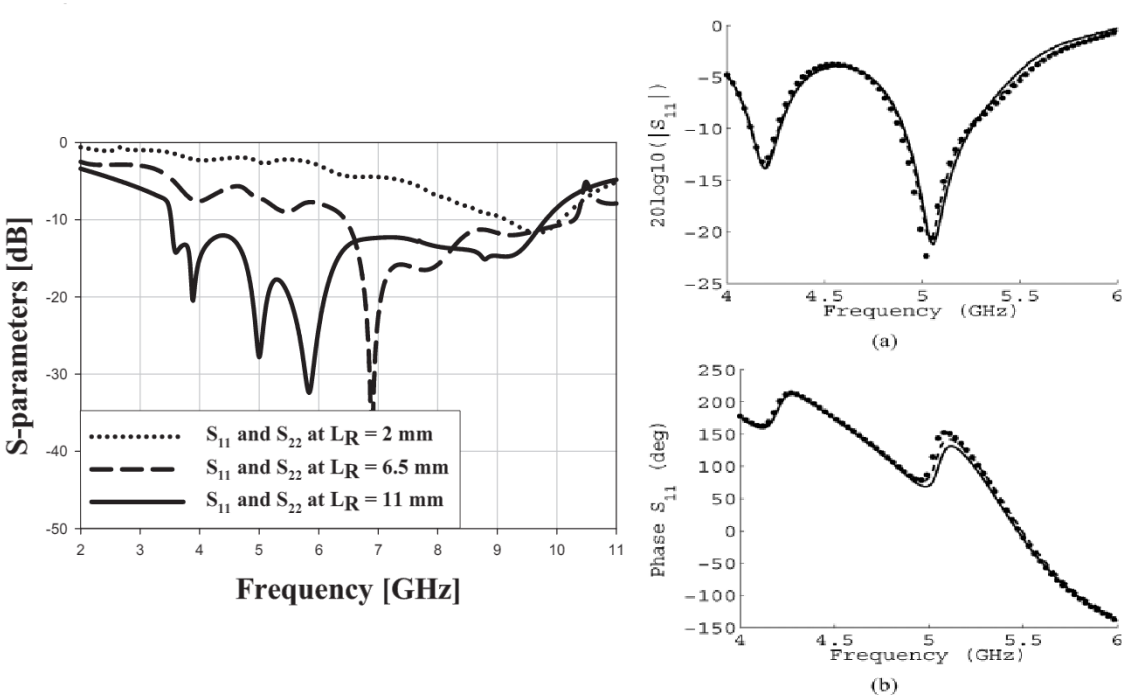

Figure 6.15

Left: S-parameter of a microstrip Dipole antenna [17]. **Right**: S-parameter of a waveguide aperture [16].

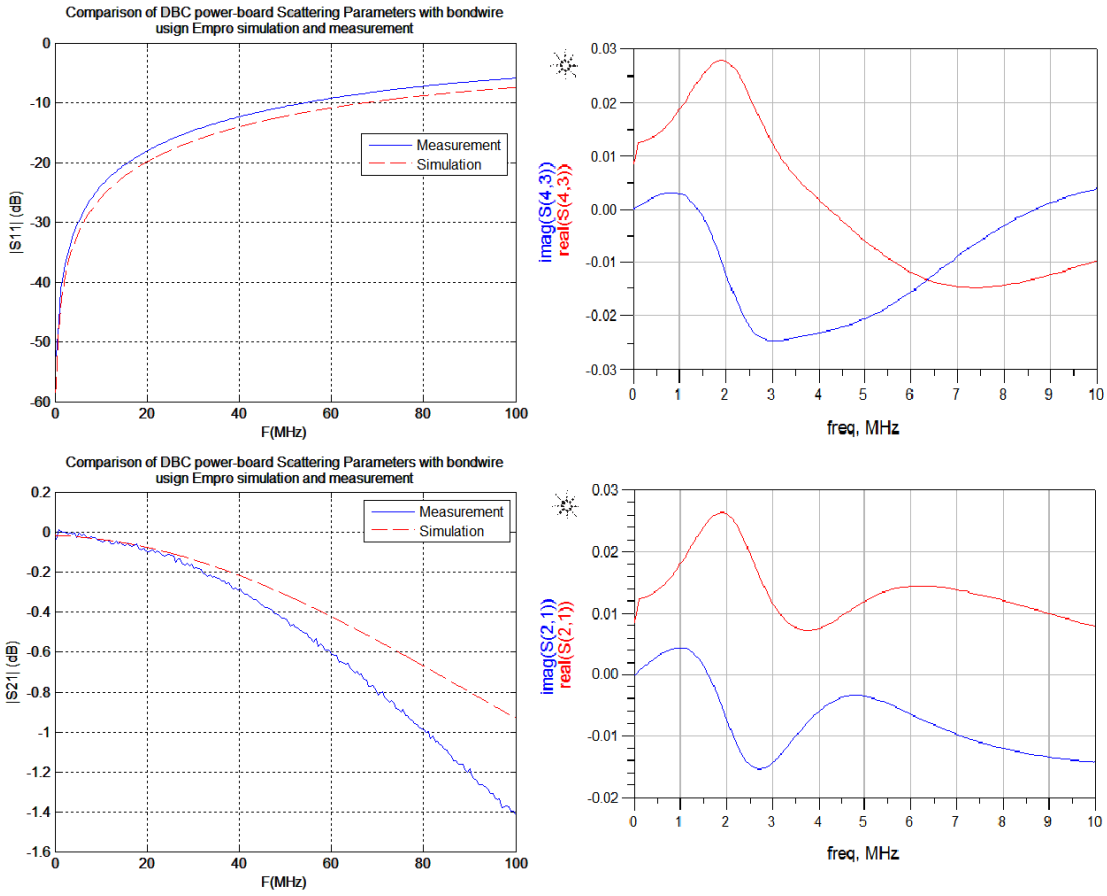

Figure 6.16

Left: S-parameter of a DBC board shown in Figure 5.18. **Right**: S-parameter of the ship hull illustrated in Figure 5.1.

$$f(t) = e^{-|t|} \qquad F(\omega) = \frac{1}{1+\omega^2} \tag{6.8}$$

For this reason, a Graphical User Interface (GUI) Matlab code is written to investigate the effects of different parameters on the signal spectrum and the reconstructed signal. At first, a frequency data is loaded to the GUI. This GUI only compares the continuous wavelet transform using fast Fourier transform (CWTFT) with fast Fourier transform (inverse FFT) methods in reconstructing the signal in the time-domain. The variables in this GUI are scaling type, wavelet type, number of scales, frequency resolution, maximum frequency and the number of the missing points. In the following the effects of changing these parameters is discussed.

6.5.1 Scaling type

Two types of scaling is used in this GUI, linear and logarithmic, which are calculated as the following:

1. Linear:

   $s_0 = 2 * T_s \qquad ds = 0.1 \qquad scales = s_0 + (0 : NbSc - 1) * ds$

2. Logarithmic:

   $s_0 = 0.02 * T_s \qquad ds = 0.4875 \qquad scales = s_0 * 2^{(0:NbSc-1)*ds}$

T_s is the sampling time, which is equal to $1/F_m$ and $NbSc$ is the number of scales. It can be resulted from the simulations that for the exponential class of functions, the logarithmic scaling fits the original signal better, so the linear scaling is not considered anymore. Figure 6.17 shows the difference between linear and logarithmic scaling types.

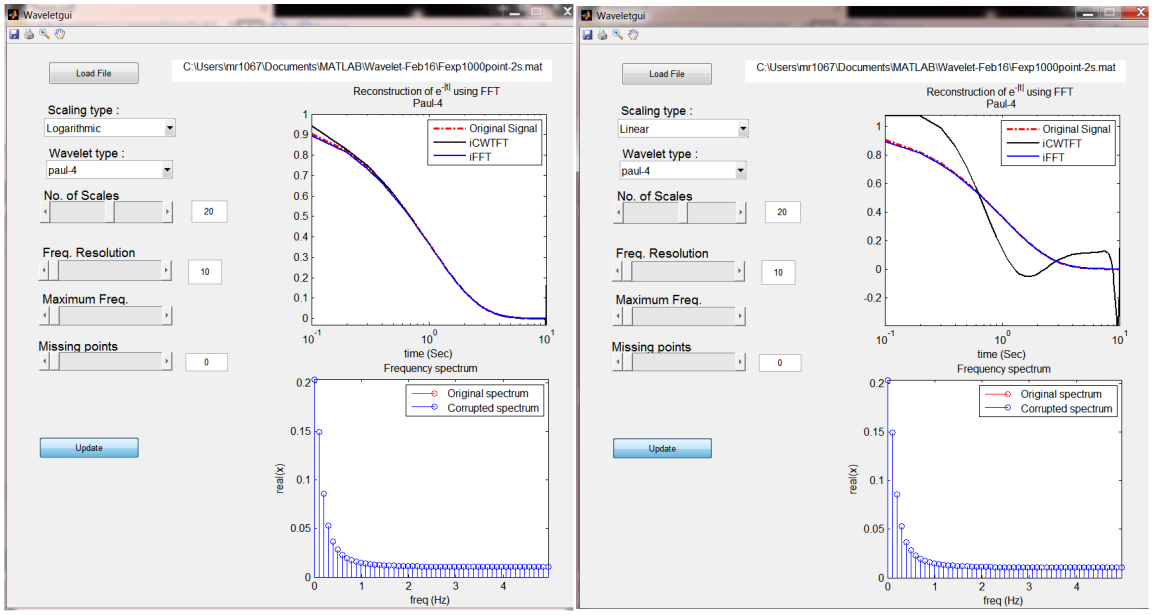

Figure 6.17

Left: Logarithmic scaling. **Right**: Linear scaling.

6.5.2 Wavelet type

Different wavelets can be used in CWT but because the applied method in this dissertation is chosen to be CWTFT, only the wavelet functions with analytical formulas are utilized. The equations of the wavelet functions and their Fourier transform is as following:

1. Derivative of Gaussian (DOG) $$\hat{\Psi}(s\omega) = -\frac{1}{\sqrt{\Gamma(m+1/2)}}(js\omega)^m e^{-(s\omega)^2/2}$$

2. Mexican Hat $$\hat{\Psi}(s\omega) = -\frac{1}{\sqrt{\Gamma(5/2)}}(js\omega)^2 e^{-(s\omega)^2/2}$$

3. Analytic Morlet $$\hat{\Psi}(s\omega) = \pi^{-1/4} e^{-(s\omega-\omega_0)^2/2} U(s\omega)$$

4. Non-Analytic Morlet $$\hat{\Psi}(s\omega) = \pi^{-1/4} e^{-(s\omega-\omega_0)^2/2}$$

5. Non-Analytic zero mean Morlet $$\hat{\Psi}(s\omega) = \pi^{-1/4}\{e^{-(s\omega-\omega_0)^2/2} - e^{-\omega_0^2/2}\}$$

6. Paul $$\hat{\Psi}(s\omega) = 2^m \sqrt{m(2m-1)!}(s\omega)^m e^{-s\omega} U(s\omega)$$

The comparison of two signals reconstructed by DOG and Paul wavelet is shown in Figure 6.18.

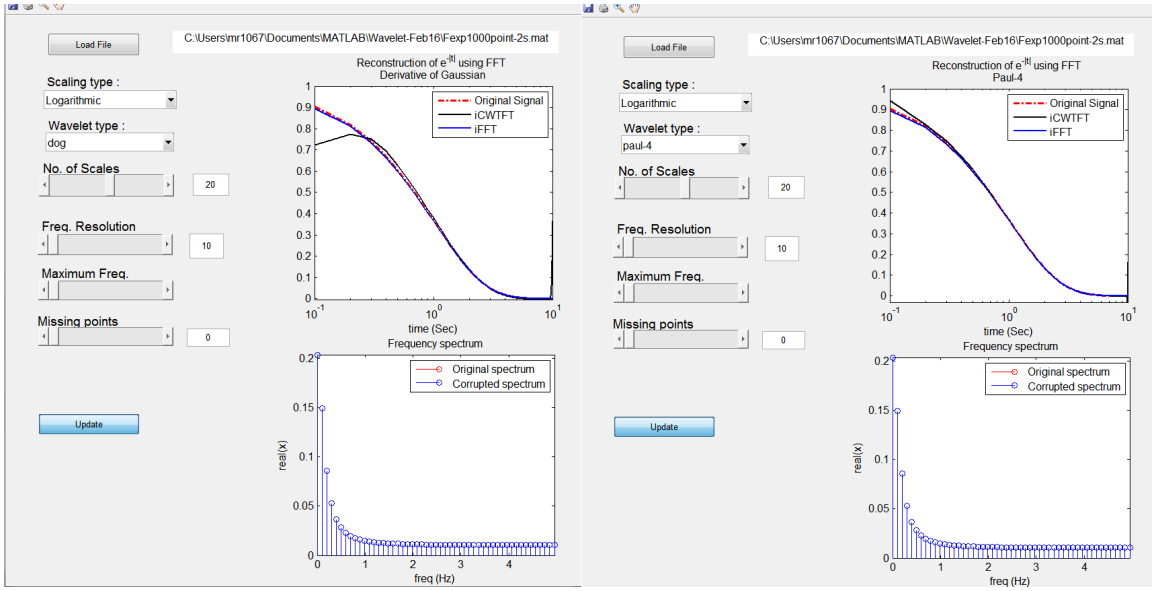

Figure 6.18

Reconstructed signal using: **Left**: DOG wavelet. **Right**: Paul wavelet.

6.5.3 Frequency Resolution and Maximum Frequency

By using these two sliders, the frequency resolution and the maximum frequency can be set on the desirable value. As much as the frequency resolution is increased the missing elements have less deteriorating effect on the reconstructed signal in the time-domain.

6.5.4 Number of Missing Points

This slider determines the number of missing points from the DC side. More missing points result in more degraded reconstructed signal in the time-domain which is shown in Figure 6.19.

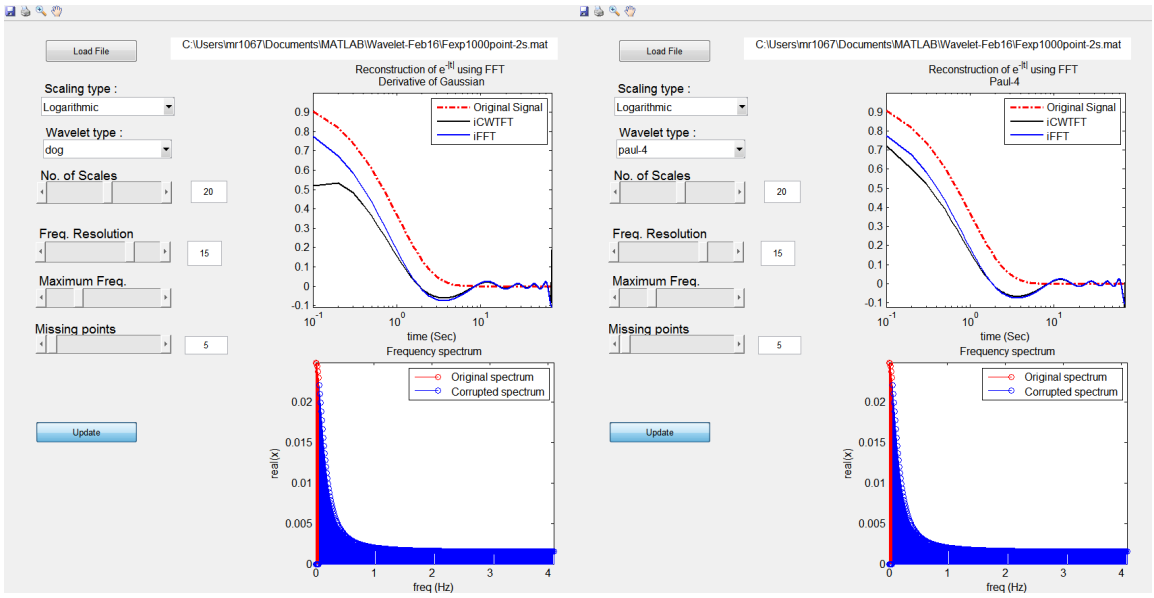

Figure 6.19

Reconstructed signal using: **Left**: DOG wavelet. **Right**: Paul wavelet with 5 missing elements from DC-side of the spectrum.

As noticed, the performance of continuous wavelet transform is not better than the Fourier transform as long as there are some missing points in the spectrum. In the next

section some enhancements are performed in the CWTFT spectrum. It is shown that the wavelet transform matches more correctly as compared to the Fourier transform.

6.6 Reconstruction of Exponential binomial

In this section, a combination of exponential terms is considered. Also an enhancement process as described in the section 4.5 is conducted. In Fig. 6.8 the reconstructed signal and the related spectrum of $7e^{-|5t|} + 8e^{-|2t|}$ are illustrated that show the wavelet transform can approximate the original signal better than the Fourier transform.

6.7 Computation of Impulse response

In this section, the extracted four-port S-parameter (discussed in the section 4.5 and shown in Figure 5.6) is transferred to a Matlab code written for the time-domain impulse response calculation. This code applies continuous wavelet transform using FFT algorithm (CWTFT) to the band-limited S-parameter and reconstructs the time-domain signal precisely. Figure 4.8 shows the flow diagram of the algorithm of the calculation process. Consider the number of the S-parameter data (spectrum) is N and the number of the missing point is k. Notice that in this research $K = 1$ because just DC frequency is missing.

After the conducted tests on the exponential and exponential binomials, the algorithm is run for the real data which is extracted by ADS as the total frequency spectrum of the entire ship hull blocks with the cables, shown in Figure 6.21 .

Through this algorithm, at first, the real part of the spectrum is extended to become an even function and the imaginary part is extended to make an odd function. Then *Wafou* transform, a special type of a wavelet transform introduced in section 4.5 is applied to both even and odd functions. As the next step, inverse wavelet transform is applied to the re-

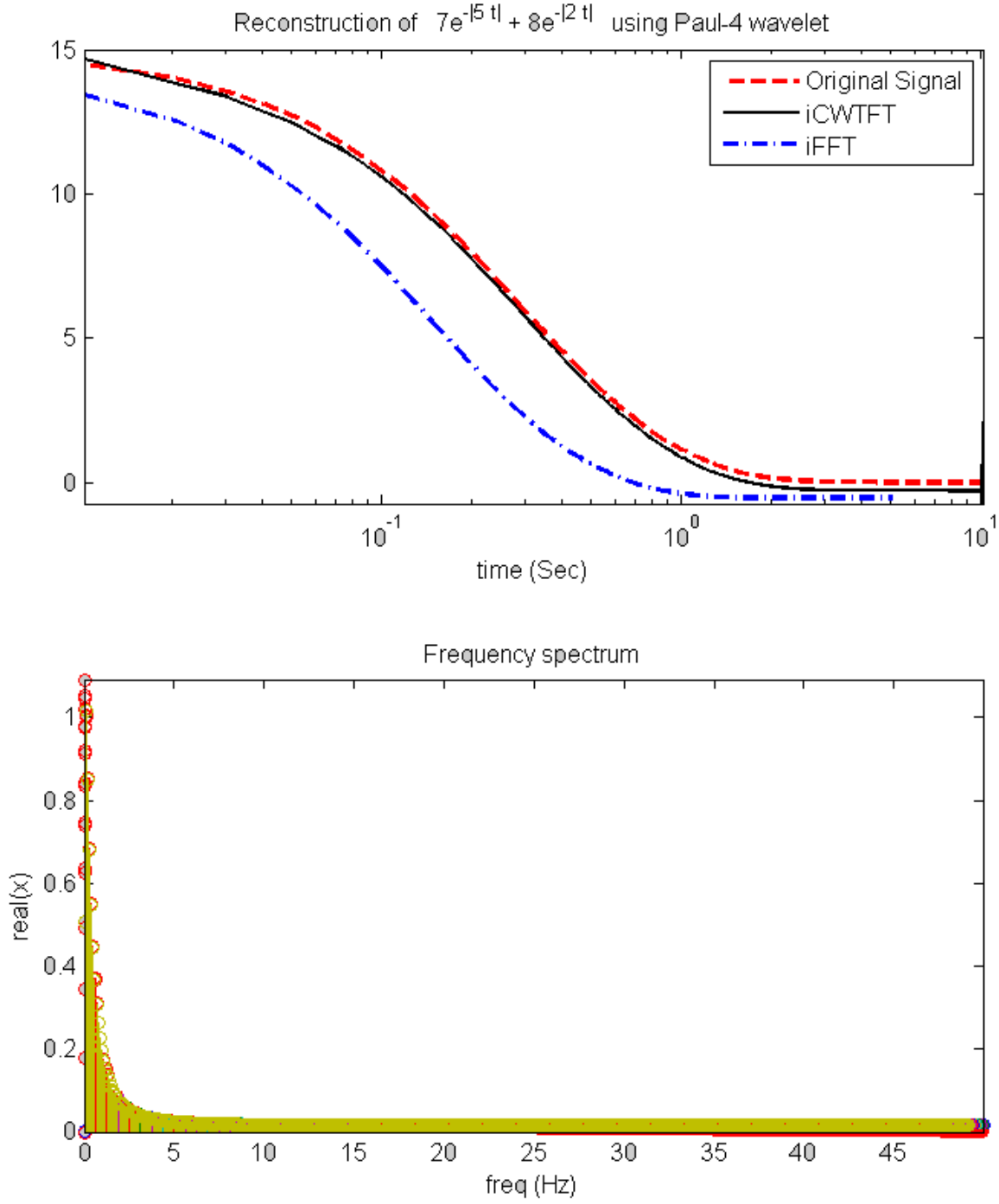

Figure 6.20

Up: Reconstruction of an exponential combination from its band-limited frequency spectrum using CWTFT and the Fourier transform.

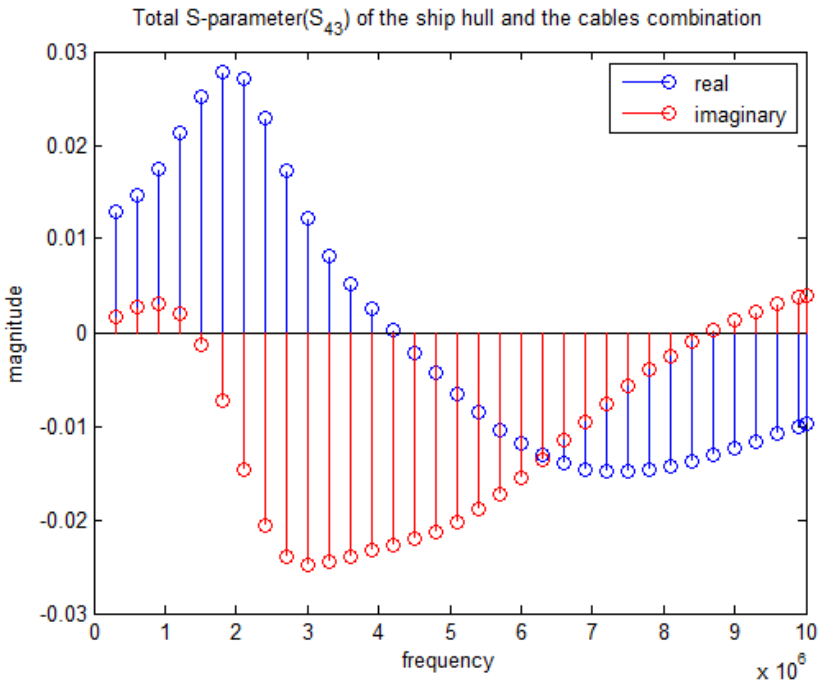

Figure 6.21

Up: S-paramter (S43; between ports 4 and 3) of the combined ship hull and cables spectrum calculated by ADS

sulting wavelet coefficients to reconstruct the signal in the time-domain. The reconstructed signal is different from the original time-domain signal. It should be noted that in this section, despite the previous experiments, the original time-domain signal is not available. From the previous observations, it can be concluded that the reconstructed signal in the time-domain differs from its original shape because of the missing DC point. at the next step, a Fourier transform is applied to the reconstructed signal and the new spectrum is generated. Then, The given S-parameter spectrum is compared with the generated spectrum. The difference between the values of the $k+1$ component in these two frequency spectra is calculated, is multiplied by a scaling factor and is assigned as the next iteration of the DC component value. The other frequency components, $k+1$ to N, in the generated spectrum is forced back to their previous value in the given S-parameter matrix. Afterwards, the process of applying *Wafou* and inverse wavelet transform is repeated with the number of s. The s is the length of the scale vector created for this particular wavelet transform. The length of this vector is determined such that the largest wavelet scale be equal to the time-domain signal. Therefore, this iteration algorithm is repeated s times. This algorithm shows a convergence in a wide range of S-parameter functions. As an example a linear combination of exponential functions is considered and the results do not match very well. Figure 6.22 is a comparison between the time-domain signals reconstructed via CWTFT, FFT and the Keysight ADS impulse response simulator. As shown the wavelet transform shows a significant superiority compared to the Fourier transform and matches the original time-domain signal better. In this experiment the Derivative of Gaussian (DOG) wavelet is used for reconstruction.

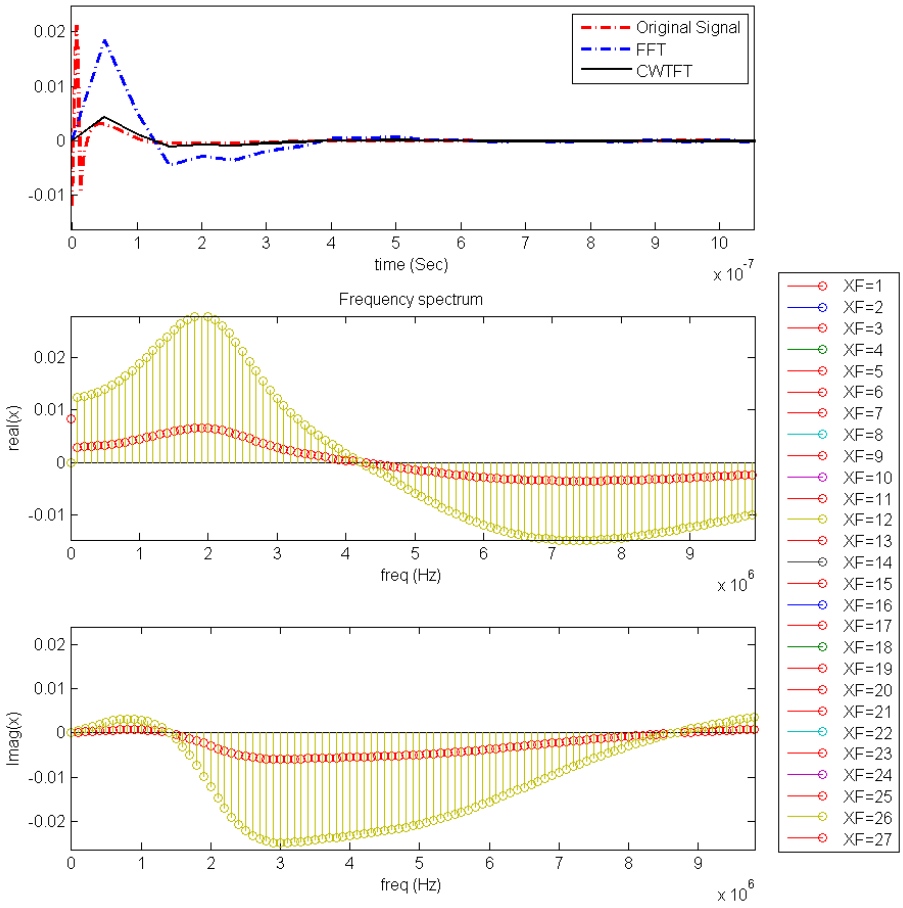

Figure 6.22

UP: Impulse response, **Middle**: real part of the spectrum, **Down**: imaginary part of the spectrum.

6.8 Convergency

In order to show convergency, at first, the developed Matlab code should be expressed in a mathematical frame, then, the convergency of the method can be evaluated by calculating the norms of the response and at last, resulting to a decreasing difference between the original signal and the reconstructed signal (error).

The original (given)S-parameter samples in the frequency domain can be shown as a set of samples (data):

$$S_0 = \{S(\omega_i)\}_{i=1}^{N} = \{S(\omega_1), ..., S(\omega_N)\} \tag{6.9}$$

In the next step, the given spectrum is extended even and odd for real and imaginary parts of the spectrum, respectively.

$$\tilde{S}_0 = \{S(\omega_{-N}), ..., S(\omega_N)\} \tag{6.10}$$

The wavelet transform of this set of data is calculated as follows:

$$[W_{ij}\{S(t)\}] = \frac{1}{2\pi}[S(\omega_i)\sqrt{|a_j|}e^{ib\omega_i}\bar{\Psi}_{ij}\frac{2\omega_N}{2N-1}] \tag{6.11}$$
$$1 \leq i \leq 2N-1 \quad , \quad 1 \leq j \leq J$$

The set of wavelet scales can be expressed as:

$$a = [a_0, a_0 2^{ds}, ..., a_0 2^{(J-1)ds}] \quad , \quad ds = \frac{39}{80} = 0.4875 \tag{6.12}$$

$$a_0 2^{(J-1)ds} \leq \frac{N}{\omega_N} \qquad \Delta a_j = a_0 2^{jds} - a_0 2^{(j-1)ds}$$

$$J \leq 1 + \frac{ln\frac{N}{a_0 \omega_N}}{dsln2} \tag{6.13}$$

The reconstructed signal in the time domain is called $f_1(t_k)$ and the related frequency domain signal $F_1(\omega_1)$ can be calculated through the following equation:

$$f_1(t_k) = \frac{1}{2\pi} \sum_{j=1}^{J} [W_{ij}\{S(t)\}\psi(\frac{t_k - \omega_j}{a_j})\frac{\Delta\omega\Delta a_j}{a_j^2}] \qquad 1 \leq k \leq N \tag{6.14}$$

$$F_1(\omega_l) = \sum_{k=1}^{N} f_1(t_k) e^{i\omega_i t_k} \frac{1}{\omega_N}$$

$$= \frac{1}{2\pi\omega_N} \sum_{j=1}^{J} [e^{i\omega_i t_k} W_{ij}\{f(t)\}\psi(\frac{t_k - \omega_j}{a_j})\frac{\Delta\omega\Delta a_j}{a_j^2}] \tag{6.15}$$

The DC component of the calculated spectrum $F_1(\omega_l)$ is determined as follows:

$$S_1(0) = |F_1(\omega_1) - S(\omega_1)|a_2 \tag{6.16}$$

$$S_1 = S_0 \cup \{S_1(0)\} = \{S_1(0)\} \cup \{S(\omega_i)\}_{i=1}^{N}$$

$$= \{S_1(0), S(\omega_1), ..., S(\omega_N)\} \tag{6.17}$$

Again, the wavelet transform is applied to the calculated spectrum ($\{S(\omega)\}$):

$$[W_{ij}\{S(t)\}] = \frac{1}{2\pi}[S(\omega_i)\sqrt{|a_j|}e^{ib\omega_i}\bar{\Psi}_{ij}\frac{2\omega_N}{2N-1}] \tag{6.18}$$

$$1 \leq i \leq 2N \quad , \quad 1 \leq j \leq J$$

In this stage, The second approximation of the original signal in the time domain ($f_2(t_k)$) is calculated:

$$f_2(t_k) = \frac{1}{2\pi}\sum_{j=1}^{J}[W_{ij}\{S(t)\}\psi(\frac{t_k-\omega_j}{a_j})\frac{\Delta\omega\Delta a_j}{a_j^2}] \qquad 1 \le k \le N+1 \tag{6.19}$$

The second approximation of the signal spectrum is calculated as following:

$$F_1(\omega_l) = \sum_{k=1}^{N} f_2(t_k)e^{i\omega_i t_k}\frac{1}{\omega_N}$$
$$= \frac{1}{2\pi\omega_N}\sum_{k=1}^{N+1}\sum_{j=1}^{J}[e^{i\omega_i t_k}W_{ij}\{f(t)\}\psi(\frac{t_k-\omega_j}{a_j})\frac{\Delta\omega\Delta a_j}{a_j^2}] \tag{6.20}$$

And the first component in the spectrum is determined as :

$$S_2(0) = |F_2(\omega_1) - F_1(\omega_1)|a_3 + S_1(0) \tag{6.21}$$

CHAPTER 7

CONCLUSION

In this dissertation a wavelet approach is addressed to reconstruct the signal in time-domain that is written in Matlab code and is evaluated by available numerical software. For this purpose the following steps were demonstrated.

7.1 Wavelet Transform Approach

1. Interpreting Matlab Wavelet Toolbox Algorithm
2. Writing a code for Discrete Wavelet Transform (DWT)
3. Applying the written code to Fourier Transform of Signal
4. Writing a code for inverse Discrete Wavelet Transform (IDWT)
5. Applying the written code to wavelet-Fourier transformed signal to reconstruct it in time-domain
6. Validating the reconstructed signal by comparison of the result with the results of numerical software.

REFERENCES

[1] "Tektronix Serial Data Link Analysis (SDLA) application note (page 6)," `http://www.tek.com/document/application-note/serial-data-link-analysis`.

[2] R. W. Anderson, L. Smith, and J. Gruszynski, "S-parameter techniques for faster, more accurate network design," *Hewlett-Packard Journal*, vol. 18, no. 6, 1967, pp. 13–24.

[3] S. Barmada, A. Musolino, and M. Raugi, "Analysis of integrated circuit system s by an innovative wavelet-based scattering matrix approach," *IEEE transactions on advanced packaging*, vol. 30, no. 1, 2007, pp. 86–96.

[4] J. B. J. baron Fourier, *The analytical theory of heat*, The University Press, 1878.

[5] R. Bayerer, D. Domes, and I. Ag, "Parasitic inductance in gate drive circuits," *Proc. Power Convers. Intell. Motion Eur*, 2012, pp. 8–10.

[6] R. M. Biernacki, Y. Chu, F. Rao, and Y. Hu, "Causality enforcement in fast EM-based simulation of multilayer transmission lines," *Microwave Symposium Digest, 2009. MTT'09. IEEE MTT-S International*. IEEE, 2009, pp. 869–872.

[7] V. Čižek, "Discrete hilbert transform," *Audio and Electroacoustics, IEEE Transactions on*, vol. 18, no. 4, 1970, pp. 340–343.

[8] R. E. Collin and H. Chang, "Field theory of guided waves," *Physics Today*, vol. 14, 1961, p. 50.

[9] V. B. Fangyi Rao and T. E. Sanjeev Gupta, Agilent Technologies Chad Morgan, "New Interconnect Models Removes Simulation Uncertainty," *IBIS Summit, 2008*. Agilent–Tyco, 2008, pp. 1–37.

[10] J. Gafford, M. Mazzola, A. Lemmon, and C. Parker, "Stable high dv/dt switching of SiC JFETs using simple drive methods," *Applied Power Electronics Conference and Exposition (APEC), 2013 Twenty-Eighth Annual IEEE*. IEEE, 2013, pp. 2450–2452.

[11] J. Gafford, M. S. Mazzola, M. Molen, C. Parker, D. Sheridan, V. Bondarenko, and J. Casady, *A 1200-V 600-A Silicon-Carbide Half-Bridge Power Module for Drop-In Replacement of an IGBT IPM*, Tech. Rep., SAE Technical Paper, 2010.

[12] X. Gong, J. Ferreira, and J. Popovic-Gerber, "Comparison and suppression of conducted EMI in SiC JFET and Si IGBT based motor drives," *Power Electronics and Motion Control Conference (EPE/PEMC), 2012 15th International*. IEEE, 2012, pp. DS2c–8.

[13] X. Gong and J. A. Ferreira, "Comparison and reduction of conducted EMI in SiC JFET and Si IGBT-based motor drives," *Power Electronics, IEEE Transactions on*, vol. 29, no. 4, 2014, pp. 1757–1767.

[14] X. Gong, I. Josifović, and J. A. Ferreira, "Modeling and reduction of conducted EMI of inverters with SiC JFETs on insulated metal substrate," *IEEE Transactions on Power Electronics*, vol. 28, no. 7, 2013, pp. 3138–3146.

[15] L. Graber, B. Mohebali, M. Bosworth, M. Steurer, A. Card, M. Rahmani, and M. Mazzola, "How scattering parameters can benefit the development of all-electric ships," *Electric Ship Technologies Symposium (ESTS), 2015 IEEE*. IEEE, 2015, pp. 353–357.

[16] M. Haynes and M. Moghaddam, "Multipole and S-parameter antenna and propagation model," *IEEE Transactions on Antennas and Propagation*, vol. 59, no. 1, 2011, pp. 225–235.

[17] S. Hong, K. Chung, J. Lee, S. Jung, S.-S. Lee, and J. Choi, "Design of a diversity antenna with stubs for UWB applications," *Microwave and Optical Technology Letters*, vol. 50, no. 5, 2008, pp. 1352–1356.

[18] D. Infante, "Guiding the Selection of Physical Experiments for the Validation of a Model Designed to Study Grounding in Dc Distribution Systems," .

[19] D. S. J. Casady, R. Schrader and V. Bondarenko, "1200 V Enhancement-mode SiC VJFET Power Modules," *Proc. Power Convers. Intell. Motion Eur*, 2011.

[20] A. J. Jerri, *Introduction to Wavelets*, Sampling Publishing, 2011.

[21] I. Kang, X. Wang, J.-H. Lin, R. Coutts, and C.-K. Cheng, "Impulse response generation from S-parameters for power delivery network simulation," *Electromagnetic Compatibility and Signal Integrity, 2015 IEEE Symposium on*. IEEE, 2015, pp. 277–282.

[22] K. Kurokawa, "Power waves and the scattering matrix," *Microwave Theory and Techniques, IEEE Transactions on*, vol. 13, no. 2, 1965, pp. 194–202.

[23] D. D. Lee, "Response surface methodology for the analysis of grounding in a medium voltage DC shipboard power system," 2010.

[24] A. Lemmon, M. Mazzola, J. Gafford, and C. Parker, "Stability considerations for silicon carbide field-effect transistors," *IEEE Transactions on Power Electronics*, vol. 28, no. 10, 2013, pp. 4453–4459.

[25] A. Lemmon, M. Mazzola, J. Gafford, and C. Parker, "Instability in half-bridge circuits switched with wide band-gap transistors," *IEEE Transactions on Power Electronics*, vol. 29, no. 5, 2014, pp. 2380–2392.

[26] E. Matthews Jr, "The use of scattering matrices in microwave circuits," *Microwave Theory and Techniques, IRE Transactions on*, vol. 3, no. 3, 1955, pp. 21–26.

[27] A. Motamedi, "S-Parameter Modeling and simulation for Signal Integrity Analysis," *Presented by GigaTest Labs*. UBM Electronics, DesignCon 2012, p. `https://blogs.synopsys.com/analoginsights/files/2012/02/Amir_slides.pdf`.

[28] C. R. Mueller and S. Buschhorn, "Impact of module parasitics on the performance of fastswitching devices," *PCIM Europe 2014; International Exhibition and Conference for Power Electronics, Intelligent Motion, Renewable Energy and Energy Management; Proceedings of*. VDE, 2014, pp. 1–8.

[29] S. Narayana, G. Rao, R. Adve, T. Sarkar, V. Vannicola, M. Wicks, and S. Scott, "Interpolation/extrapolation of frequency domain responses using the Hilbert transform," *Microwave Theory and Techniques, IEEE Transactions on*, vol. 44, no. 10, Oct 1996, pp. 1621–1627.

[30] S. Narayana, G. Rao, R. Adve, T. Sarkar, M. Wicks, and S. Scott, "Interpolation/extrapolation of frequency domain responses using the Hilbert transform," *Signals, Systems, and Electronics, 1995. ISSSE '95, Proceedings., 1995 URSI International Symposium on*, Oct 1995, pp. 335–338.

[31] S. Narayana, T. K. Sarkar, R. Adve, M. Wicks, and V. Vannicola, "A comparison of two techniques for the interpolation/extrapolation of frequency domain responses," *Digital Signal Processing*, vol. 6, no. 1, 1996, pp. 51–67.

[32] G. Otonari and O. Bell, "Advances in Measurement Based Transient Simulation, http://www.keysight.com/upload/cmc-upload/All/Meas-Based-Transient-Simulation-Gigatest.pdf," *Presented by GigaTest Labs*, 2008.

[33] K. Park, "Structural system identification using systems theory and wavelets," *Tutorial in Celebration of the 50th Anniversary on DYNAMICS, SYSTEMS and DESIGN*, 1996, pp. 1–120.

[34] M. Rahmani and M. Mazzola, "Modeling of common mode currents on electric ship hull using scattering parameters," *Electric Ship Technologies Symposium (ESTS), 2015 IEEE*. IEEE, 2015, pp. 156–160.

[35] F. Rao, "Optimization of spectrum extrapolation for causal impulse response calculation using the hilbert transform,", June 14 2011, US Patent 7,962,541.

[36] F. Rao, S. Gupta, and V. Borich, "The need for impulse response models and an accurate method for impulse generation from band-limited S-parameters," 2008.

[37] A. Robertson, K. Park, and K. Alvin, "Extraction of impulse response data via wavelet transform for structural system identification," *Journal of vibration and acoustics*, vol. 120, no. 1, 1998, pp. 252–260.

[38] M. Shahverdi, M. Mazzola, R. Schrader, A. Lemmon, C. Parker, and J. Gafford, "Active gate drive solutions for improving SiC JFET switching dynamics," *Applied Power Electronics Conference and Exposition (APEC), 2013 Twenty-Eighth Annual IEEE*. IEEE, 2013, pp. 2739–2743.

[39] C. Warwick and F. Rao, "S-parameters Without iTears,Understand this critical frequency-domain measurement and its interpretations," 2010.